The Institute of Paper Science and Technology

Atlanta, Georgia

Doctor's Dissertation

The Permeability of Compressed Fiber Mats and the Effects of Surface Area Reduction and Fiber Geometry

Fung-jou Chen

June, 1982

TABLE OF CONTENTS

THE PERMEABILITY OF COMPRESSED FIBER MATS AND THE EFFECTS OF SURFACE AREA REDUCTION AND FIBER GEOMETRY

A thesis submitted by Fung-Jou Chen

B.S. 1970, Provincial Chung-Hsing University

M.S. 1975, Lawrence University

in partial fulfillment of the requirements
of The Institute of Paper Chemistry
for the degree of Doctor of Philosophy
from Lawrence University,
Appleton, Wisconsin

SUMMARY

A study was made to determine the permeability of compressed fiber mats and to examine the effects of surface area reduction and fiber geometry. Three batches of polyester fibers with cross-sectional aspect ratio 1.00, 1.80, and 3.18 were used to form mats through a constant-rate filtration technique. Their permeability results were obtained in the porosity range from 0.85 to 0.40, and were represented in terms of the Kozeny factor. By assuming that all the fiber surface is exposed to the permeating fluid, the Kozeny factor was found to decrease monotonically with decreasing porosity without leveling off to the commonly found value of 5.0. The progressive deviation of the Kozeny factor at low porosities was most pronounced for cylindrical-fiber mats, and became less so as the fiber aspect ratio was increased.

A polymer adsorption technique using cationic polyethylenimine PEI-1000 was employed to determine the exposed surface area of the compressed mats. The exposed surface areas so measured were then used to recalculate the Kozeny factors and it was found that the Kozeny factors of all the three types of fibers level off to a fairly constant value of 4.7 at lower porosities, in good agreement with the value found for particle beds. These results suggest that particle shape, either longitudinal or cross-sectional, plays no role in mat permeability. The particle shape, however, influences the extent of surface area reduction and concurrently the apparent Kozeny factors.

The compression responses of these three types of mats were found to match the responses of surface area reduction as a function of porosity. A direct plot of the applied compressive load against the surface area reduction gave a unique correlation independent of mat porosity and fiber shape, suggesting that the surface area reduction is induced by mechanical load.

INTRODUCTION

Fluid flow through porous media has long been a subject to interest in many branches of science and technology. By far the largest amount of research which has explored the basic relationship guiding such flow has been on beds composed of granular particles, and many useful results have been obtained.

Studies on fluid flow through fibrous beds are of great importance to paper-makers who are concerned with pulp washing, formation and dewatering of the paper web on the paper machine, and water removal in the wet presses.

Because of the extreme complexity of the fiber mats, it is virtually impossible to obtain an exact geometrical description of their pore geometries, and it is therefore impossible to apply the fundamental principles of hydrodynamics to characterize the flow properties of the mats. Consequently, in attempts to study the fundamental relationships of the flow of fluid through fiber mats, it has been necessary to revert to a more phenomenological approach.

There are some analytical studies on the fluid flow through regular arrays of fiberlike cylinders, but these are of little importance to practical systems in which fibers are not well ordered. They may, however, provide some insight into the effect of structural variation on the permeability of porous media in general.

In this work, filtration-formed mats with fibers randomly oriented in the plane normal to flow are the porous media of primary concern. Early studies have established the basic relationships of fluid flow through such mats at high porosities. Recent studies, however, have given anomalous results when porosities are extended to the lower range. The objective of this thesis is,

therefore, to investigate the flow properties of the lower porosity fiber mats and the effect of some suggested complicating factors.

LITERATURE REVIEW

This review is divided into three major parts. Part One presents the fundamental relationships of fluid flow through particle beds, including Darcy's Law and two most successful approaches to correlate Darcy's permeability to the structural properties of porous media, namely the phenomenological approach and the analytical approach. Part Two summarizes the studies of fluid flow through fiber beds, including studies on random mats and studies on regular arrays of fibers. In Part Three, some complicating factors encountered in recent work are presented. These form the basis for this thesis work.

FUNDAMENTAL RELATIONSHIPS

Darcy's Equation

The fundamental relationship describing slow, steady-state, isothermal flow of an incompressible Newtonian fluid through a homogeneous porous medium is the Darcy's equation (1),

$$U = Q/A = K_o \Delta P/L \tag{1}$$

where U = superficial velocity, cm/sec

Q = volumetric flow rate, cm^3/sec

A = cross-sectional area of porous medium presented to flow, cm^2

ΔP = pressure drop across the medium, $dyne/cm^2$

L = thickness of the medium, cm

K_o = proportionality factor, cm/poise

The Darcy equation simply states that the flow rate is directly proportional to the pressure drop. It is applicable for laminar flow where inertial effects

are negligible and where the resistance to flow, as expressed by $1/\underline{K}_o$, is due entirely to the viscous drag of the fluid.

The proportionality factor, $\underline{K}_o$, combines the structural properties of the porous medium and the characteristics of the permeating fluid. The fluid properties can be separated from those of the medium by the commonly accepted relationship (2):

$$K_o = K/\mu \tag{2}$$

where μ is the viscosity of the fluid. The factor, $\underline{K}$, is generally referred to as the Darcy permeability or called the specific permeability. It is dependent only on the characteristics of the porous structure and has the dimension of length squared. Combining Eq. (1) and (2), the Dary equation becomes:

$$U = \frac{K}{\mu} \frac{\Delta P}{L} \tag{3}$$

Darcy's Law was empirically determined in 1856, from the flow of water through a sand filter bed, but recently a theoretical basis for it has been demonstrated. Irmay (3) showed that the equation was valid on a macroscopic scale by a space average of the microscopic flow obeying the creeping flow form of the Navier-Stokes equation. A theoretical derivation of Darcy's Law was presented by Whittaker (4), who applied the conservation principles to the flow in an anisotropic medium and derived the Darcy equation.

Since the Darcy permeability, $\underline{K}$, is structure dependent, numerous approaches have been proposed to correlate it to the measurable quantities of the porous structure. The most successful of these are: (1) the phenomenological or semi-empirical approach, for which the best known is the hydraulic radius theory as

represented by the Kozeny-Carman equation, and (2) the analytical approach as represented by the drag theory of permeability.

Phenomenological Approach

In the phenomenological approach, the flow of fluids through porous media is considered to be analogous to flow through a system of capillaries. This approach may be further divided into studies on cylindrical capillary models and studies on noncylindrical capillary models. Studies of the latter models are also referred to as the hydraulic radius theory or Kozeny-Carman theory.

In the hydraulic radius theory, a porous medium is considered to be analogous to be a bundle of parallel, noncylindrical capillaries, the size of which is represented by the hydraulic radius, $\underline{m}$. The hydraulic radius of a capillary is defined as the ratio of cross-sectional area to wetted perimeter. Extending the definition to a porous medium, $\underline{m}$ is the ratio of porosity, ε (volumetric void fraction), to specific surface $\underline{S_o}$ (surface area per unit volume of the medium). By dimensional considerations, the Darcy permeability of the model is taken to be proportional to the hydraulic radius squared. Since the average velocity in pores is equal to $\underline{U}/\varepsilon$, the ratio of $\underline{K}$ for the porous medium to $\underline{m}^2$ of the model is proportional to ε. The resulting Kozeny-Carman expression (5) of Darcy's permeability is

$$K = \frac{\varepsilon^3}{k\, S_o^2} \tag{4}$$

with $\underline{k}$ referred to as the Kozeny factor. It is an unknown factor and must be empirically determined for each particular porous medium in question.

The specific surface of the medium, $\underline{S_o}$, can be converted to specific surface based on particle volume, $\underline{S_v}$ (area per unit volume of particles), assuming point contact between particles, by

$$S_o = S_v(1-\varepsilon) \tag{5}$$

Thus, the Kozeny-Carman equation becomes

$$K = \varepsilon^3/[k\ S_v^2\ (1 - \varepsilon)^2] \tag{6}$$

Carman (5) attempted to further break down the Kozeny factor into the product of a pore shape factor and a tortuosity factor squared. The value of the pore shape factor for straight flow channels of various cross-sectional shapes lies in the range 2-3. The tortuosity factor, defined as the ratio of the average length for fluid flow to the thickness of the porous medium, is estimated to be $\sqrt{2}$ from beds of spheres. Thus, according to Carman, the Kozeny factor should have a value between 4-6; with the average value of 5.0, if average shape factor of 2.5 is chosen.

Carman (6) later accumulated and discussed a huge volume of literature which evaluated and utilized the Kozeny-Carman equation. For randomly packed beds of uniform spheres in which the porosity ranged from 0.26 to 0.48, he concludes that the Kozeny factor is 4.8 with a probable range of variation, due to experimental uncertainty, of 4.5 to 5.1. A considerable mass of experimental data (6) on randomly packed beds of various shape particles, some rather extreme, also indicate that the Kozeny factor is about 5.0, independent of particle shape and porosity from about 0.26 to 0.80. The Kozeny factor, therefore, has been termed the "Kozeny constant."

Although the Kozeny-Carman equation appears to be semiempirical in nature, partial justification from hydrodynamic consideration has been made. Snyder and Stewart (7) solved the basic hydrodynamic equations of continuity and motion for creeping flow of a Newtonian fluid through loose cubic packing ($\varepsilon = 0.476$) and dense cubic packing ($\varepsilon = 0.26$) arrangements of uniform spheres under exact boundary conditions. Their solution is in almost complete agreement with the Kozeny-Carman equation, the theoretical values of the Kozeny factor for the high and low porosities being 4.16 and 4.86, respectively. Scarlett (8), using a three-dimensional description for an irregular pore, obtained an equation for creeping flow that gives a value of the Kozeny factor of 4.93.

The Kozeny-Carman theory has also received much criticism, largely on the indiscriminate use of the Kozeny constant of 5.0 for the entire class of porous media. Particle beds represent only a part of the entire class of porous media. In general, particles can be packed uniformly in a column so that the void space is randomly distributed and interconnected. Fluid can thus permeate the structure in all directions. The Kozeny constant of 5.0, derived from particle beds, cannot be indiscriminately applied to another type of porous media. Monographs by Carman (6) and Scheidegger (2) discuss in detail the limitations on the use of the Kozeny constant of 5.0. Because of this, and because of the fact that the Kozeny factor does contain unknown variables (tortuosity, shape factor, pore uniformity, pore distribution, to name just a few), it is usually considered advisable to determine experimentally the Kozeny factor for the particular system in question. For practical purposes, the Kozeny factor has also been used as a relative measure of the resistance to flow through a porous sample and can serve as a basis for comparison of porous media having known structural characteristics.

The constancy of the Kozeny factor breaks down and increases sharply when the porosity exceeds 0.8. Carman (6) points out that the assumption of flow through capillaries used in deriving the Kozeny-Carman equation no longer applies at these high porosities. As the particles move farther apart, the flow pattern changes from the flow through capillaries to a flow in relative motion around the particles. The Kozeny factor would go to infinity when the porosity approaches unity (where the particles exert essentially no mutual influence and Stokes' Law must be applied to each).

Analytical Approaches

The analytical approaches are represented by the various drag theories, treating permeation as flow around particles instead of flow through capillaries. These involve starting with Stokes' Law for the frictional drag of a single particle, and assuming a certain geometrical model to take into account the flow interference due to the neighboring particles as the particle population increases. There are numerous models dealing with sphere beds, but only the cell models of Happel (9) and Kuwabara (10), which have been extended to fibrous beds, will be discussed. The other approaches have been summarized by Happel (11).

In the cell model, the population of sphere particles is divided into a number of identical unit cells. Each cell contains a spherical particle surrounded by a concentric spherical fluid envelope. The fluid volume is such that the porosity of the cell is identical to that of the entire system of particles. In Happel's analysis, boundary conditions are specified for the solid sphere moving within the fluid. A no-slip condition is imposed on the solid surface and the conditions of zero normal velocity and zero shear stress are

assumed on the outer fluid boundary. Kuwabara uses the condition of zero vorticity on the outer fluid boundary instead of zero shear stress.

The cell model has the characteristics that the fluid flow is around the particle and the flow interference due to neighboring particles is the restriction of the size of the fluid envelope. With these assumptions, the complete Navier-Stokes equations, omitting inertia terms, can be solved. An equation similar to Darcy's is obtained, which describes the permeability of the unit cell and represents that of the entire system.

Figure 1 shows both Happel and Kuwabara's solutions expressed in terms of the Kozeny factor, along with experimental results for comparison. The experimental Kozeny factor for spheres at porosities lower than 0.7 was taken as 4.8 as reviewed by Carman (6). The Kozeny factors at porosities higher than 0.7 are taken from Brinkman's equation (12) which, as also reviewed by Carman (6, p. 26), has been supported by the data of Steinour (13) on sedimentation, Mertes and Rhodes (14) on fluidization and sedimentation, the fluidization experiments of Verschoor (15) on sand beds in water and on closely graded glass spheres in toluene, the data of Happel and Epstein (16) with stationary, regular arrays of spheres, and the data of Wilson (17) who was able to prepare more or less random assemblages of spheres without the need for support up to values of $\varepsilon = 0.84$ (using dilute gelatin to promote adhesion between particles).

Happel's solution is in better agreement with the experimental data than Kuwabara's. This occurs, as Happel (11) points out, because the vorticity model yields a higher energy dissipation in the envelope than that due just to particle drag alone, owing to the additional work done by the stress at the outer boundary. Since the cell model provides a rigorous solution based on hydrodynamic principles and accounts for a broader range of porosity than the

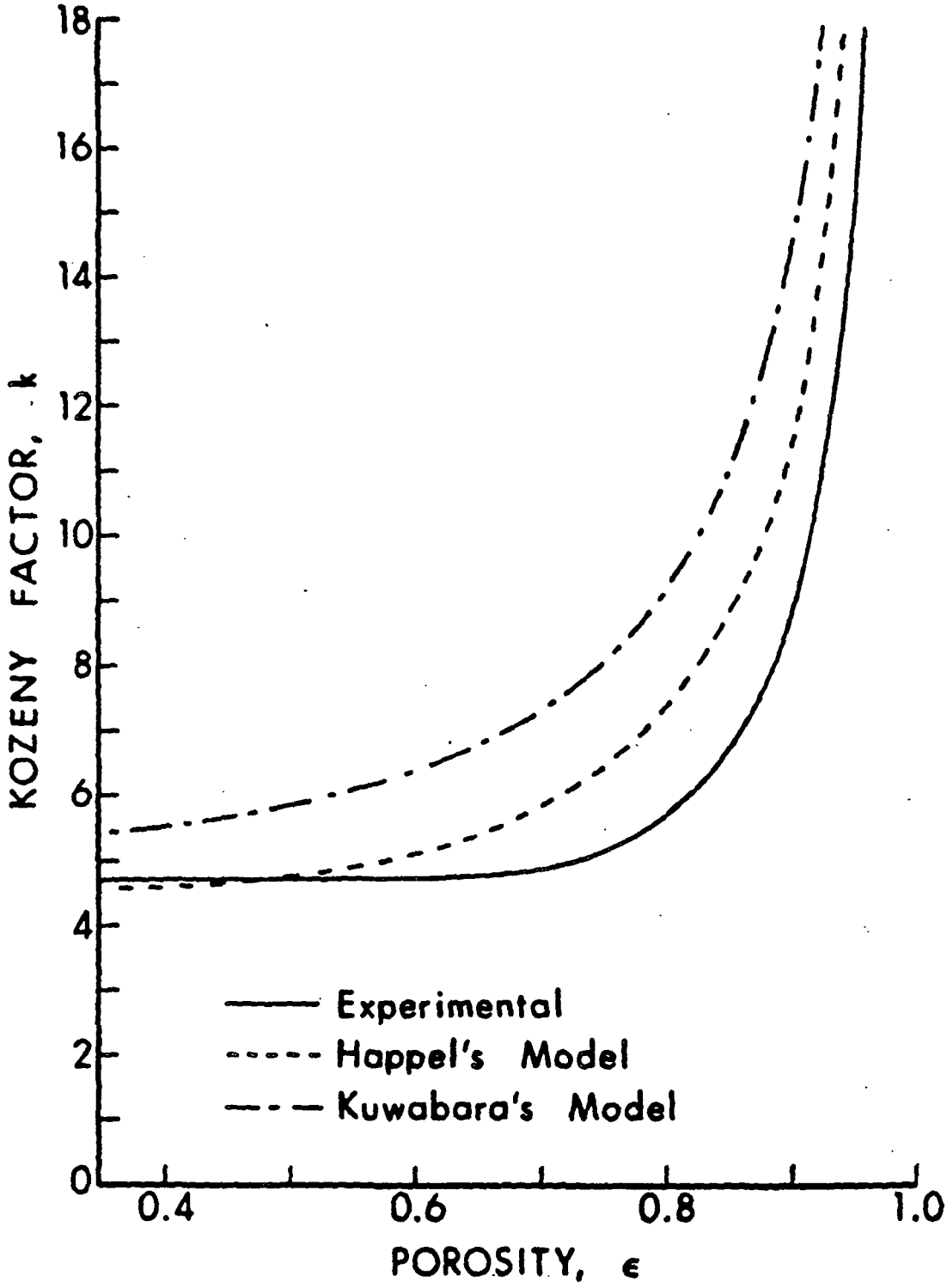

Figure 1. Correlation of Kozeny factors for beds of spherical particles.

Kozeny-Carman model, this approach has attracted general attention. One serious drawback of this approach, however, is that it bears no physical meaning at lower porosities ($\varepsilon < 0.5$) where the spheres have in fact touched each other and the spherical fluid envelope assumed in the theory would be severely distorted. The agreement of the solution with the experimental value therefore gives at most the plausibility of the approximation approach based on the space averaging technique.

FLUID FLOW THROUGH FIBER MATS

In this section, studies concerned primarily with fluid flow through mats of fibers, rather than any porous medium, will be discussed. A review of fiber mat permeation is given by Han (18). The Darcy equation combined with the Kozeny-Carman equation will be used as the basic relationship for flow through fiber mats. Because of the easier definition of circular fiber (or cylinders) and because of the simpler analysis of flow past such fibers, the flow through fiber mats has been usually studied with circular fibers.

Flow Through Random Fiber Mats

By virtue of their elongated shape, fibers can be randomly formed into mats of high porosities. In early work, it was also demonstrated that the Kozeny factor is dependent on porosity at high porosities. An empirical equation was given first by Davies (19),

$$k = k_1 \frac{\varepsilon^3}{(1 - \varepsilon)^{1/2}} [1 + k_2(1 - \varepsilon)^3] \tag{7}$$

where k_1 and k_2 are two constants and have the values 4.0 and 56, respectively, based on air permeability data for fiber filters over the porosity range 0.994 to 0.70.

Ingmanson and associates (20) made very careful water permeability experiments with uniform mats of glass and nylon fibers of circular cross section oriented randomly in the x-y plane with their axes principally perpendicular to flow. Their measurements yielded the values 3.5 and 57 for k_1 and k_2, respectively. The experimental data, as shown in Fig. 2, were obtained from porosity 0.96 down to 0.68. Porosities lower than 0.68 were not obtained because glass fibers shatter appreciably under the increasing compressive loading. It was expected, however, that the Kozeny factor would level off to 5.0 at lower porosities, based on the trend of their data and the amply demonstrated constancy from other types of beds.

Carroll (21) has presented a three-parameter correlation of Kozeny factor and porosity for beds of cylindrical synthetic fibers which fits the data below a porosity of 0.80 better than does the more widely used Davies-Ingmanson equation. The Carroll expression is

$$k = 5.0 + \exp\,[14(\varepsilon - 0.80)] \qquad (8)$$

One drawback to this equation is the failure to approach infinity as the porosity goes to unity.

Flow Through Regular Array of Fibers

Rigorous solutions from an analytical approach for describing the fluid flow through the random fiber mats of interest in this work is virtually impossible. This is due to the difficulties in specifying exact boundary conditions. Only simple cases, namely flow parallel or perpendicular to regular arrays of infinitely long parallel cylinders of equal radii, have been considered by investigators. These are reviewed below.

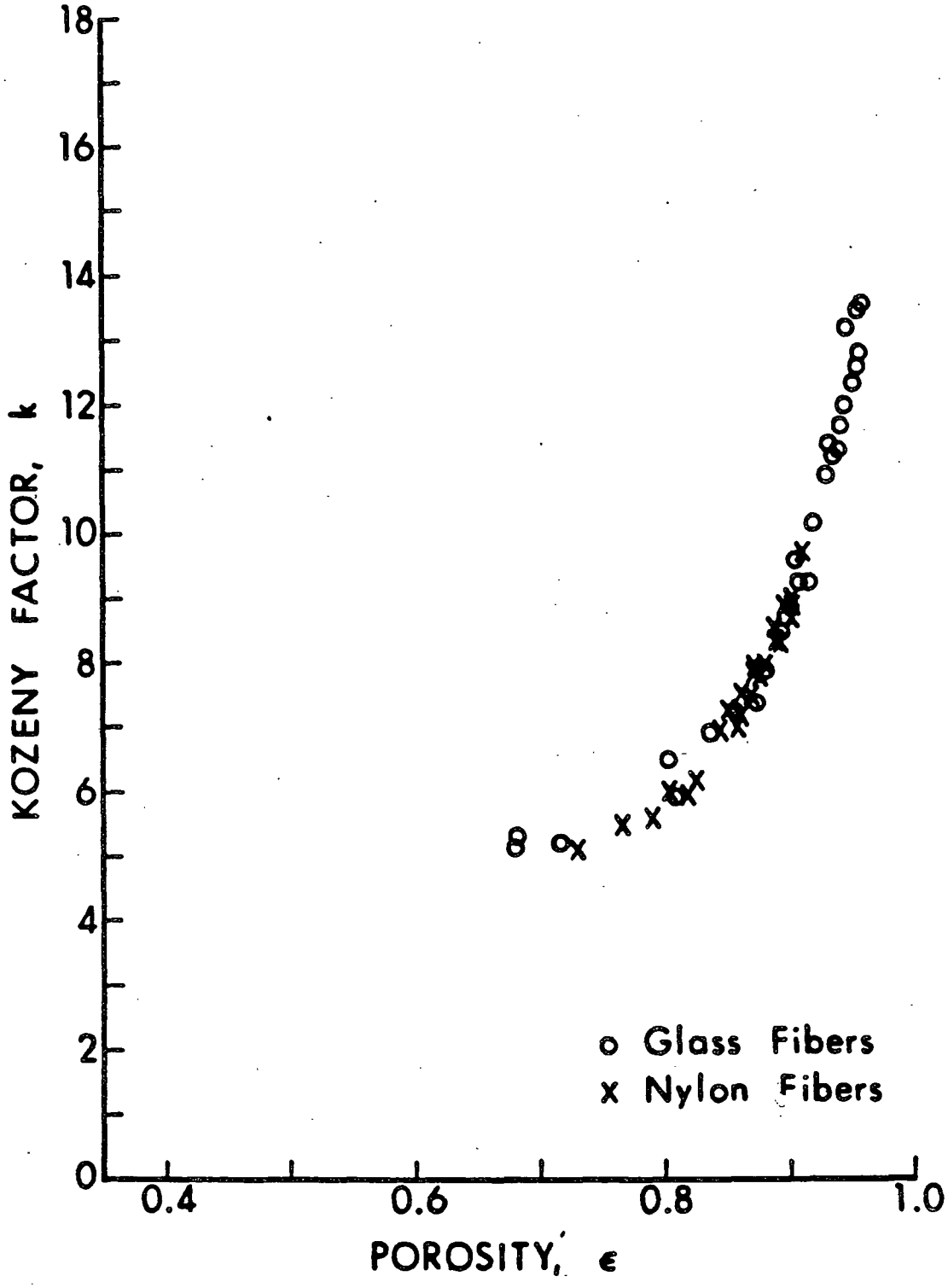

Figure 2. Correlation of Kozeny factors for beds of cylindrical fibers (20).

Emersleben (22) was the first to solve the Navier-Stokes equation for the problem of flow parallel to parallel cylinders in a square array. The square array of circular sections was represented by contours of constant value for a special periodic function, namely the second-order Epstein Zeta function. This function represents the contours well, above a porosity of about 0.8, but gives a progressively poorer approximation at lower porosities, since the cylinders represented by the function becomes noncircular. His solution for the Kozeny factor as a function of porosity is shown as Curve 1 in Fig. 3.

The parallel flow problem was also solved by Langmuir (23). In this work a concentric flow contour was assumed throughout the entire porosity range. This assumption implies that the flow is parallel to an equilateral triangular array of parallel cylinders. Langmuir's solution yields,

$$k = \frac{2\,\varepsilon^3}{(1-\varepsilon)\left[2\ln\left(\frac{1}{1-\varepsilon}\right) - 3 + 4(1-\varepsilon) - (1-\varepsilon)^2\right]} \qquad (9)$$

The success of the free-surface cell model in describing the fluid flow through sphere beds had also led Happel (24) to extend the same treatment to the case that Langmuir investigated. His model is, in principle, the same as that of Langmuir and yields exactly the same solution as that of Langmuir. The zero-vorticity cell model of Kuwabara (10) was checked by Brown (25) for the same case mentioned above; the result is identical to that of Langmuir and Happel. The results of these three investigations are plotted as Curve 4 in Fig. 3.

The laminar flow parallel to the parallel cylinders arranged in both square and equilateral triangular arrays were also considered by Sparrow and Loeffler (26). Their solution was obtained using series expression, and are also plotted

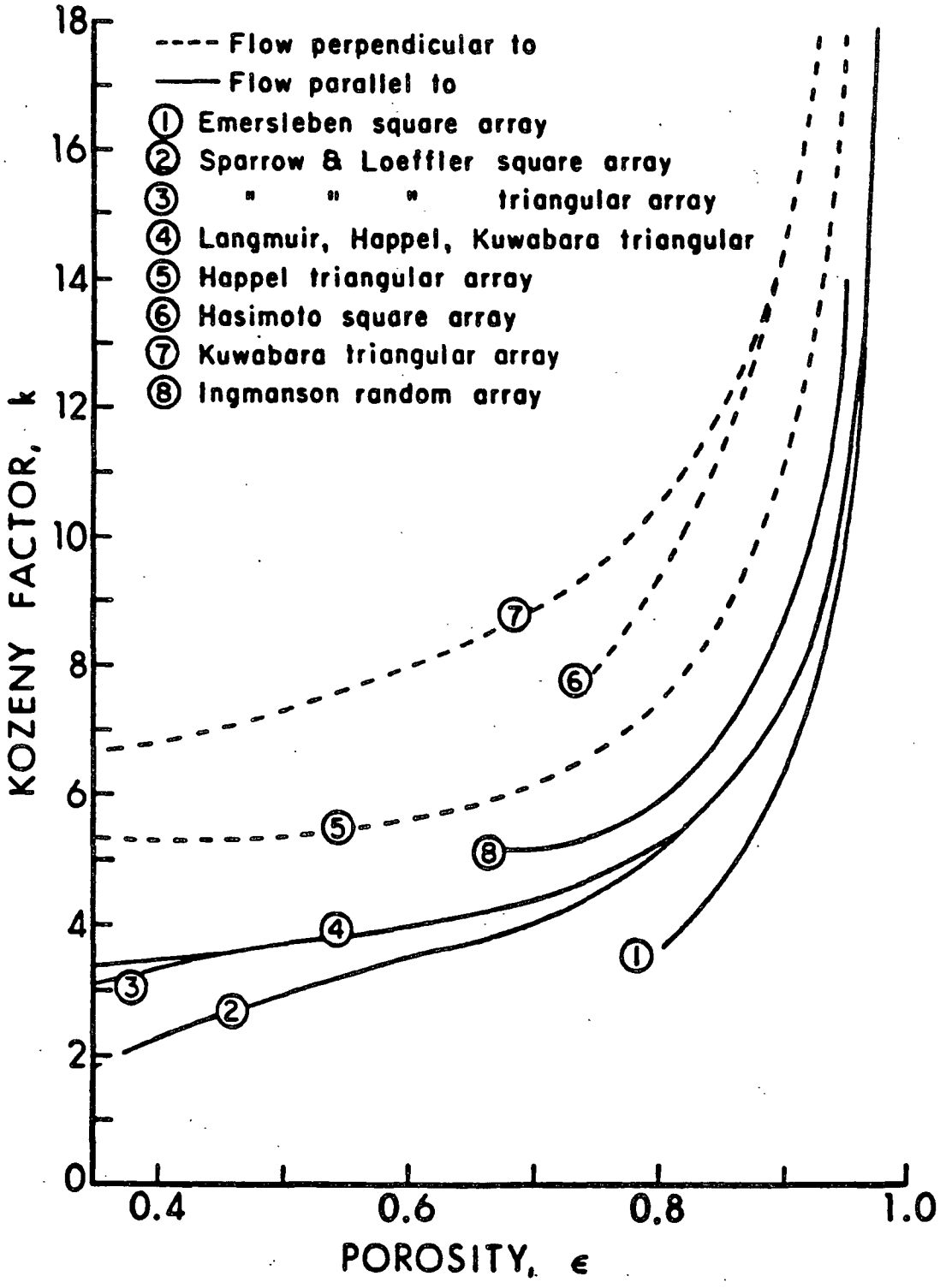

Figure 3. Correlations of Kozeny factors for beds of cylindrical fibers of regular arrays.

as Curves 2 and 3 in Fig. 3. It indicates that at high porosities, the two types of cylinder arrangements do not affect permeability and agrees exactly with the Langmuir, Happel, and Kuwabara's solutions. At lower porosities, substantial deviation between the two arrangements is indicated. The solution of the equilateral triangular case still agrees with that of Langmuir, Happel, and Kuwabara down to a porosity of about 0.45 and then diverges. The solution of the square array case gives a lower value of the Kozeny factor than that of the triangular array case at lower porosities. A similar result for this square spacing was also obtained by Leibenson (27).

Another case of flow problem has also been considered by some investigators, namely fluid flow perpendicular to regular arrays of parallel cylinders.

Hasimoto (28) solved the two-dimensional problem of flow perpendicular to the longitudinal axes of parallel cylinders in a square array. He represented the square array of circular sections by contours of constant value for a special periodic function derived from the Epstein Zeta function of the third order. His solution at porosity lower than 0.8 is poor, since the cylinders represented by the function becomes noncircular. The solution is only plotted to a porosity of 0.7 in Curve 6 of Fig. 3.

Happel (24) solved the two-dimensional problem of flow perpendicular to parallel cylinders in an equilateral triangular array by using the free-surface cell model mentioned previously. His solution yields,

$$k = \frac{2\,\varepsilon^3}{(1-\varepsilon)\left\{\ln\left[\frac{1}{(1-\varepsilon)}\right] - \frac{1-(1-\varepsilon)^2}{1+(1-\varepsilon)^2}\right\}} \qquad (10)$$

This expression is also plotted as Curve 5 in Fig. 3 for comparison.

The same problem was also solved by Kuwabara (10) using the same cell model except that zero vorticity was assumed on the virtual fluid surface instead of zero shear stress as a boundary condition. The resulting Kozeny factor from the Kuwabara analysis is,

$$k = \frac{4\,\varepsilon^3}{(1-\varepsilon)\left[2\ln\left(\frac{1}{1-\varepsilon}\right) - 3 + 4(1-\varepsilon) - (1-\varepsilon)^2\right]} \qquad (11)$$

This relationship is also plotted as Curve 7 in Fig. 3. As is evident, Kuwabara's solution predicts a higher value for the Kozeny factor than Happel's at all porosities, and is exactly twice his solution for the parallel flow case expressed in Eq. (9). This effect had been suggested by Langmuir (23) prior to Kuwabara's solution. It should be noted that at porosities higher than 0.86 Kuwabara's solution merges with Hasimoto's, indicating that the triangular and square array have the same permeability at such high porosities.

The abovementioned analytical solutions for both flow parallel and flow perpendicular to the regular arrays of cylinders are all based on approximate solutions of the Navier-Stokes equations. These solutions certainly need verification by experimental evidence before confidence in them can be established.

For the parallel flow case, Sullivan's experiments (29) for flow parallel to cylindrical rods in contact give a value of $\underline{k} = 0.83$ for the square array ($\varepsilon = 0.215$), and $\underline{k} = 0.81$ for the equilateral triangular array ($\varepsilon = 0.093$). These two data points are in good agreement with Sparrow and Loeffler's theoretical treatment. However, Sullivan also performed parallel flow to bundles of fibers combed parallel to each other, including goat wool, hairs, copper wires, and glass wool, and showed that the Kozeny factor increases very mildly from 1.0 to

2.0 at very low porosities and at about $\varepsilon = 0.80$ rises sharply. Sparrow and Loeffler suggest that this discrepancy may be due to experimental problems in that the fibers are not arranged exactly as required by theory. Unfortunately, there is no other data in the literature to verify the analytical solutions for parallel flow through regular arrays of parallel cylinders.

For the perpendicular flow case, some evaluation of the theoretical treatments was made by Kirsch and Fuchs (30). They used small particles having density identical to the permeating fluid to trace out the flow pattern and velocity profile through a system of parallel cylinders in an equilateral array with the flow perpendicular to it. The flow pattern and velocity profile were measured photographically on an equatorial plane of one of the cylinders at different distances from the surface, and compared with the theoretical values calculated from the expressions for the streamline function according to Happel and Kuwabara's analysis. The experimental velocities measured at porosity 0.95 and 0.80 agreed closely with the values from Kuwabara's formulae but differed significantly from those of Happel.

In their follow-up study, Kirsch and Fuchs (31) made model filters having several parallel sheets of parallel cylinders set accurately perpendicular to the direction of flow. The cylinders were alternatingly staggered to form the equilateral triangular array. Down to porosity of 0.73, Kuwabara's expression for flow resistance was again followed closely. They also studied the perpendicular flow through the model with a square array of cylinders, down to porosity of 0.86, and showed the same results as that of the triangular array. This is in substantial agreement with the prediction of Kuwabara and Hasimoto.

A most remarkable observation was also made by Kirsch and Fuchs in similar studies on model filters. Since their concerns were over the fluid flow through real filters in which the fibers are randomly laid on the plane perpendicular to the flow, the models considered above are much too unrealistic for practical purposes. They studied "fan" models, obtained from those considered earlier by turning each layer of parallel cylinders through an arbitrary angle in its plane. Their results showed that the flow resistance predicted by Kuwabara was reduced drastically when the parallelism between the cylinders was impaired, and was almost independent of the angle of rotation (unless all the angles came back to zero again). From porosity 0.992 to 0.83, the results of the "fan" model closely agree with Ingmanson's data for random fiber mats.

Since Ingmanson's data falls between the Kozeny factors of the parallel flow, $\underline{k}_{(p)}$, and the perpendicular (transverse) flow, $\underline{k}_{(t)}$, in the cell model analysis, both Happel (11) and Meyer (32) suggested that the two directional values can be mixed for that of random mats. Meyer employed a weighting function, $\underline{W}(\varepsilon)$, in the following manner:

$$1/k = W(\varepsilon)/k_{(p)} + [1 - W(\varepsilon)]/k_{(t)} \tag{12}$$

And based on the solutions of Happel's free surface cell model, the weighting function chosen by Meyer was

$$W(\varepsilon) = 1.6\ (\varepsilon - 0.5) \tag{13}$$

The Kozeny factor curve using this approach fits the experimental data very well. This method, in essence, assumes that a real fiber mat has fibers or fiber segments oriented at various angles to the flow direction. The flow velocity and drag vectors can thus be resolved into components both parallel and

perpendicular to the fiber segment. Such an approach, however, makes it difficult to explain Kirsch and Fuchs' "fan" model filter in which layers of fibers are all perpendicular to the direction of flow.

COMPLICATING FACTORS IN STUDIES ON FLUID FLOW THROUGH FIBER BEDS

Several experimental programs have been conducted in which the mat permeability of wood fiber mats was the principal concern. For a discussion of these, the reader is referred to the reviews by Meyer (33) and Han and coworkers (34). With wood fibers, the permeability measurements have been rather complicated.

Permeability studies of man-made fibers, such as glass and nylon fibers, have been conducted with relative ease because specific volume and surface area of such fibers can be obtained directly through pycnometric and microscopic measurements. In contrast, the specific volume and specific surface area of wood fibers are ill-defined, because the shape of wood fibers is irregular, and the cell wall is porous and swells in water. Furthermore, a wood fiber has a lumen, which does not contribute to flow. Under compressive stress, the lumen collapses, the apparent cell wall density may change, the fiber shape becomes more ribbonlike, and the external surface reduces. The study of permeability of wood fiber mats has therefore been rather difficult, and requires considerable "juggling" in interpreting the obtained permeability data.

In an investigation of the water permeability of wood pulp, rayon, and cotton fibers, Robertson and Mason (35) recognized that the porosity, ε, used in permeation consideration should represent the fraction of the bed volume actually available to the flowing liquid, and should exclude the portion of

stagnant liquid in the cell wall and lumen. They, therefore expressed the bed porosity as:

$$\varepsilon = 1 - vc \tag{14}$$

where c is the mass of the fibers per unit volume of the mat and v is the effective specific volume of the fibers. Since the porosity could not be determined directly from the mat density, c, they rearranged the Kozeny-Carman equation in such a manner that a graphical treatment of permeability data taken at different bed densities would yield directly the values of effective specific volume, v, and the product of the Kozeny constant and the square of the specific surface, S_w, defined on a mass basis. The equation that they used, obtained by substituting the expression for ε given by Eq. (14) in the Kozeny-Carman equation, is

$$(Kc^2)^{1/3} = \left(\frac{1}{k\ S_w^2}\right)^{1/3} (a - vc) \tag{15}$$

where S_w, the surface area per unit mass, is equal to $v\ S_v$. A plot of $(K\ c^2)^{1/3}$ against c will be linear if the Kozeny-Carman equation applies, that is k, v, S_w are all constants, and the slope and intercept will yield respective values of $k\ S_w^2$ and v. In their work, a constant Kozeny factor of $k = 5.55$ was used, which was in accordance with the state of affairs at that time.

Deviations of the data from the linear relationship predicted by Eq. (15) were observed by Robertson and Mason (35) for porosities greater than 0.8, which they attributed to increasing values of the Kozeny constant with increasing porosity. This speculation was later shown to be the case by Ingmanson (20). Deviations in the water permeability data from the predicted linear relationship, at porosities below 0.5 were also observed for bleached sulfite wood pulp by Carroll and Mason (36) and Mason (37). They believe this deviation is due to

deformation of the fiber either by collapse of the lumen or deswelling of the fiber wall by the applied compressive load.

These same investigators (36-37) also observed a decay in permeability with continued flow of liquid through the fibrous bed. Systematic experiments by Carroll and Mason (36) showed that the decay was most serious with highly swollen or very flexible fibers and was accelerated by liquid flow. They believe the decrease in permeability was caused by a relaxation of internal stresses in the compressed mats causing a movement of fibers which would cause the Kozeny constant to increase.

Another form of Kozeny-Carman equation, used in analyzing flow through compressible porous beds, is given by Fowler and Hertel (38). They suggest that if one considers a porous bed so highly compressed that its void volume is zero, then the effective particle density and the bed density are the same and equal to W/AL_o, where L_o is the bed thickness at zero porosity and W is the mass of particles in the bed. Since the solid fraction of an actual bed is L_o/L, the porosity is given by

$$\varepsilon = 1 - L_o/L \tag{16}$$

If this value of ε is substituted in Eq. (15), the following form is obtained

$$(KL)^{1/3} = \left(\frac{1}{k\, S_v^2 L_o^2}\right)^{1/3} (L - L_o) \tag{17}$$

A plot of $(KL)^{1/3}$ against L will be linear if the Kozeny-Carman equation applies - that is, if k, S_v, and L_o are constants. The value of S_v can then be

calculated from the slope of this plot, and the effective particle density from the intercept, L_o.

A plot of Brown's (39) air permeability in the above form for beaten sulfite pulp fibers shows linearity at initial steps of reducing mat thickness, L, but becomes curved as the mat thickness is further reduced. He noted that the curvature may be interpreted in terms of a decreased L_o or increasing k or S_v under compaction. The intercept L_o value, extrapolated from the linear portion, indicates an effective fiber density of 0.72 g/cm^3, whereas the curved portion gives 1.49 g/cm^3. This latter value is very close to the density of solid cellulose. Brown believed that it is more probable that the Kozeny constant increased with decreasing mat thickness based on the tortuosity concept, because the individual fibers are flattened out under compression. Mason (37) pointed out that under the compressive pressure (up to 13,000 psi) used by Brown, it is more likely that the effective specific volume of the fiber decreases and gradually approaches the specific volume of cellulose. It is evident, therefore, that at this time the interpretation of permeability data of wood fiber mats had been complicated by the possibility that the three parameters (Kozeny factor, specific surface area, and specific volume, the latter can be converted to porosity) in the Kozeny-Carman equation are all variables. The problem is difficult since it is impossible to interpret three unknowns in one equation.

In a study of air permeability in mats of bleached sulfite pulp, Bliesner (40) employed the rearranged form of Kozeny-Carman equation proposed by Fowler and Hertel (38). By fixing the value of Kozeny factor at 5.55, he attempted to solve the two variables, i.e., specific surface area and specific volume of fibers, from one equation by graphical means. In his work, mats prepared under wet pressures of 0.1, 25, 50, 75, and 100 psi gave respective fiber densities of

1.39, 1.45, 1.50, 1.54, and 1.56 g/cm^3, and respective surface areas of 3688, 3928, 4176, 4091, and 4250 cm^2/g. The increase of fiber density with the increasing wet pressure was expected. However, the result that the mat being wet-pressed at 100 psi produced individual fibers having densities equivalent to crystalline cellulose is surprising. Furthermore, the increase in the specific surface area with increasing wet pressure is also contrary to what one would expect.

In order to explain these unexpected data, he proposed that the collapse of the hollow wood fibers into ribbonlike structure may explain his findings. Thus, he was concerned about the effect of fiber shape on the value of the Kozeny factor. Beds of synthetic fibers of three different cross-sectional shapes were examined. One set of fibers was 15-denier* nylon with a circular cross section. Another set was prepared by flattening the circular nylon fibers in a press nip and had an approximately elliptic cross section of aspect ratio** 2.91. The third set was 10-denier orlon fibers with "dog-bone" shape cross section with an aspect ratio 4.14.

Bliesner's experimental Kozeny factors as a function of porosity are shown as the solid curves in Fig. 4. They provide no obvious conclusion about the effect of fiber shape on the Kozeny factor. Bliesner reasoned that the flatter fibers should overlap more easily than circular ones, thereby excluding more surface area from the permeating fluid as a result of this interfiber contact. To account for this, he corrected for the surface area and showed a significant effect of fiber shape on the Kozeny factors, shown as the dotted curves in Fig. 4.

*Denier - g/9000 m.
**Aspect ratio - the ratio of width to thickness of fiber cross section or the ratio of major to minor axes of an elliptical cross section.

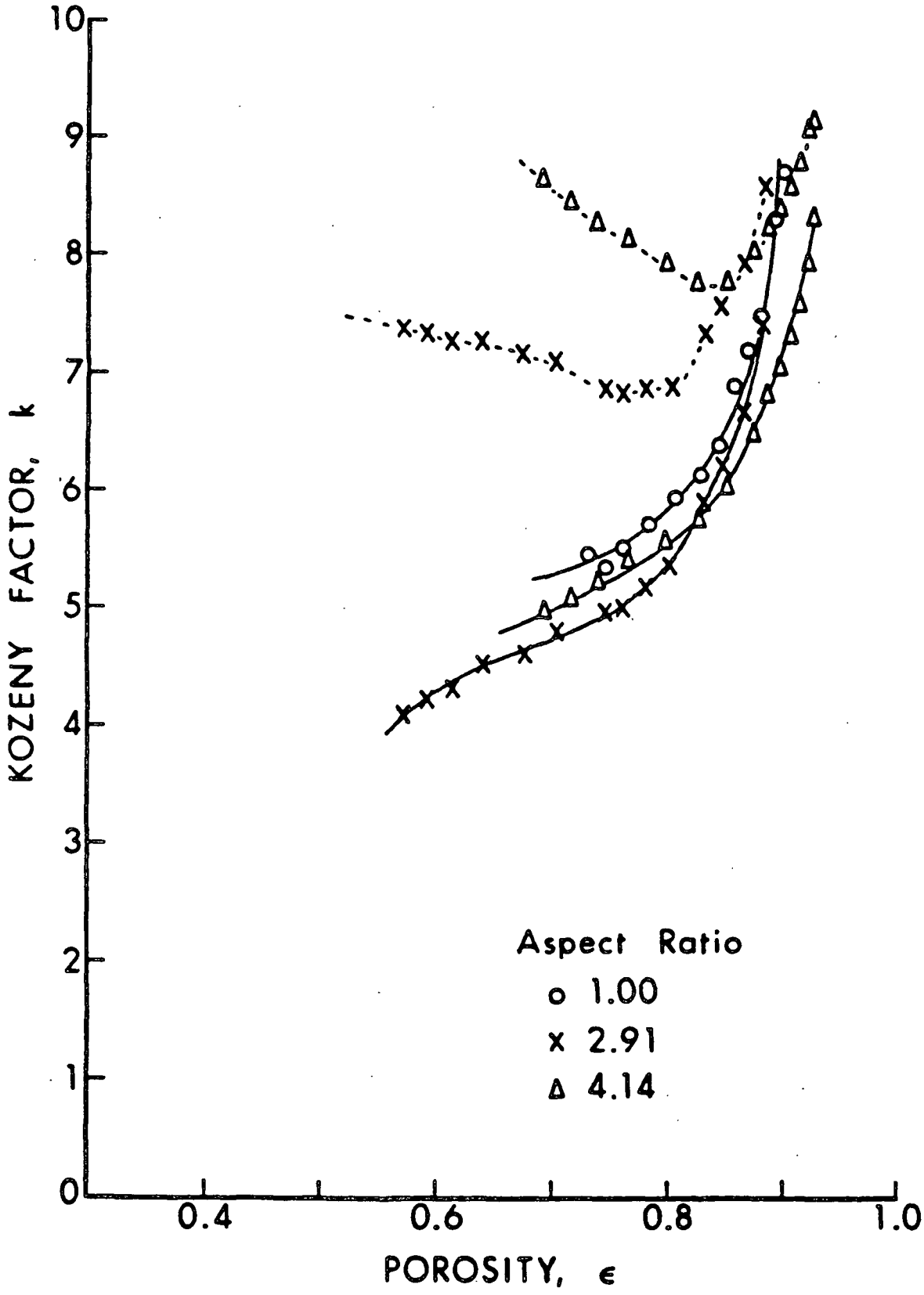

Figure 4. Bliesner's experimental and surface-area-corrected Kozeny factors.

The contact area calculations were performed by multiplying the projected area of a fiber-to-fiber intersection by the number of intersections at a given mat porosity. The number of intersections at a given mat porosity was calculated using the idealized fiber network model of Onogi-Sasaguri (41).

Because of the uncertainties in Bliesner's contact area calculations, Labrecque (42) investigated further the effect of fiber shape on mat permeability. Four experimental batches of Nylon 6 fibers with aspect ratios ranging from 1.00 to 4.69 were used. His experimental Kozeny factors as a function of porosity are shown by the solid curves in Fig. 5. These data showed no significant differences among fibers with aspect ratios of 1.00, 2.64, and 4.12, but a significant difference for those with aspect ratio 4.69. Of interest, however, is the fact that the Kozeny factor of all the fibers of various aspect ratios continued to drop and deviated significantly from Davies-Ingmanson's correlation at porosities below 0.8. The Kozeny factor would have been expected to level off to 5.0, at least for cylindrical fibers. Labrecque's data were questioned seriously (25) because of the disagreement with the previous works, and also because of fiber curling problems which prevented proper mat formation in water. His mats were ultimately prepared in ethanol.

Labrecque also attempted to correct the surface area exposed to flow by using a dye adsorption technique. Labrecque found that a dozen of commercial dyes can all penetrate into his nylon fibers and the interfiber contacts. A light-scattering technique was also attempted and did give some evidence of surface area reduction. His corrected Kozeny factor data also showed a significant effect of fiber shape, as seen from the dotted curves in Fig. 5. Clearly, Labrecque's uncorrected and corrected data are in total disagreement with those of Bliesner (40).

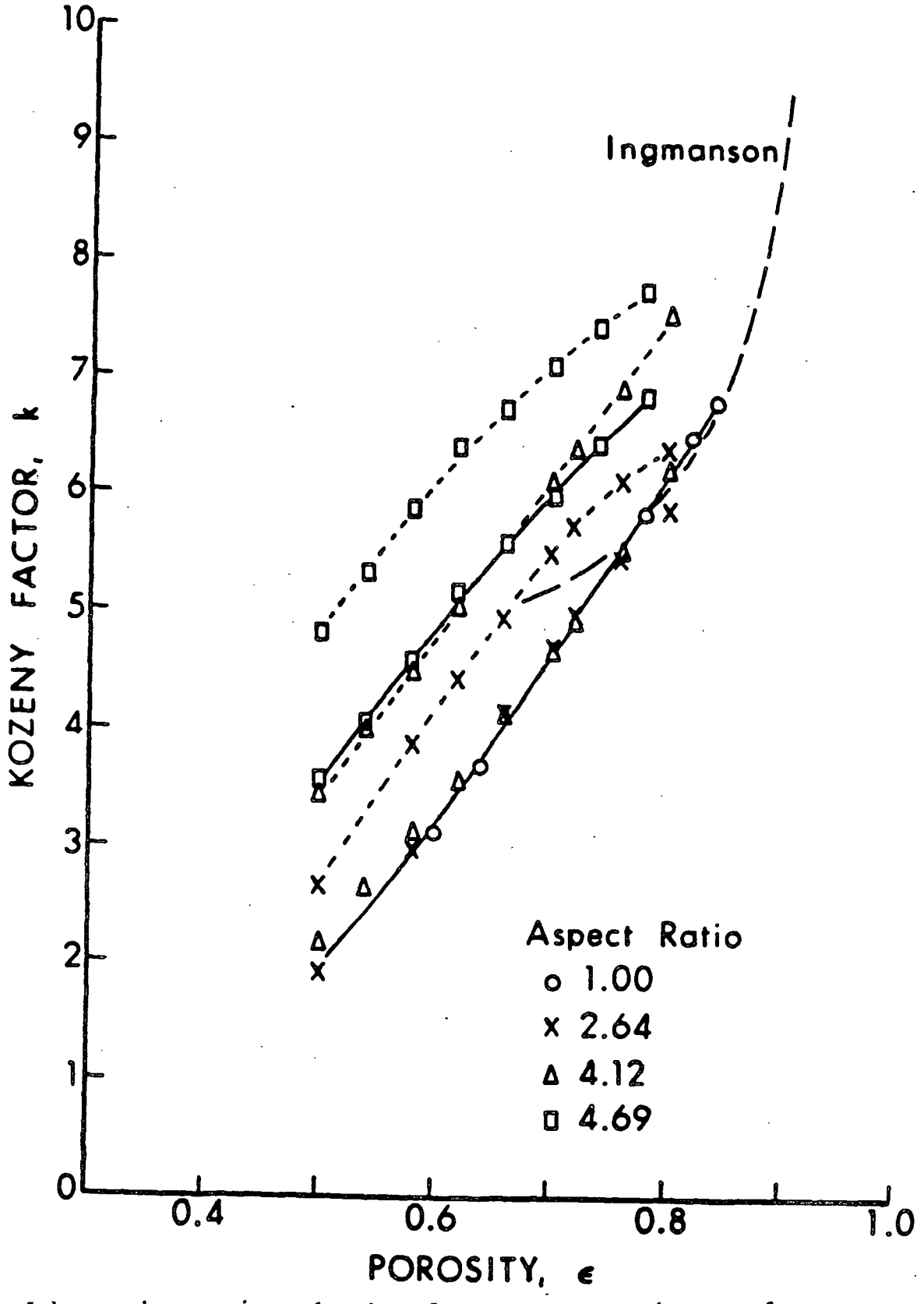

Figure 5. Labrecque's experimental and surface-area-corrected Kozeny factors.

In an attempt to clarify the effect of fiber shape on mat permeability, Brown (25) recently extended Kuwabara's (10) zero-vorticity cell model from circular to elliptical cylinders. Solutions were determined for both flow parallel to the central fiber axis and flow perpendicular to the fiber axis. For the latter, two cases were considered, flow perpendicular to the major axis and flow perpendicular to the minor axis.

Solutions for flow parallel to the central fiber axis indicated little effect of fiber shape on permeability. Solutions for flow perpendicular to the central fiber axis showed a significant effect of fiber shape both along the major and the minor cross-sectional axes. Flow along the minor axis experienced a higher flow resistance than flow along major axis, as shown in Fig. 6. The effect of fiber aspect ratio on flow resistance is relatively mild at high porosities, but becomes rather significant at the lower porosities.

These solutions still assume that the fiber assemblage is a regular array and thus are not applicable to a random mat. This means a weighing method for obtaining the composite mat Kozeny factors must be used. Unfortunately, none of the estimated composite mat Kozeny factors as a function of porosity agrees with either Bliesner's or Labrecque's results, corrected or uncorrected for surface area.

Recently, Nguyen (43) performed some water permeability experiments on cylindrical dacron fiber mats. His data, interestingly, indicated a similar trend to the long-questioned data of Labrecque. The experimental Kozeny factor at low porosities continued to decrease without leveling off at about 5.0. He attributed this deviation to the surface area reduction of the fibers by showing microscopically the increasing number and magnitude of fiber indentations with

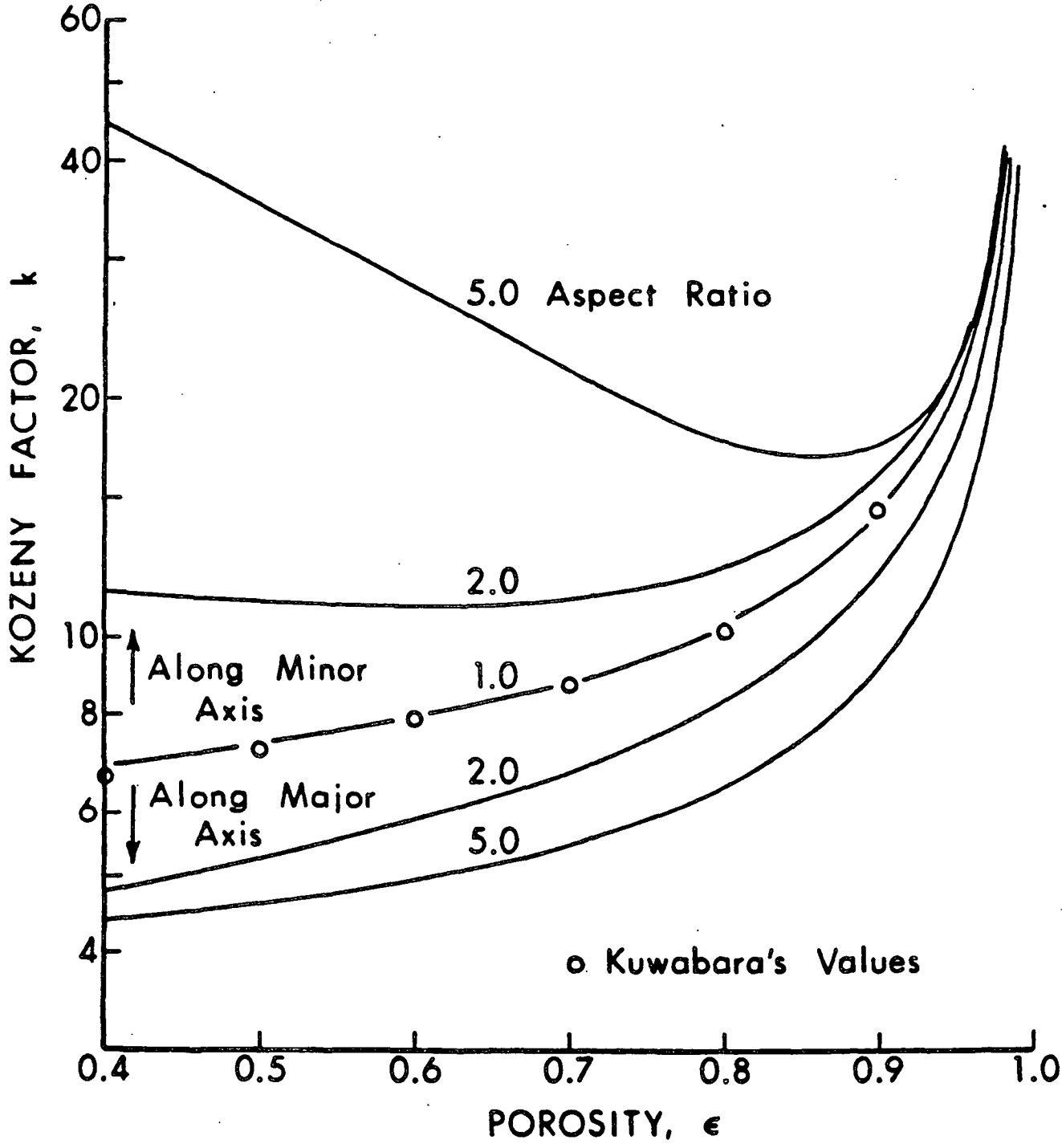

Figure 6. Brown's solutions of Kozeny factors using cell model analysis.

decreasing mat porosity. This, in essence, has challenged both Bliesner and Labrecque's results which indicated no surface area reduction for mats of cylindrical fibers at low porosities.

PRESENTATION OF THE PROBLEM

It is quite evident from the previous review that the permeability of filtration-formed fiber mats with random orientation in the X-Y plane has only been explained in the high porosity range where point contacts at the fiber intersections can be reasonably assumed.

However, when the mat is compressed to lower porosities, there is conflicting theoretical and experimental evidence on how the permeability of the mat should behave. The three experimental investigations (40,42,43) and one theoretical analysis (25) are not in agreement, as reviewed in the preceding section.

The analysis of the permeability of the compressed mats is further complicated by the suggested effects of the surface area reduction and the fiber shape change.

The objective of this thesis is to investigate the permeability of fiber mat compressed to lower porosities and to verify the suggested effects of surface area reduction and fiber geometry.

EXPERIMENTAL MATERIAL, EQUIPMENT, AND PROCEDURES

The objectives of this work were to study the permeability of fiber mats compressed to low porosities, and to verify the suggested effects due to surface area reduction and fiber geometry. To achieve these objectives, it was necessary

(1) to select, procure, and characterize fibers with the required properties,

(2) to select and characterize a technique for estimating the change of surface area of the fiber mat at various levels of compaction,

(3) to design a flow system which allowed the measurement of mat permeability and surface area change.

The experimental work carried out in this investigation may therefore be conveniently separated into three groups corresponding to these three requirements.

FIBER SELECTION AND CHARACTERIZATION

The selection of the fibers is extremely critical. It is important to choose fibers which will permit easy definition of parameters such as specific surface area, density, cross-sectional shape and size, etc., without introducing factors which would complicate the interpretation of the final results.

Experience has shown that man-made fibers, such as glass, nylon and polyester, allow definable characteristics and reproducible results. Glass fiber was not considered since it shatters under compressive loading. Conformable polyester and nylon fibers were more suitable for this work. Nylon

fibers, however, swell about 4% in water and, as Labrecque (42) found, the elliptical nylon fibers, after drawing, tend to curl into coils when wetted in water. Polyester fiber was thus chosen because it does not swell in water (44).

The polyester fibers used were obtained as experimental samples from the American Enka Corporation. By varying the shape of the spinnerets, they were able to extrude and supply continuous filament of polyester fibers with cross-sectional aspect ratios of 1.00, 1.80, and 3.18 (see Fig. 12, p. 60).

To prepare the fibers to the desired length, the continuous filaments were cut in the same way described by Arnold (45). The filaments were unwound from the bobbin and rewound onto eight rectangles of chipboard which were fastened to the faces of an octagonal wheel about 2 feet in diameter. The rewinding was completed when the skein of fiber on the chipboards was about one inch wide and 1/8-inch thick. The skein was then secured with Duco cement at each of the corners of the octagon; and, when the glue was dry, the fiber bundle and chipboard were cut from the wheel leaving the bundle secured at ech end to a chipboard strip.

The cutting was accomplished with razor blade gang cutters. These cutters consisted of a number of single-edged razor blades mounted on steel rods and spaced with washers to give the desired fiber length. A polyethylene sheet was placed over the fiber bundle. The cutter was in turn placed over the polyethylene sheet and forced through the bundle by means of a hydraulic press. The polyethylene sheet was then pulled out from the gang cutter such that the fibers embedded between blades were easily removed from the cutter.

To remove any occluded impurities which might have been introduced during fiber manufacturing and preparation, the fibers were cleaned in the sequence: 50°C water, 95% ethanol, and 50°C water for two cycles prior to any experimental work. The water was deionized, distilled and filtered through a Millipore unit (0.45 μm average pore size). The ethanol was also filtered through the same system.

The density of the polyester fibers was measured pycnometrically. The density determinations were performed in triplicate. Clean fibers were deaerated in water in a vacuum desiccator, and pycnometers were filled with air-free fiber slurry by carrying out the filling operation below the water surface. Density was calculated from the equation

$$\rho = W \rho_w/(W - y) \tag{18}$$

where ρ = density of fiber, g/cc

W = weight of fiber dried in 105° oven, g

ρ_w = density of water at the test temperature, g/cc

y = difference in weight between the slurry-filled and water-filled pycnometer, g.

The cross-sectional dimensions of these fibers were determined microscopically. Bundles of each type of fibers were embedded in butyl methacrylate and microtomed cross sections of each obtained. Photomicrographs of the cross sections and a micrometer grid were tkan at a magnification of 300X. For the convenience of the fiber dimensional determination, the film negatives were projected and enlarged to 2500X on tracing papers. The width and thickness of about 200 fibers were measured against the micrometer grid with a ruler. The aspect ratio for each fiber was calculated by dividing the width by the

thickness. The fiber perimeters were measured with the aid of a calibrated map reader and the cross-sectional area measured with a planimeter. The volumetric surface area was then calculated by dividing the fiber perimeter by its cross-sectional area.

In order to determine whether the fibers swell in water, the diameter of a circular fiber before and after being soaked in water for a week was measured under a microscope at 400X with a micrometer eyepiece. No diameter change was found. In addition, all fibers used in this study remained straight when soaked in water and did not show the curling problem found by Labrecque (42) for his nylon fibers.

The moduli of elasticity for each fiber sample was determined. Load-elongation curves for single filaments of known cross-sectional areas were measured and recorded with an Instron Tensile Tester. The slope of these curves provide the necessary data for the calculation of Young's modulus through the relationship

$$E = F\ell/A_f\ (\Delta\ell) \tag{19}$$

where E = modulus of elasticity, g/cm^2

F = load, g

A_f = fiber cross-section area, cm^2

$\Delta\ell$ = elongation, cm

ℓ = initial fiber length, cm

SELECTION AND CHARACTERIZATION OF POLYMER ADSORPTION TECHNIQUE FOR EXTERNAL SURFACE AREA MEASUREMENT

Selection of Technique

Because of the importance of the surface area in the permeability considerations, an accurate technique was required to estimate the external surface area of a mat at various states of compaction. It was believed that the most suitable method of measuring the surface area of a compressed fiber mat should use the same flow system as used for the permeability determination. In this way, the system would be in the same state of mat condition and the surface area determined would relate directly to the actual exposed area. Because of this consideration, an attempt was made to employ an adsorption technique which could be incorporated into the same aqueous system used in the permeability determination.

In general, the adsorption techniques for measuring surface area depend on bringing a second substance (or adsorbate) into contact with the surface of adsorbent to be measured. The number of adsorbed molecules of the adsorbate multiplied by its "effective" planar molecular dimension gives the exposed surface area of the adsorbent. The value of surface area so measured, varies depending upon the specific adsorbate-solvent-adsorbent being used (55). Some solvent swells and opens up the internal structure of the adsorbent, and if the size of the adsorbate molecules is small enough to reach the internal surfaces of the adsorbent, the surface area measured will be the total surface area (external and internal). Labrecque (42) attempted to use dye adsorption methods for the measurement of external surface area of fibers, but was not successful because his nylon fiber swelled in water and the dye molecules were so small that penetration into the fibers occurred.

As noted earlier, the polyester fiber used in this work does not swell in water, but is difficult to dye due to the close packing of the polymer chains in its bulk (44). To overcome these difficulties it has been found (44) necessary to (1) select small and reactive dye molecules, (2) evaluate the solution temperature, usually above 100°C, and (3) use a swelling agent. Without high temperatures or a swelling agent, even the smallest and most reactive dyestuff will be adsorbed only on the external surfaces of the fibers and rubbing fastness will be very poor. In view of these difficulties for dye molecules to penetrate, the dye adsorption technique appears to be a feasible technique for measuring the external surface area of polyester fibers in an aqueous system.

However, it has been shown (46) that the surface structure of synthetic fibers can be heterogeneous and porous. Small dye molecules may detect a larger surface area than the geometrically measured one. A polymer adsorption technique was therefore preferred, since the polymer size can be chosen large enough to prevent penetration, to ignore minute surface heterogeneities, and to adsorb only on the very external surfaces of the fibers.

Because the geometric surface area of fibers as measured microscopically is used in the permeability consideration, the specific polymer adsorption (mg of polymer adsorbed/m^2 surface area) will also be based on the geometric area and will be determined in a fiber slurry in which all the fiber surfaces are exposed. The reduction of specific polymer adsorption measured at various levels of mat compaction can then be used as the indication of the reduction of available surface area.

Selection, Description, and Source of Polyethylenimine (PEI)

Polyethylenimine (PEI) was selected for development of the polymer adsorption technique. This would allow estimates of the change of surface area of polyester fiber mat under compression. This polymer has been well characterized in three dissertations (47,48,49) at The Institute of Paper Chemistry. Its adsorption characteristics on porous cellulose fibers were studied by Kindler (47), on porous silica gel by Hostetler (48), and on nonporous silica by Lindquist (49). These works thus provide excellent background for this work.

PEI is produced by an acid-catalyzed polymerization of aziridine and contains primary, secondary, and tertiary amino groups in the ratio of 1:2:1 (50). This ratio results in a structure of monomer units, $-CH_2-CH_2-NH-$, which is highly branched with branch points at every 3 to 3.5 monomer units (50). The three-dimensional branched network implies a spherically shaped macromolecule in solution (48,51), with tertiary amines being the branch sites and primary amino nitrogens being the terminal groups.

The point of zero cationic charge on PEI occurs at pH 10.8-10.9. At pH less than 10.8, the amine groups can accept a proton and become positively charged. However, the amine groups become protonated in a successive manner as the pH is lowered because of the reduced basicity of specific amine groups as adjacent amine groups become protonated. Therefore, the extent of cationic charge on the polymer is dependent on the pH of the solution. If the source of hydrogen ions is from water, the pH is shifted to the alkaline side.

The electrokinetic properties of charged PEI molecules change moderately from acidic conditions up to pH around 8.0, then sharply beyond pH 8.0 until reaching its isoelectric point of pH 10.8. The mobility data by Hostetler (48)

and Lindquist (49) showed that the effective charge-to-size ratio of PEI decreases slightly from low pH up to 8.0, and then drastically from pH 8.0 to 10.8. The data of Allan (52) and Lindquist (49) showed that the viscosity of PEI solutions drop sharply also from pH 8.0 to 10.8.

Corresponding to its electrokinetic properties in aqueous solution, the adsorption of PEI on adsorbents is highly dependent on pH. Kindler (47), Hostetler (48), Lindquist (49), and Allan (52) have all shown that the adsorption of PEI increases moderately from acidic conditions up to pH around 8.0, then sharply toward its isoelectric point of pH 10.8. Though the trend of pH dependency is similar, the magnitude of adsorption varies depending upon the nature of the adsorbent being used.

The PEI samples used in this study were obtained from the Dow Chemical Company. Eight samples designated as PEI-3, PEI-6, PEI-12, PEI-18, PEI-200, PEI-400, PEI-600, and PEI-1000 were obtained. The number average molecular weights of these samples were 300, 600, 1200, 1800, 25,000, 35,000, 50,000 and 75,000, respectively. The samples were clear, having no discoloration or visible debris. These polymers were used in the following studies without further fractionation.

Polyester Fiber - PEI Adsorption Experiments

Preliminary experiments were done so that the adsorption process could be characterized and the optimum adsorption condition could be chosen for later studies. This was accomplished by examining the effects of pH, time, concentration, and molecular weight. A polyester fiber suspension was used in the PEI adsorption studies.

The adsorption experiments were conducted according to the following basic procedure.

Ten grams of clean polyester fibers were suspended in 200 mL of water, dispersed by constant stirring, and adjusted to the desired pH with 0.5N HCl and 1N NaOH. A known quantity of polymer solution of known molecular weight was added to the slurry drop by drop in a time interval of 1-2 minutes. The pH was constantly adjusted and maintained at the desired value during the polymer addition. After a desired contact time (counting from the completion of polymer addition), 5 mL of solution was removed from the slurry for the quantitative analysis of the concentration of PEI in solution. The quantity of PEI adsorbed by the fibers was calculated from the change in the solution phase concentration. The quantitative analysis of the PEI solution concentration was performed by means of a colorimetric technique to be described in the next section.

The effect of pH was determined by running adsorption experiments with batches of fiber suspensions at various pH's. A one mL solution containing three milligrams of PEI-1000 was added to the slurry. The adsorption was allowed to have 30 minutes contact time.

The effect of contact time was studied at pH = 10.2 with 3 mg of PEI-1000 added. To determine the effect of concentration and molecular weight, the condition of pH = 10.2 and 30 minutes contact time was chosen. The basic adsorption procedure was followed. All experiments were carried out at room temperature.

To determine whether PEI can be desorbed from polyester fibers, an adsorption experiment was conducted, using 3 mg of PEI-1000 with pH = 10.2 and 30

minutes contact time. The slurry was then subsequently eluted and soaked in pure water (1) at pH 10.2 for 3 hours, (2) at pH 12.0 overnight, and (3) at pH 2.0 overnight. The first step of this procedure was to examine the possible reversibility due to the lowering of the PEI solution concentration, whereas the second and third looked at the effect of extreme pH's at which adsorption of PEI on polyester fibers was found to not take place. The fibers treated with this procedure were then subjected to the preceding adsorption experiment again. The reversibility was determined by the percent reestablishment of the original PEI adsorptivity.

As will be shown in the Results and Discussion section, PEI exhibits an irreversibility using the preceding procedure. Another procedure (76) using sodium hypochlorite for dispersing paper broke with PEI as a wet strength resin was found to reestablish the PEI adsorptivity on polyester fibers. The procedure involves (1) treating the fibers with 0.65% NaOCl at pH 10.0 for 10 minutes, then displacing by distilled water, (2) treating the fibers with NaOH solution at pH 12.5 for 3 minutes and then with an ample amount of water. This procedure was subsequently used to reestablish the PEI adsorptivity of a compressed polyester mat.

Quantitative Analysis of PEI Solutions

The concentration of PEI in solution was determined colorimetrically by measuring the color intensity of a complex of PEI with cupric ion, in the presence of hydrochloric acid and acetate ion. The reaction was discovered by Perrine and Landis (53), developed for PEI analysis by Kindler (47), and used recently by Hostetler (48), and Lindquist (49).

The experimental technique which measures the PEI concentration, up to 60 mg/L, may be described as follows. Five milliliters (mL) of the unknown PEI solution are mixed with 1 mL of a color reagent consisting of 0.01M cupric acetate and 0.01M hydrochloric acid. The absorbance of the mixed solution is measured at 269 nm wavelength of UV light with a Beckman Model DU spectrophotometer zeroed with a blank consiting of 1 mL of color reagent in 5 mL of distilled water. The concentration is determined by comparing the absorbance with a standard curve.

A typical calibration of standard curve is shown in Fig. 7. The concentration of PEI in the standard solutions is obtained by determining the organic nitrogen content by a Hengar technique (56) and calculating the PEI content based on a theoretical nitrogen content of 32.53%. The standard curve obeys Beer's Law,

$$\text{PEI Concn. } (mg/\ell) = (45.51)(\text{absorbance})(V_t/V_s) \qquad (20)$$

where V_t = total volume (sample + reagent)

V_s = sample volume

The complex formation between PEI and the cupric ion is pH sensitive. The copper reagent is buffered with sufficient HCl such that the pH of the solution after addition of the PEI solution is about 5.3. If the pH of the PEI solution is such that the buffering capacity is exceeded upon addition to the color reagent, then less PEI-copper chelate formation occurs for PEI solutions at low pH or increased formation of pale blue gelatinous cupric hydroxide at high pH. The former results in less solution absorbance while the latter yields high absorbance values. The range of PEI solution pH which does not exceed the

buffering capacity is about 5-9. For cases when the pH of the PEI solution was beyond the pH buffering range, a drop of 1N HCl or 1N NaOH is added to the test solution before the copper reagent is added. In these cases, a 10 mL sample is usually procured so as to reduce the dilution error introduced through addition of acid or base.

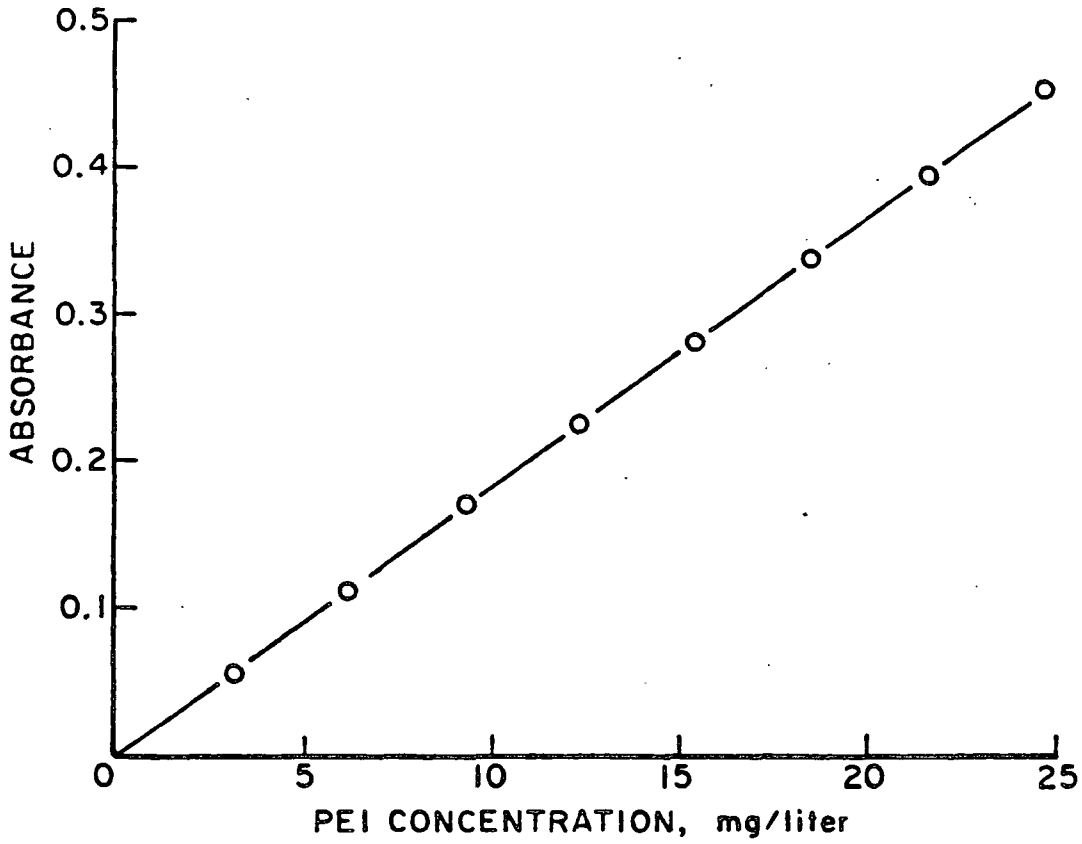

Figure 7. Colorimetric analysis of PEI: standard curve.

STUDIES OF PERMEABILITY AND POLYMER ADSORPTION OF COMPRESSED MATS

As was mentioned previously, it was desirable to study the permeability and the surface area of the compressed fiber mat with the same flow system. This way the system would have the same mat conditions and the two quantities measured would relate directly to each other. A flow system was therefore

designed with this consideration in mind. For the convenience of discussion, the structure of the permeating cell and the procedure for preparing a fiber mat in the cell will be described before discussing the flow system and procedures for studying the permeability and polymer adsorption of a compressed mat.

Description of Permeating Cell

The permeating cell designed in this study was made of 316 stainless steel, chosen for its rigidity and chemical inertness. As shown in Fig. 8, it consists of a central cylinder having its inner surface honed, two movable perforated pistons fitted at each end of the central cylinder, and two caps set on the top of each piston. Neoprene "O" rings are used throughout for sealing. Six studs are located on each end of the central cylinder. The caps, along with the pistons, could be tightened down from either end to compress the fiber mat, sandwiched between the two pistons, to the desired thickness.

The mat thickness was determined by the gap clearances between the cylinders and the two caps. For accurate control, shims of accurate thicknesses were inserted into these two gaps.

The permeable pistons, shown in Fig. 9, were drilled with 1/8-inch holes arranged in a concentric pattern. Three layers of stainless steel wire screen (35 mesh backing wire, 60 mesh central wire, and 100 mesh face wire) were soldered onto each. The 35 mesh wire minimized deflection of wire into the holes under the compressive force.

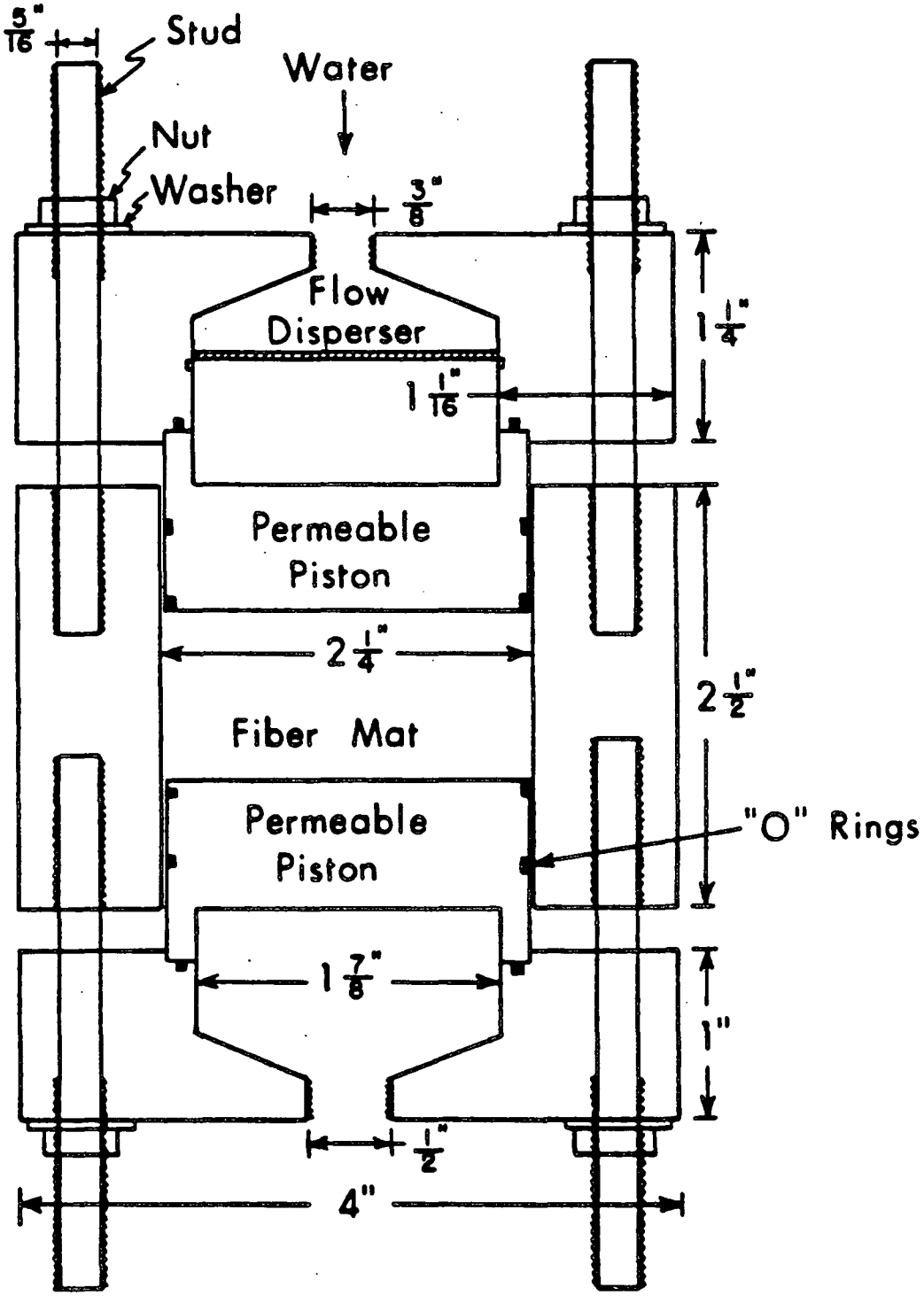

Figure 8. Assembly of permeating cell.

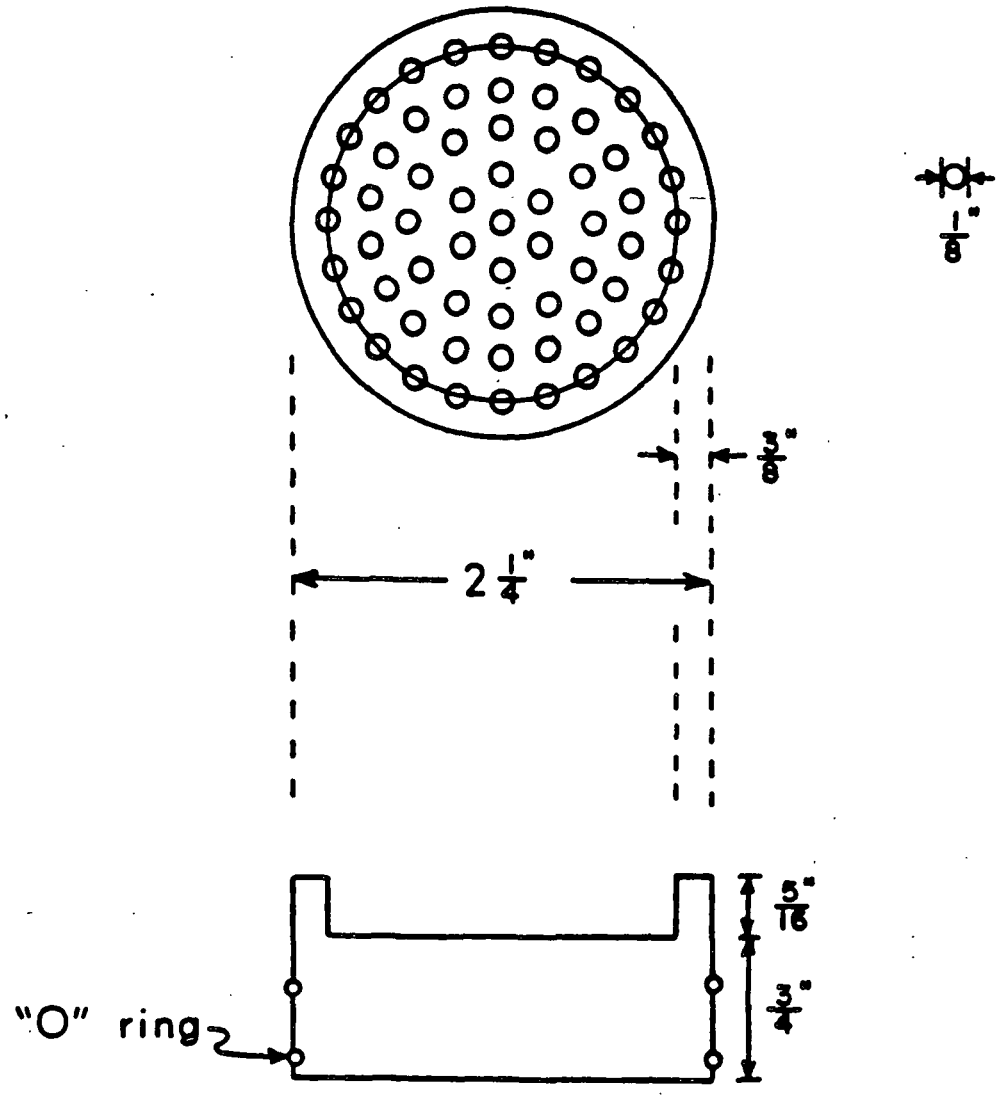

Figure 9. Construction of permeable piston.

Fiber Mat Preparation

A schematic diagram of the mat-forming assembly is shown in Fig. 10. The cylinder of the permeating cell (E) was clamped on a table (D) and had its bottom piston and cap fixed in its lowest possible position in order to provide the maximum mat forming space. The upper piston and cap were replaced by a 2-section lucite forming tube (C) having the same inside diameter. The lower forming tube was 8 inches long, whereas the upper one was 13 inches and contained a flow

stabilizer (54) to steady out the flow pattern during the mat formation. The forming tube was connected to a slurry tank above it.

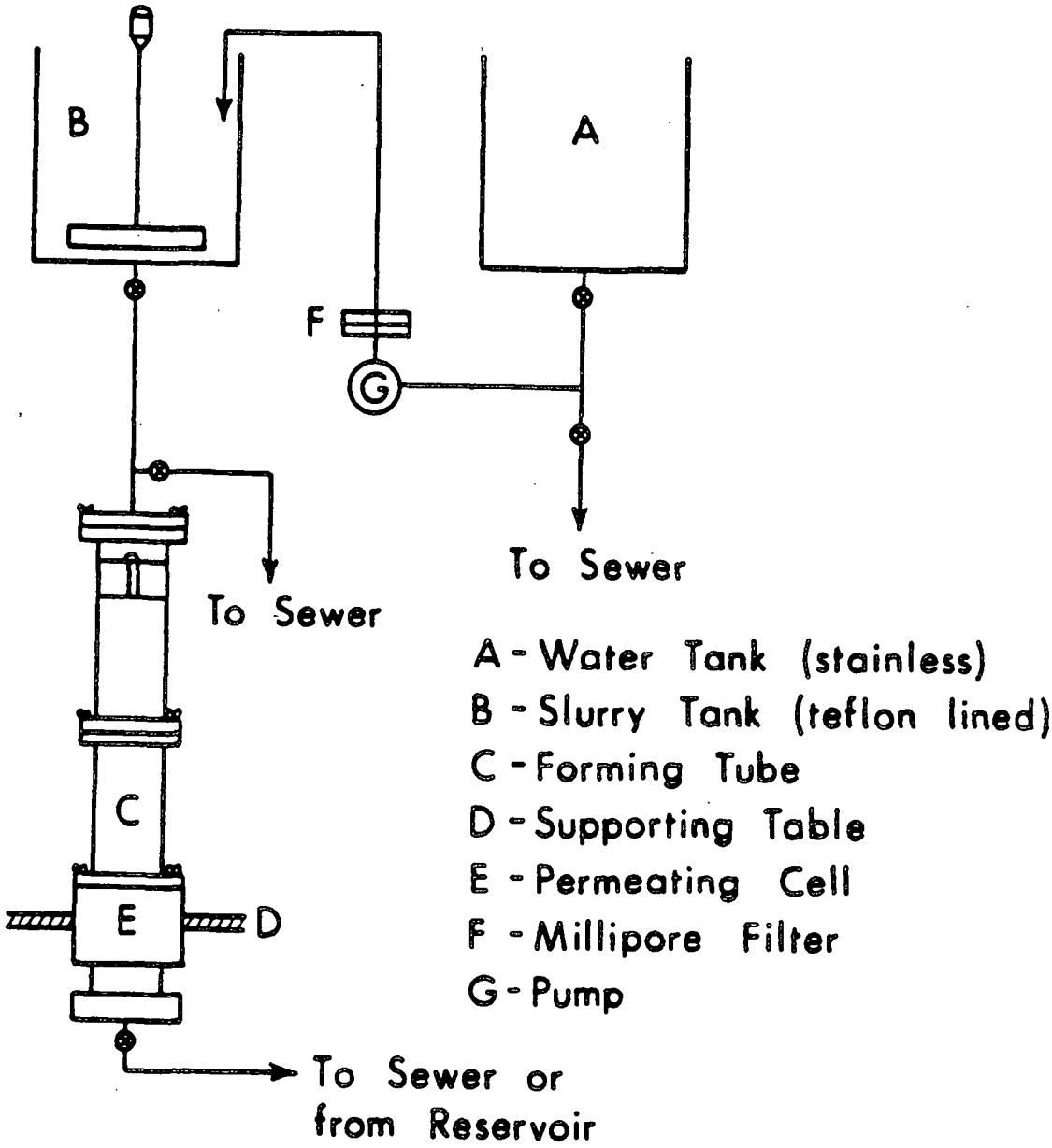

Figure 10. Schematic diagram of the mat-forming assembly.

When a mat was to be formed, freshly prepared distilled water was pumped from a large stainless steel tank (A) through a Millipore filter (F) to a 30-gallon, Teflon linked mixing tank (B). The forming tube and permeating cell assembly was then filled by flowing water from a water reservoir, upward through the bottom permeable piston such that any entrapped air below the piston could be forced out. After the forming tube was completely filled by the upward flow, the two valves between forming tube and mixing tank were operated such that the whole system was completely filled with water.

Fiber suspensions were prepared as follows. Dry and clean fibers were first introduced into warm water in a 4 liter suction flask which was gradually evacuated to a gently boiling condition for the purpose of deaeration. This deaerated slurry was next transferred into the slurry tank (B), taking care to avoid disturbances to the free surface which might cause entrainment of air bubbles on the fiber surfaces. The dilute fiber suspension in the tank was mildly agitated by a puddle stirrer to break up any fiber bundles and to maintain a state of uniform dispersion. The consistency of the suspension was kept about 0.01%.

The valve below the permeating cell was then opened and the fiber suspension was fed by gravity into the forming tube at a rate of 3 cm/sec. This flow rate is in the laminar flow region which is desirable in order to prevent continued disturbance of the fibers at the slurry-mat interface. The mat so formed has been demonstrated (54) to be highly reproducible with the fibers randomly oriented in the x-y plane normal to the direction of flow, but with little orientation in the z-direction parallel to flow.

After a sufficiently thick mat had been formed, the valve below the slurry tank was closed. The valve adjacent to the top of the forming tube was then opened to allow air to enter the tube. The water level in the tube was lowered slowly until it reached the bottom of the upper forming tube. The upper forming tube was then removed, and the upper permeable piston guided by a stainless steel rod was lowered through the forming tube to evenly push the mat into the permeating cell. The guiding rod was then removed, the lower forming tube was dismounted, and the upper cap was finally placed on the top of the upper piston to complete the mat preparation process.

Permeability and Adsorption Measurements

Figure 11 shows the flow diagram used for the measurements of permeability and polymer adsorption of a compressed fiber mat. The permeating cell containing a prepared mat is shown as (D). The flow was driven by a variable speed positive-displacement tubing pump (E), and went counterclockwise from the closed vessel (A), through the permeating cell (D), rotameter (C) to the open vessel (B) which was set parallel to the closed vessel (A). At a given flow rate, the water level in vessel (A) and (B) was balanced by introducing air from valve (F), such that the pressure drop from vessel (A) to (B) was indicated by the water manometer (G) which had one leg connected to the vessel (A) and the other leg to the open atmosphere. The flow rate was read from the calibrated rotameter (C). The water temperature needed for determining the viscosity was read from a thermometer set in the open vessel (B).

The vessels (A) and (B) were two 80 mL sections cut from a 200 mL graduated cylinder and were clamped between two parallel stainless steel plates which had holes drilled for air or water inlets and outlets as indicated in the diagram.

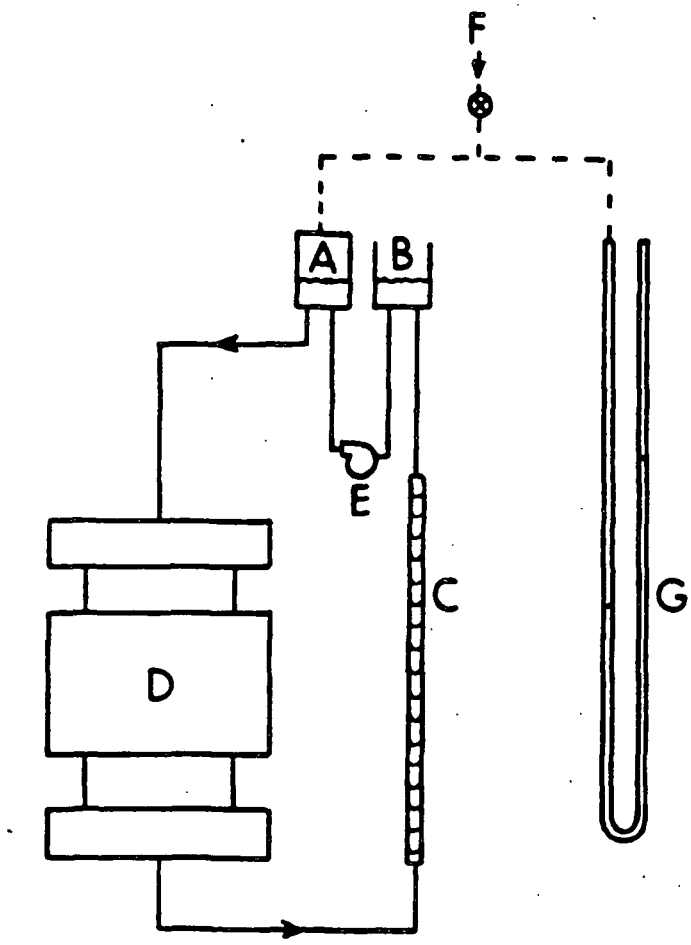

A - Closed Vessel
B - Open Vessel
C - Rotameter
D - Permeating Cell
E - Pump
F - Air Inlet
G - Water Manometer

Figure 11. Schematic flow diagram for the measurements of mat permeability and polymer adsorption.

Without the presence of the fiber mat, this closed flow system contained 321 mL of water filled to a control mark on vessel (A) and (B). With the presence of fibers (usually 20-30 g) in the permeating cell, the volume of water in the system filled to the control mark was 321 mL minus that displaced by the fibers.

In order to obtain the Darcy permeability of the mat at a given thickness, a series of flow rates and their respective pressure drops across the mat was obtained. This is needed in order to ensure the direct proportionality between flow rate and pressure drop indicated in Darcy's Law. The mat thickness was then reduced to another desired value by tightening down either one of the pistons, and another series of flow rates and the respective pressure drops were determined. This process was repeated until the desired rang eof mat thicknesses had been covered. In all cases, the mat thickness was approached from a high to low value. The flow rates were approached from the low to the high.

In order to account for the potion of the pressure drop across the mat that was due to the apparatus, pressure drops across the apparatus at various flow rates were determined in the absence of a fiber mat. The results are given in Appendix I, and were always taken into account in the mat permeability calculations.

It should be noted that the maximum flow rate was adjusted so that the pressure drop resulting at that flow rate was always less than 1% of the mechanical load required to compress that mat to the thickness at which the data were obtained. This was necessary for high porosity mats in order to ensure that no significant porosity gradient, from top face of the mat to the bottom, was established. For mats compressed to the low porosity range, this precaution was not necessary.

After the permeability measurements had been completed, the fiber mat was removed from the cell, dried at 105°C to a constant weight, and weighed to 10^{-4} g accuracy on an analytical balance. The mat weight, W, was used to calculate the mat porosity, ε, at each mat thickness, L, according to:

$$\varepsilon = 1 - \frac{W}{\rho A L} \tag{21}$$

where ρ is the fiber density and A is the cross-sectional area of the mat.

With the permeability relationships established for each type of mat, a subsequent study was carried out in which the permeability experiment was again performed as a duplicate run and then followed by the adsorption measurement at each given mat thickness.

The experimental procedure of these measurements can be described as follows. The permeability measurements were done in the same manner as described earlier. When the permeability run had been completed, the flow rate was reduced to 100 mL/min across the mat area of 26.65 cm^2 such that the recycling rate of 1 cycle per 3 minutes was set for the system. While the water was circulating, the electrodes of the pH meter were lowered into vessel (B) and the pH of the system was adjusted to the desired level which usually took 5-6 minutes to reach equilibrium. A known quantity of PEI of given molecular weight was added gradually to the system over a time interval of 3 minutes corresponding to the recycling rate. The pH was maintained at the desired value during the addition of PEI and also throughout the desired contact time. The adsorption equilibrium was usually completed after 15 minutes. Five milliliters of solution was then removed from vessel (B) for colorimetric analysis after 30 minutes of contact time and another five milliliters after 45 minutes to ensure a state of equilibrium.

Upon completion of the adsorption measurement, the PEI solution was eluted out of the system using distilled water. The elution was done by connecting a supply line to the flow inlet inside vessel (B) to the pump line, and by connecting a discharge line to the flow outlet inside vessel (B) from a rotameter line. The elution was completed when the pH of the discharge reached the pH of distilled water (about pH 6.7). Subsequent displacement of other solutions was done in the same manner. The system was displaced with 0.65% NaOCl at pH 10.0 for 10 minutes, followed by distilled water, then by NaOH solution at pH 12.5 for 3 minutes, and finally by an ample amount of water.

The mat was then compressed to another thickness. The permeability and adsorption measurements were done in the same manner and were then followed by the elution procedures. This was repeated until the desired range of porosity was covered.

It has to be noted that the water used in all phases of this thesis work was deionized, distilled, and filtered. The conductivity of this water was less than 2.0×10^{-6} mho/cm. The Millipore filters having 0.45 μm average pore size were also used to filter all other solutions that needed to come in contact with the fibers or fiber mats.

Fiber Mat Compressibility Measurements

Fiber mat compressibility is an important physical property. Its measurement is a routine procedure in which a mat is compacted with known pressure and the mat density is determined. In this work, compressibility data for mats of three types of fibers were obtained in a hope that some qualitative interpretation of mat behaviors may be made.

The compressibility measurements were carried out in two stages in order to cover a wide range of porosities. Up to 500 g/cm^2, the experiments were performed using a procedure similar to Ingmanson's (78) and can be described as follows. After the mat was formed and with the upper section of the forming tube removed, the upper piston, (with "O" ring removed) guided by a piston rod which was in turn guided by a central hole in the cover of the lower section of forming tube, was placed on the top of the mat. The weight of piston and rod minus the piston buoyance force constituted the first applied load. Subsequent loads were then applied by a series of brass weights placed on the lock-nut weight support located at the upper portion of the piston rod. Time interval between loading was 3 minutes. Mat thickness at each load was measured with the aid of a cathetometer.

From 500 g/cm^2 up to 10^5 g/cm^2, the wet mat in the permeating cell was subjected to a force applied by a Baldwin-Southwark Universal Tester, using a compression rate of 0.0125 inch per minute.

PRESENTATION OF DATA AND DISCUSSION OF RESULTS

The experimental data obtained in this investigation are presented in the same order given in the experimental program section. They are (1) fiber characterization, (2) the study of polymer-fiber interaction, and (3) the study of permeability and polymer adsorption of compressed mats. A discussion section is added which brings to light the implication of the results obtained in this study.

FIBER CHARACTERIZATION

Figure 12 shows the photomicrographs of the microtomed cross sections of the three sets of fibers, imbedded in butyl methacrylate, at a magnification of 300X. These fibers are characterized by their different cross-sectional shape which is a variable to be examined in the permeability determinations. The fiber properties pertaining to the permeability and adsorption determinations are summarized in Table 1.

Table 1. Summary of fiber properties.

Fiber identification	310A	313B	315D
Fiber length, μm	2770	2770	2770
Fiber width, μm	13.8	14.8	20.1
Fiber thickness, μm	13.8	8.23	6.31
Aspect ratio	1.00	1.80	3.18
Fiber perimeter, μm	43.3	38.9	43.8
Fiber cross-sectional area, μm^2	148.9	104.9	108.7
Fiber density, g/cc	1.41	1.39	1.39
Denier, g/9000 m	1.86	1.31	1.36
Draw ratio	2.48	2.50	2.44
Specific surface area, cm^2/cc	2905	3703	4031
Modulus of elasticity, $g/cm^2 \times 10^{-7}$	6.75	6.62	6.55

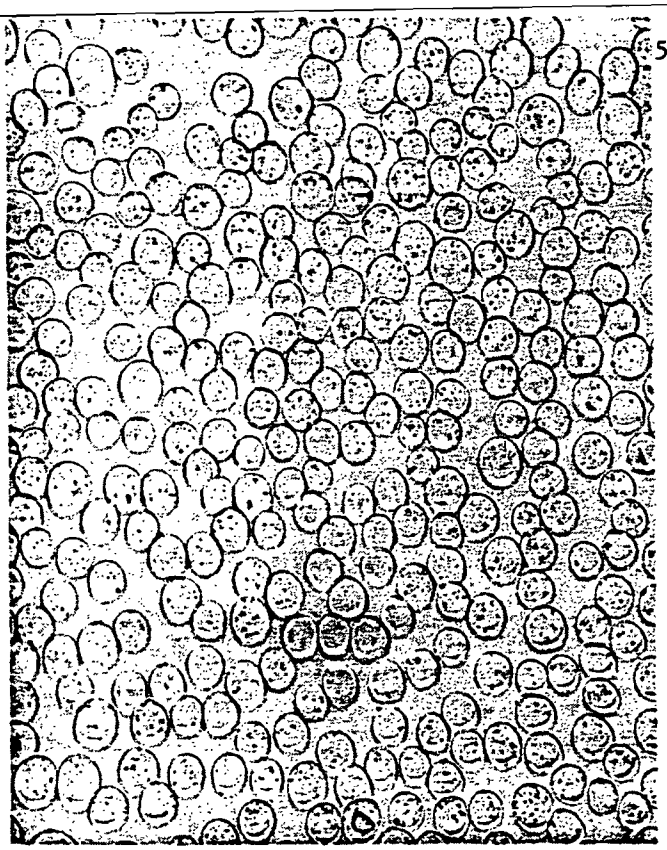

Aspect Ratio = 1.00

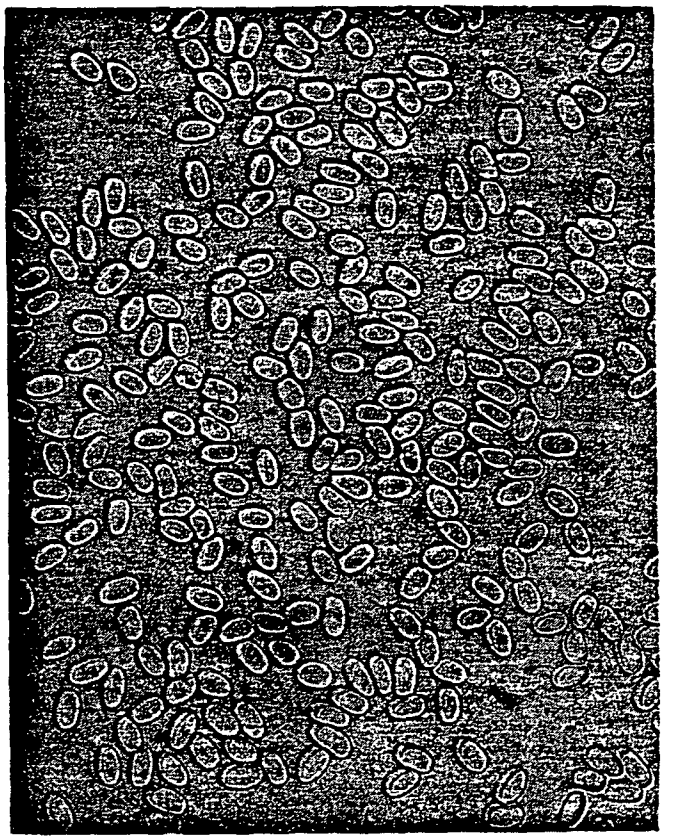

Aspect Ratio = 1.80

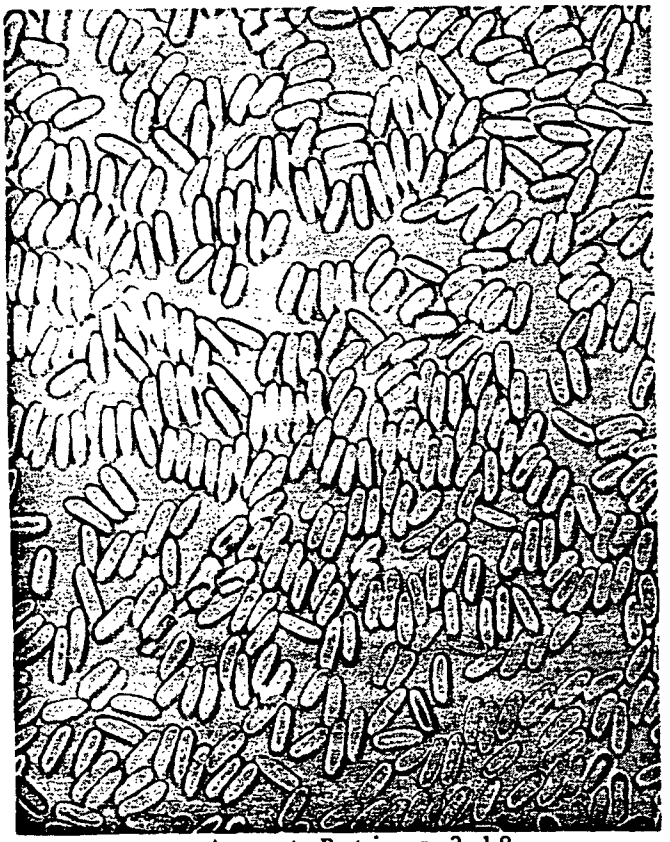

Aspect Ratio = 3.18

Figure 12. Cross-sectional shapes of fibers used in this study (magnification 300X).

CHARACTERIZATION OF POLYMER ADSORPTION

General Aspects of Polymer Adsorption

Polymer adsorption is a broad subject. Nearly each specific adsorbent-solvent-adsorbate system has its specific beavhior of adsorption (57-59). There are, however, some generalities for most systems. These are to be briefly mentioned to bring to light important aspects considered in the present adsorption system.

It has been found that most polymer adsorption data fit the simple Langmuir equation within experimental error (55). The amount of polymer adsorbed at equilibrium is usually only slightly dependent on temperature, but is very sensitive to solvent power; less polymer is adsorbed out of a good solvent than a poor one. In systems involving polyelectrolytes, adsorption is highly dependent on pH. The nature of this dependence is, of course, contingent upon the adsorbate and adsorbent being used.

Studies (60-63) on the kinetics of polymer adsorption often show a fairly rapid initial rise in adsorption with time followed by a slow asymptotic approach to equilibrium. Most systems reach equilibrium after several hours but in some cases the time required is as short as 10-15 minutes.

Only a fraction of the segments of the adsorbed chain are in direct contact with the surface, either physically or chemically. The remaining sequences of segments are looped into the solution phase. The configuration of the adsorbed polymer is difficult to determine experimentally. Recent work indicates that the configuration is closely related to the configuration of the polymer in solution (64,65).

Once adsorbed, most systems exhibit an apparent irreversibility with respect to solution concentration. Even washing with pure solvent will often remove only a small fraction of adsorbed polymer. In a generalized picture of the adsorption of a polymer molecule, multiple points of segmental attachment to the adsorbent surface and looping of chain segments into solution between attachments are though to occur (58,66-68). Desorption of the entire molecular chain is though to happen only when all bonds are broken simultaneously which is statistically improbable.

It has been found (60-63) that the rate of adsorption increases as the molecular weight decreases. The effect of molecular weight is generally interpreted in terms of a diffusion controlled adsorption process. The slowly diffusing high molecular weight species require more time to arrive at the adsorption site than do the smaller, more mobile molecules. For a polymer solution containing both high and low molecular weight molecules, the smaller molecules are adsorbed more quickly and in greater number than are the larger molecules. Later they are displaced by larger molecules whose adsorption is thermodynamically favored. This phenomenon was demonstrated by Emery (69) and Farrer (70) and is termed "molecular reshuffling."

Diffusion-controlled adsorption is a characteristic of porous substrates. Larger molecules can be excluded from the smaller pores accessible to the smaller molecules (71,47,48) such that decreasing the molecular weight increases the amount of adsorption.

With this general behavior of polymer adsorption in mind, initial adsorption experiments were designed to characterize the adsorption of PEI on polyester fibers. The results of these experiments were then used as the basis for

determining whether the system was suitable for the purpose of this work and, if suitable, the proper conditions to be used. Since the main reason for using the polymer adsorption technique in this study was to ensure that adsorption take place only on the external surface, the highest molecular weight PEI-1000 was preferred at the very outset of this study and its adsorption was thus more fully characterized.

Adsorption Characteristics of PEI-Polyester Fiber System

Effect of pH

In systems involving polyelectrolytes, adsorption is highly dependent on pH. The effect of pH on the amount of PEI adsorbed on polyester fibers was therefore investigated first. PEI-1000 (number average molecular weight 75,000) was used as the adsorbate and the cylindrical fibers as the adsorbent. Ten grams of cylindrical fibers were dispersed in 200 mL of solution yielding 2.057 m^2 of available surface for adsorption. Three milligrams of PEI-1000 was added to each slurry at a given pH. Thirty minutes contact time was allowed.

The upper curve in Fig. 13 shows the amount of PEI-1000 adsorbed per meter squared of fiber surface over the pH range 3.0 to 11.5. The experimental data are given in Appendix II. Adsorption starts at pH 3.5, increases gradually until a pH about 9, then more rapidly to a maximum at pH 10.2, and from there drops sharply to zero at pH 10.8. This overall trend agrees very well with most of the PEI adsorption studies using other types of adsorbent (47-49,52).

The increase of PEI adsorption on polyester fibers from pH 3.5 to 9.0 may be attributed to the increasing ionization of the surface carboxyl groups of polyester fibers. It has been stressed by Wilfinger (72) that the carboxyl groups on the cellulose surface are responsible for adsorbing PEI. Trout (73) also

reported a linear correlation between the amount of PEI adsorbed and the carboxyl content of a pulp. The polyester fiber is made from polyethylene terephthalate which contains terminal carboxyl groups. It was shown by Clapp (74), using a potentiometric titration technique, that the dissociation of the carboxyl groups of polyester fibers starts at pH 3.5, increases almost linearly with the increasing pH, and reaches completion at pH 9.0. The PEI adsorption data in Fig. 13 appear to agree with this trend, suggesting that the adsorption is attributable to the electrostatic interaction between the cationic PEI and the anionic carboxyl groups on fiber surfaces.

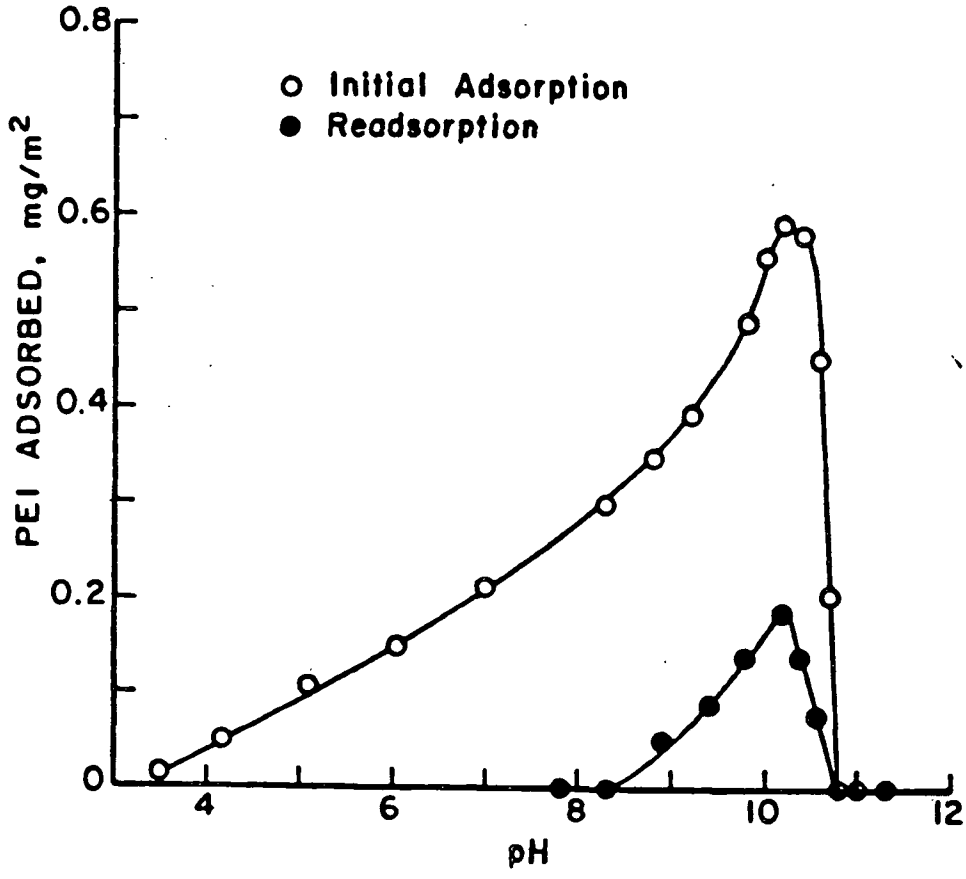

Figure 13. Adsorption of PEI on polyester fibers as a function of pH.

The sharper increase of PEI adsorption on polyester fibers above pH 9 is attributable to the closer molecular packing of PEI on fiber surfaces. Lindquist (49) has shown a drastic reduction of protonation of PEI when pH is increased from pH 8.0 to pH 10.8, resulting in the decreased size of PEI molecule and the reduced lateral electrostatic repulsion between adjacently adsorbed molecules. This, in turn, results in a greater amount of adsorption.

Maximum adsorption occurs at pH 10.2 where PEI and polyester fiber probably carry equal and opposite charges. At pH 10.8, PEI reaches its isoelectric point, i.e., carrying no net positive charge. Even though the surface carboxyl groups of the fibers are fully ionized, electrostatic interaction becomes inoperative and adsorption does not occur. The optimum pH of 10.2 was chosen for all the subsequent studies.

Since PEI does not adsorb on polyester fibers at pH higher than 10.8 or lower than 3.5, it appeared possible to desorb the PEI from the fibers by simply increasing or decreasing the pH to the two extremes. Fibers having been treated with PEI-1000 at pH 10.2 were subsequently (1) eluted and soaked in pure water at pH 10.2 for 3 hours, (2) eluted and soaked at pH 12.0 overnight, and then (3) eluted and soaked at pH 2.0 overnight. The first step of this procedure was to include the possible reversibility due to the lowering of the solution concentration, whereas the second and third were due to the effect of pH. It was planned that if this procedure did reestablish the original PEI adsorptivity of the fibers, subsequent studies would pinpoint the specific contributing step. The fibers so treated, however, did not reestablish the original adsorption characteristics. The readsorption as a function of pH using these washed fibers is shown by the lower curve of Fig. 13 which indicates that only a fraction of PEI adsorptivity is recoverable. The readsorption data is given in Appendix II.

Irreversibility of PEI adsorption has been found on cellulose fibers by Allan and Reif (75). They postulated that the PEI molecules may be physically entrapped within small aperture pores of cellulose fibers if washed with acid, since acid would cause the molecule to expand about 1.6 times its isoelectric point diameter. This mechanism has been examined in a study of PEI adsorption on well defined porous silica gels by Hostetler (48). He found that such a mechanism is plausible when the pore apertures are of the same order of magnitude as the expanded size of PEI molecules. Irreversibility was also found by Hostetler for a PEI-porous silica system having the sizes of pore aperture orders of magnitude smaller than the PEI molecular diameter. This was attributed to the improbable simultaneous breakage of the multiple-attached bonds.

Irreversibility of PEI in attaching and bridging cellulose fiber surfaces has allowed papermakers to use PEI as an excellent wet-strength resin. However, it has also caused papermakers considerable difficulty in redispersing their broke. A procedure to break the bonds was developed later on (76). This procedure was found in this study to reestablish the PEI adsorptivity of the polyester fibers. The procedure involves elution with 0.65% NaOCl at pH 10.0 for 10 minutes, washing with water, followed by elution with NaOH at pH 12.5 for 1 minute and then an ample amount of water. Ten cycles of readsorption were conducted using the same fibers treated with this procedure. The results shown in Fig. 14 indicate good reproducibility. The mechanism for reestablishing PEI adsorptivity is not certain. It may be due to the formation of chloroamine (77) which is known to hydrolyze readily.

It was found during the adsorption studies that the PEI-treated fibers exhibit noticeable improvement of their dyeability by anionic dyes (e.g., Acid Blue B from American Cyanamid Co.). An attempt was therefore made to examine if the

dyed layer of PEI on the fiber surface could be identified under a microscope, in a hope that differentiation of it from the PEI-absent areas of interfiber contacts may provide some additional information in the later studies of a compressed mat. Unfortunately, the color intensity of a single fiber at 300X magnification was found too low to be useful. Association of the adsorbed PEI with a metallic ion (e.g., cupric ion) for surface analysis by an Energy Dispersive X-ray Analyzer was also attempted, but the intensity was here also a problem.

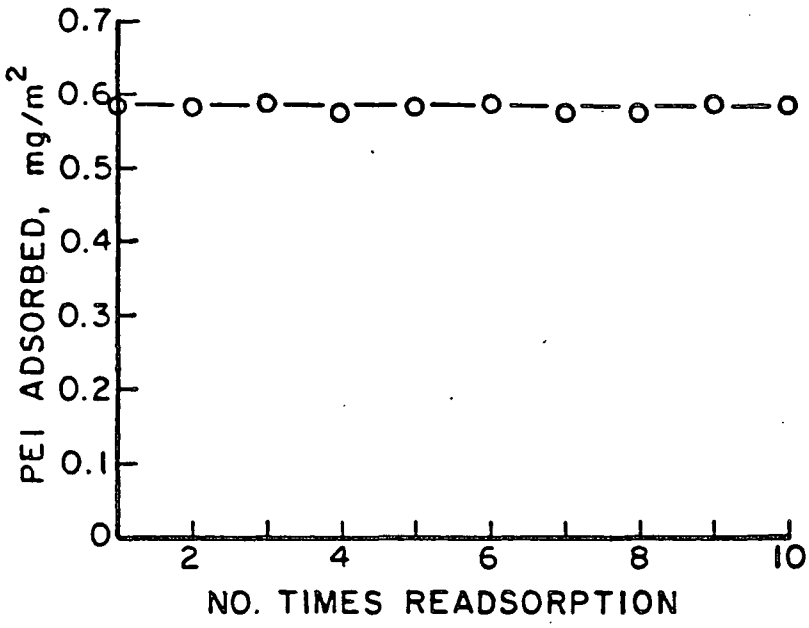

Figure 14. Reproducibility of PEI adsorption in ten cycles of desorption.

Effect of Contact Time

Figure 15 presents the PEI adsorption on polyester fibers as a function of contact time. Ten grams of cylindrical fibers were dispersed in 200 milliliters of distilled water and the slurry pH was controlled at 10.2. Three milligrams of PEI-1000 was added to each slurry with the pH maintained at 10.2. The

results show a very rapid initial adsorption and a subsequent leveling off to a nearly constant value. The adsorption is almost complete within 15 minutes of contact. The data are included in Appendix II.

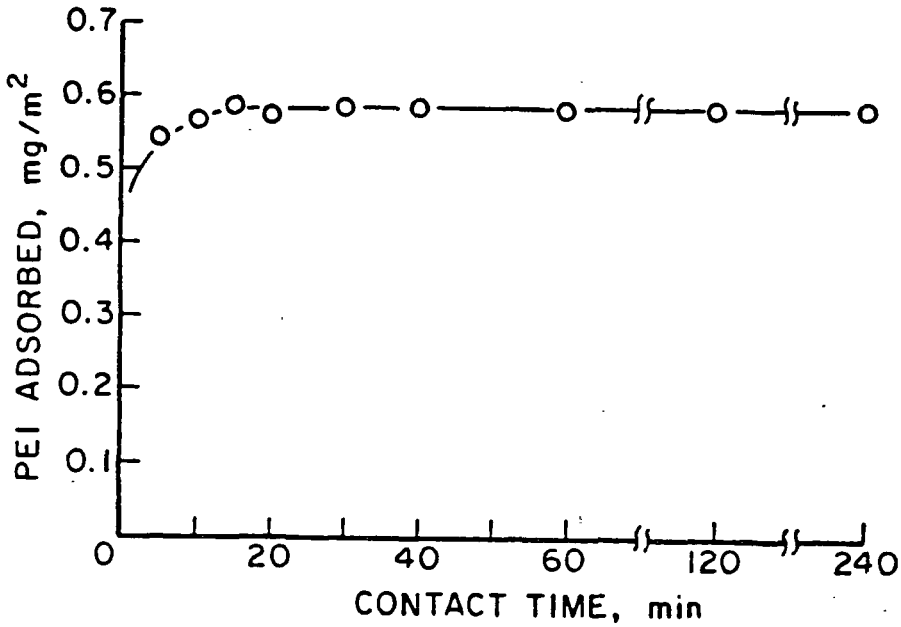

Figure 15. Adsorption of PEI on polyester fibers as a function of contact time.

Almost complete adsorption within 15 minutes of contact time was also observed by Lindquist (49) for adsorption of PEI on nonporous Ludox silica particles, and by Birkner and Morgan (80) who found the electrophoretic mobility of latex particles was reversed by PEI and stayed constant within 15 minutes contact time. Likewise, Kasper (81) has shown that the adsorption of a cationic polymer (1,2-dimethyl-5-viny pyridinium bromide, $M = 6 \times 10^3$ to 5×10^6) onto nonporous colloidal silica was more than 50% complete within two minutes and more than 90% complete within ten minutes. The rate of adsorption was also independent of the initial concentration of polymer. The kinetic adsorption data of Kindler (47) of PEI onto cellulose showed in general much longer time

(more than 100 minutes) to reach equilibrium due to the slow internal diffusion of PEI into porous cellulose.

The results of this work indicate that the adsorption of PEI on polyester fibers is more akin to the characteristics of nonporous surface adsorption than to those porous materials. The amount of adsorption stays constant, indicating little "molecular reshuffling" or internal diffusion.

Effect of Concentration

It has been generally found that most polymer adsorption data fir the simple Langmuir isotherm. That is, the amount of polymer adsorbed per unit surface area increases with the concentration of polymer in solution up to some saturation value beyond which point the curve levels off. The saturation point is believed to correspond to the formation of a monolayer of polymer on the surfaces. The Langmuir equation is given as follows.

$$\Gamma_A = K_{\perp} \Gamma_m C_e/(1 + K_{\perp} C_e) \qquad (22)$$

where Γ_A is the specific adsorption at equilibrium concentration, $\underline{C_e}$, $\underline{K_{\perp}}$ is the Langmuir constant, and Γ_m is the specific adsorption at surface saturation. The Langmuir constant is often referred to as a measure of the "affinity" for adsorption.

Ten grams of each type of fibers were dispersed in 200 mL of distilled water and the slurry pH was controlled at 10.2. A known amount of PEI-1000 was added to each slurry and the pH was maintained at 10.2. Thirty minutes contact time was allowed. The adsorption data of PEI-1000 on the fibers with different aspect ratios are shown in Fig. 16, where the specific adsorption Γ_A is plotted against equilibrium concentration $\underline{C_e}$. The adsorption data are given in Appendix

II. The adsorption isotherm is of the high affinity type; no PEI remains in solution at low levels of addition. As the concentration of PEI increases further, a plateau develops. The Langmuir type of adsorption indicates the formation of a monolayer. The agreement of adsorption among the three batches of fibers indicates these fibers have the same surface properties.

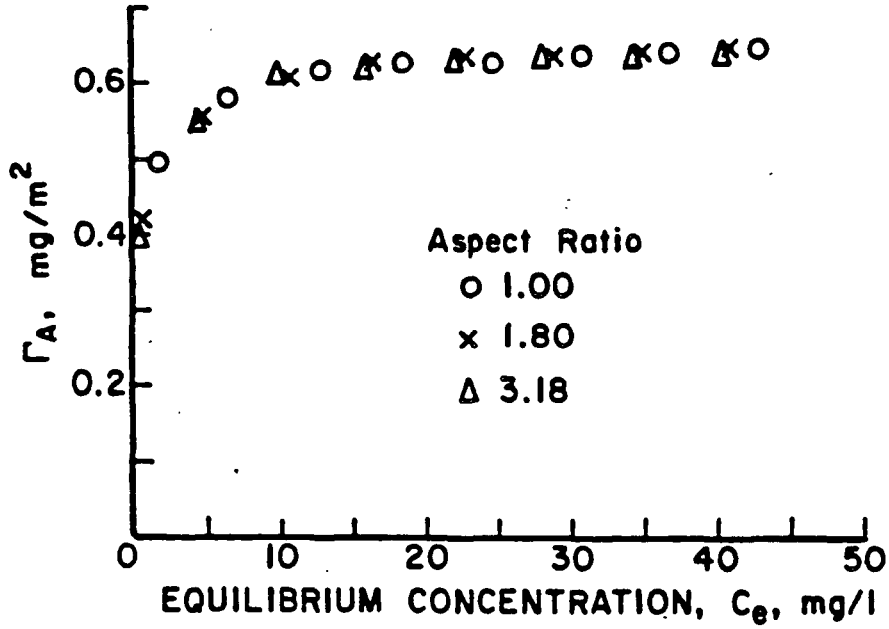

Figure 16. Equilibrium adsorption isotherms.

The Langmuir equation can be rearranged to

$$\frac{C_e}{\Gamma_A} = \frac{1}{K_L \Gamma_m} + \frac{C_e}{\Gamma_m} \qquad (23)$$

A plot of C_e/Γ_A vs. C_e will be linear with slope L/Γ_m and intercept $1/K \Gamma_m$ if the adsorption is characterized by Langmuir type behavior. Such a plot is given in Fig. 17. Very good compliance to the Langmuir form was indicated. The value for Γ_m and K_L were then obtained from this plot and has values of 0.655 mg/m^2 and 1.138 L/mg, respectively.

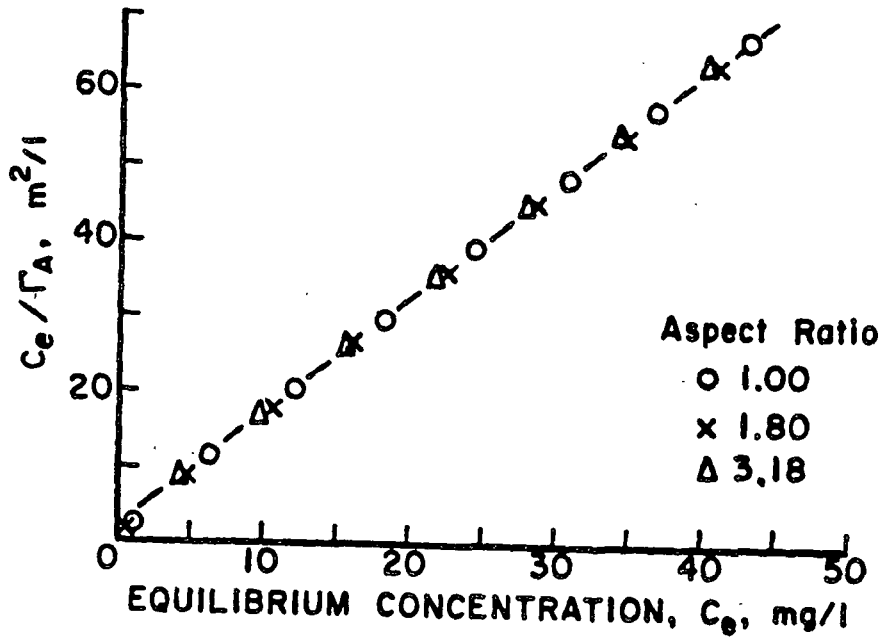

Figure 17. Equilibrium adsorption isotherms - Langmuir linear form.

With the specific adsorption at surface saturation, Γ_m, obtained, an attempt was made to examine whether the monolayer adsorption can be assumed to be on the external surfaces. As was reviewed previously, it has been difficult to determine experimentally the precise size and configuration of an adsorbed polymer molecule. Some studies have indicated that the adsorbed molecules retain approximately the same size and shape on the adsorbent surface as they had in solution (64,65). The solution sizes of spherical PEI of various molecular weights at various pH's in solution have been characterized by Hostetler (48) and Lindquist (49), using intrinsic viscosity data and the Einstein-Stokes equation. The diameter of PEI-1000 at pH 10.2 is 147 Å estimated from the results of Lindquist (49). With the information of molecular size in solution available, and assuming the size and shape of molecules remaining the same and having a (hexagonal) close packing on the substrate surface, it is possible to calculate the geometric saturated adsorption of PEI on surface, $\Gamma_{m,g}$, according to

$$A_m = \pi d^2/4 \tag{24}$$

$$\Gamma_{m,g} = M/(1.11\ A_m\ N_A) \tag{25}$$

where A_m is the projected area of a molecule of diameter d at pH 10.2. N_A is the Avogadro number and M is the molecular weight. The hexagonal close packing arrangement has a projected area amounting to 90.6% of the area of a flat surface on which the monolayer rests, accounting for the factor of 1.11. The geometric maximum adsorption, $\Gamma_{m,g}$, for PEI-1000 at pH 10.2 so calculated was 0.66 mg/m^2, which compared favorably with the experimentally obtained saturation adsorption, Γ_m, of 0.655 mg/m^2.

The adsorption characteristics of PEI-1000 on polyester fibers carried out to this point indicated that the molecules of PEI-1000 are sufficiently large to ensure the external adsorption. This is important since the reduction of specific PEI adsorption at various levels of mat compression to be studied later can then be used as the indication of the reduction of the external surface area but not that of the internal surface area.

Effect of Molecular Weight

Although not essential to the present work, it is of interest to know the minimum molecular size below which the penetration of PEI into polyester fibers may occur. The effect of molecular weight on adsorption was thus studied.

This study was carried out in the permeation cell. Mats of cylindrical fibers of 30.5416 grams were present in the cell with 300 mL circulating water at pH 10.2. A known quantity of PEI was added to the system and the equilibrium concentration was determined after 30 minutes contact time by removing 5 mL solution from the system for colorimetric determination. After measuring the

equilibrium concentration, a give milliliter PEI solution of the same concentration was made up and was returned to the adsorption system. Another known dosage of PEI was added to the system, and its respective equilibrium concentration was noted. This process was repeated until the desired equilibrium concentration range for establishing an adsorption isotherm for the given sample of PEI was covered. The PEI was then removed from the fibers in the same manner as was described in the experimental section, and another adsorption isotherm was obtained for a sample of another molecular weight.

The adsorption data of eight different molecular weights of PEI are shown in Fig. 18 in which the specific adsorption Γ_A is plotted against equilibrium concentration $\underline{C_e}$. The experimental data are given in Appendix II. All the adsorption isotherms are of the Langmuir type. Good compliance to the linear form of Langmuir equation was also found over the conditions studied, as shown in Fig. 19. The values of Γ_m and $\underline{K_L}$ were then obtained from the linear plot and are summarized in Table 2 for the various molecular weights. Table 2 also gives the molecular diameter of various molecular weights estimated from Lindquist's data (49), and the geometrically allowed specific adsorption, $\Gamma_{m,g}$, calculated in the same manner as was described in the preceding section.

As shown in Fig. 20, the experimental saturation adsorption, Γ_m, compares favorably with the calculated $\Gamma_{m,g}$ for the four highest molecular weights. However, for the lower molecular weights, the amount of PEI actually adsorbed becomes progressively less than that geometrically allowed. The same results were also obtained on adsorption studies of PEI-nonporous silica system by Lindquist (49). He suggested that for an adsorption system involving electrostatic interaction, the molecule would be adsorbed in a somewhat flattened configuration due to the strong force involved, and the shape and size will

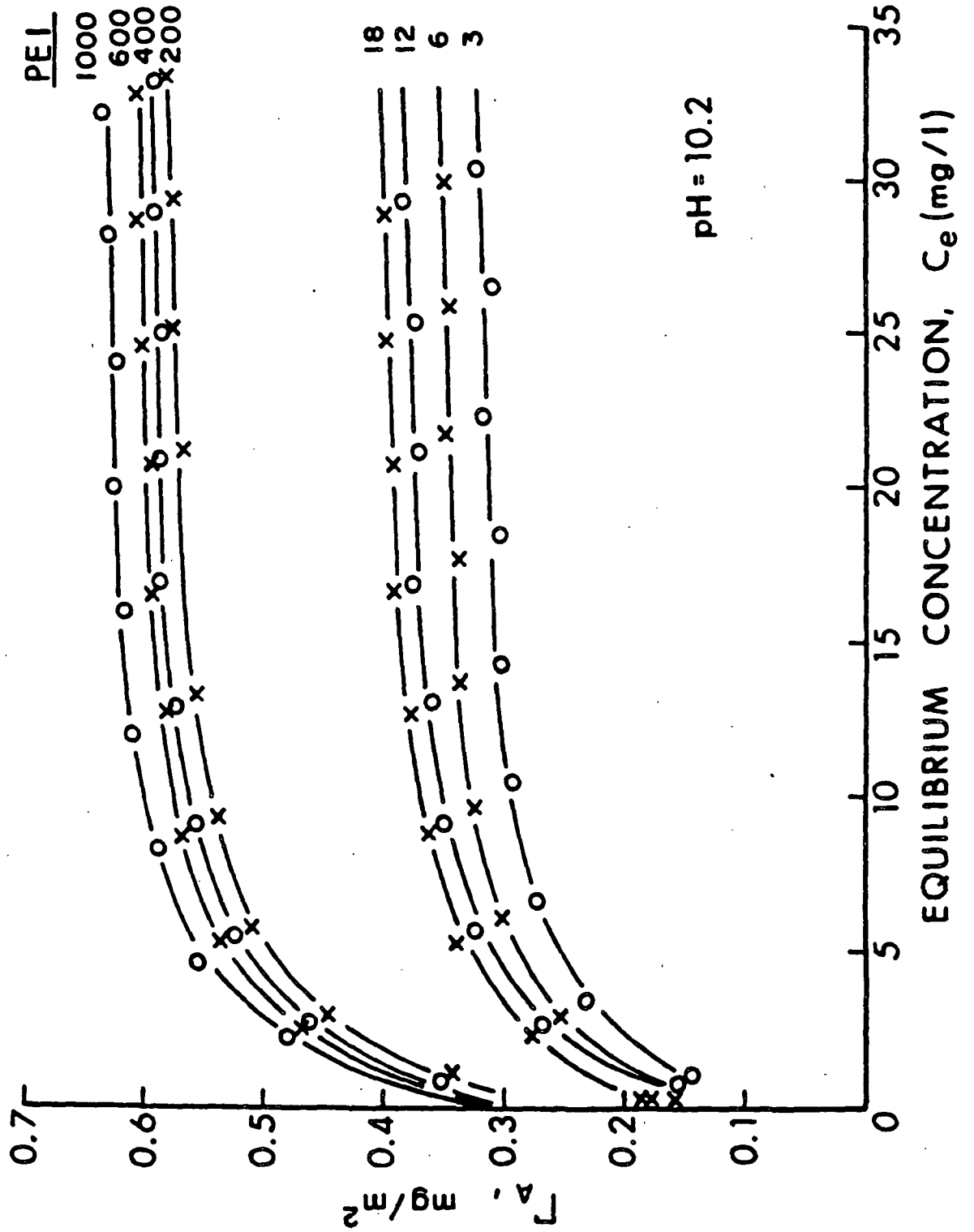

Fiure 18. Adsorption isotherms of various molecular weight PEI.

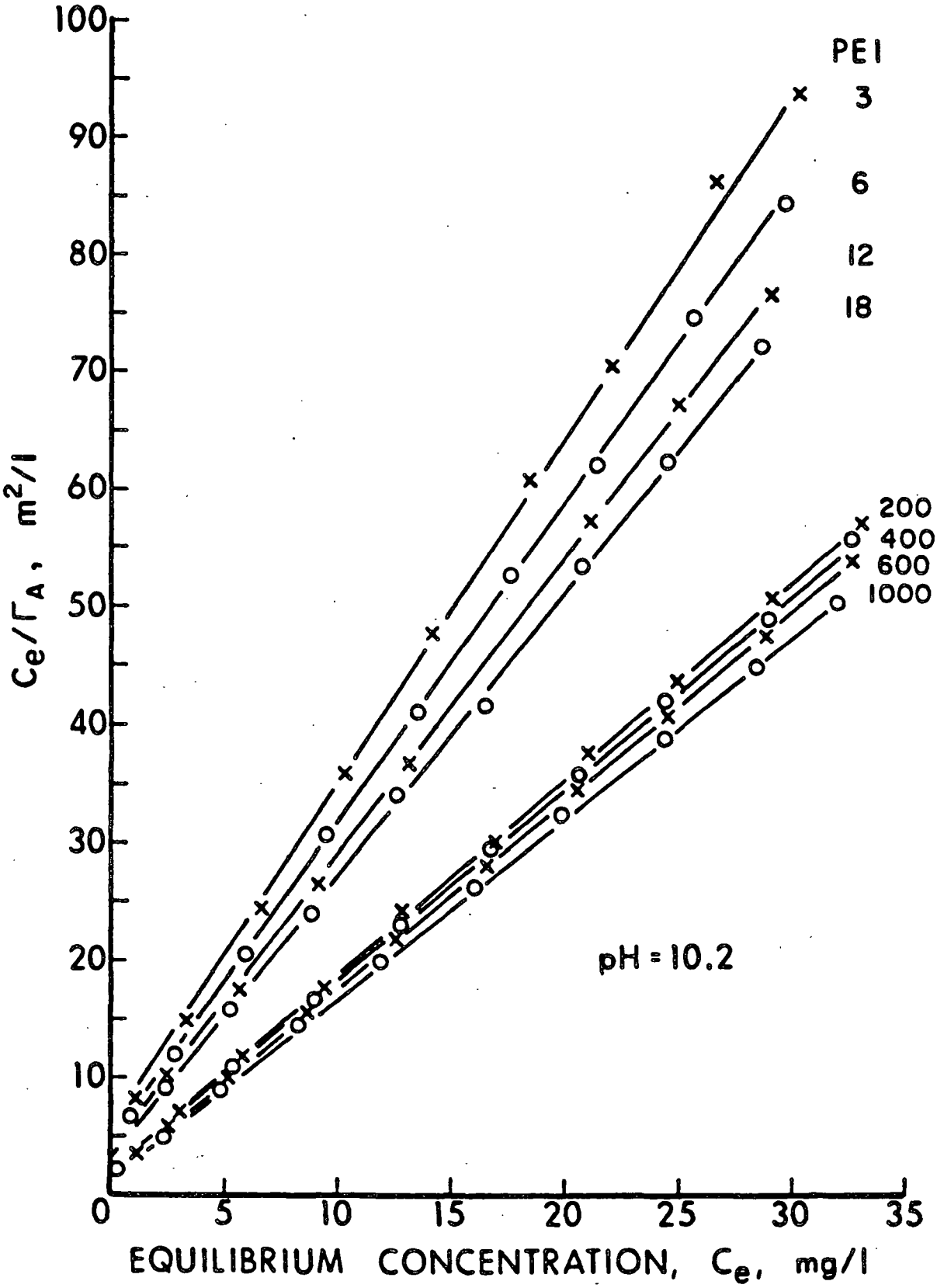

Figure 19. Adsorption isotherms of various molecular weights - Langmuir form.

somewhat deviate from that in solution. Since the attractive force is the strongest at the absorbent surface and diminishes with distance, the smaller molecule being subject to stronger surface force may be attracted to a flatter configuration and its adsorbed diameter will become larger than its solution diameter, rendering a smaller quantity of adsorption than the calculated one. Evidently, this proposed mechanism is not easily verifiable. However, it seems fair to say that the agreement of the present result with Lindquist's data characterized on a nonporous substrate gives an indication that there has been no internal penetration occurring down to the lowest molecular weight PEI examined in this series.

Table 2. Summary of some PEI properties, Langmuir parameters and geometrical allowed specific adsorption at pH = 10.2.

PEI	M_n	Diameter, Å at pH = 10.2	$\Gamma_{m,g}$, mg/m^2	Γ_m, mg/m^2	K_L, l/mg
1000	75,000	147	0.66	0.655	1.138
600	50,000	121	0.65	0.626	1.112
400	35,000	102	0.65	0.613	1.099
200	25,000	86	0.64	0.598	1.002
18	1,800	24	0.60	0.416	0.834
12	1,200	20	0.57	0.398	0.759
6	600	14.5	0.54	0.363	0.768
3	300	10.5	0.52	0.337	0.734

In the case of PEI adsorption on porous substrate such as on cellulose studied by Kindler (47) and on porous silica gel by Hostetler (48), the amount of adsorption has been shown to increase with decreasing molecular weight. For example, Hostetler had shown close agreement between Γ_m and $\Gamma_{m,g}$ only for the lower molecular weight PEI on porasil A, but Γ_m becomes significantly less than the geometrically allowed $\Gamma_{m,g}$ as the PEI molecular weight increases, because of the increasing amount of inaccessible surface area hidden in the pores for larger molecules.

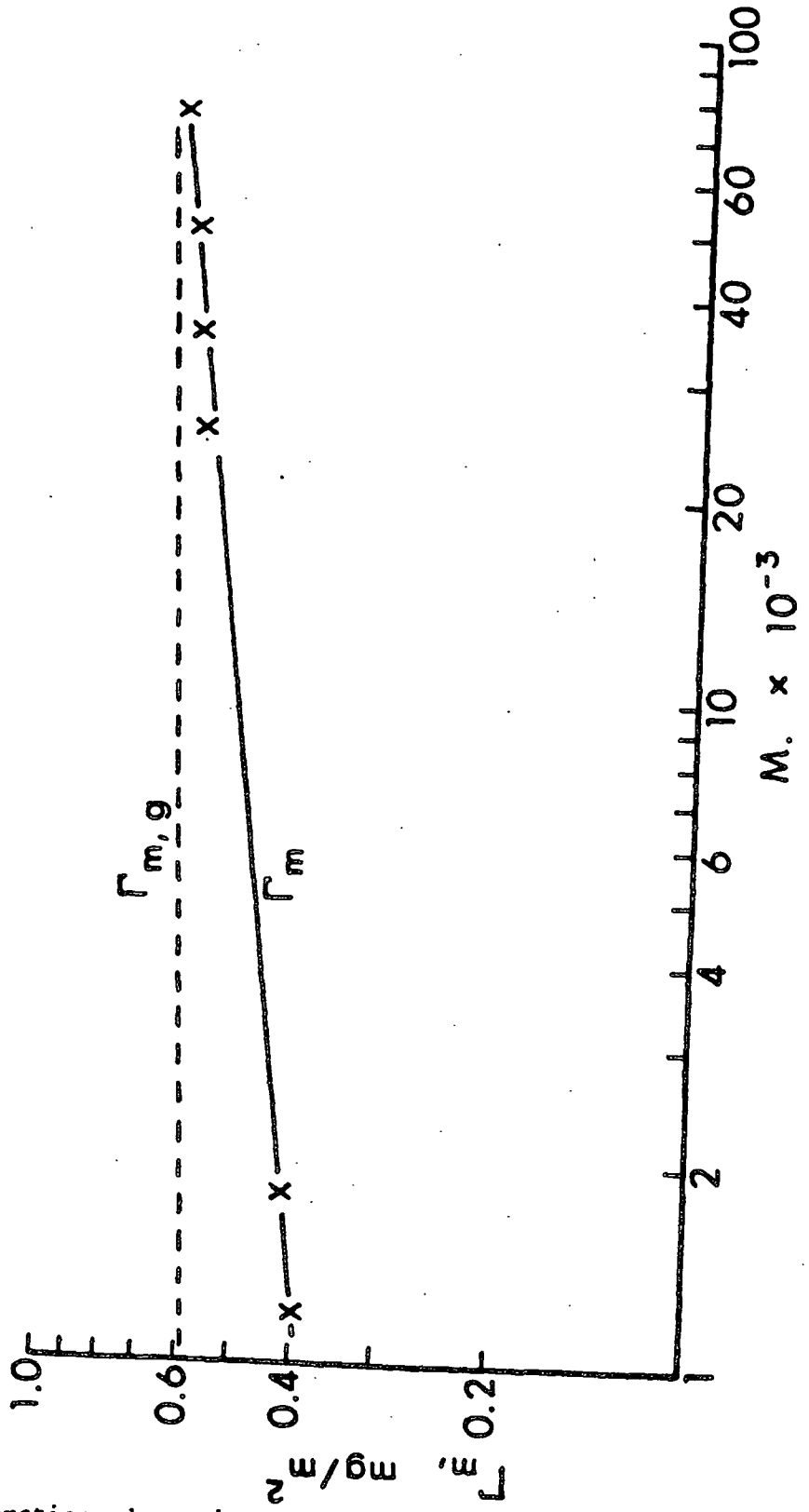

Figure 20. Saturation adsorption as a function of molecular weight: experimental vs. theoretical.

In summary, the study of the effect of molecular weight of PEI adsorption on polyester fibers gives an indication that the adsorption is more akin to the monolayer formation on the external surfaces as was studied by Lindquist (49).

Summary of PEI Adsorption on Polyester Fibers

The preceding studies indicate that the adsorption of PEI on polyester fibers is a rapid and strong electrostatic type of interaction, probably resulting in a somewhat flattened layer of polymer molecules on the fiber surfaces. The Langmuir type adsorption, along with the fact that the maximum amount of adsorption has the same magnitude as that of geometrically allowed, indicate the formation of a monolayer of PEI on the external surfaces of fibers.

Optimum adsorption condition using PEI-1000 at pH 10.2 was chosen for later studies. Thirty minutes contact time was allowed. The reduction of specific PEI adsorption of fiber mats at various levels of compaction will be used as the indication of the reduction of external surface area. It should be clear that the use of PEI-1000 at pH 10.2 automatically implies that only the surface area accessible to the molecule of 147 Å was accounted for.

PERMEABILITY AND POLYMER ADSORPTION OF COMPRESSED MATS

General Aspects of Compressed Fiber Mats

Fiber possess varied and numerous physical forms and properties. The fibers can be arranged and assembled into mats in a myriad of modes; each mode would conceivably possess its own characteristic physical properties. The importance of mode of packing on permeability properties has been given in the literature review section in which a distinct variation of permeability was brought to light among flow perpendicular and parallel to regular arrays and to random array of fibers.

A fiber mat formed by constant-rate filtration from a dilute suspension is the fibrous structure of primary concern in this work. The fiber mat so prepared is characterized by the random orientation of fibers in the horizontal plane with their axes mostly perpendicular to the vertical direction (54). Among the fibers passages exist allowing the fluid to flow through. An important feature of this fibrous structure is its high initial porosity. In order to reduce the mat porosity, it is necessary to apply mechanical stress, usually from the vertical direction perpendicular to the plane of the mat, to force fibers closer together. At early stages of mat porosity reduction, fiber bending associated with an increasing number of fiber intersections has been viewed as the predominant mechanism. The fibers may also reposition themselves, the extent of which may depend upon the properties of fibers. And, eventually, the fibers have little space to bend or slip and must undergo interfiber compaction. Interfiber compaction would occur to ductile fibers, whereas fiber breakage would occur for glass fibers at high degrees of loading. Han (18) has reviewed the mat compression studies and compression mechanisms. The reviewed studies concerned mainly mat compression in the high porosities and the mechanisms of fiber bending and repositioning. Compression to lower porosities where interfiber compaction becomes important has received little attention.

While the fibers in the mat undergo complex modes of movement and interaction in the process of porosity reduction, the pore geometry would also go through a series of changes. The exact geometrical description of the complex structure of a compressed fiber network and its pore geometry has been difficult to achieve. Consequently, in attempts to study the fundamental relationships of the fluid flow through fiber mats, it has been necessary to revert to a more phenomenological approach.

Permeability of Compressed Mats

It has been generally assumed in permeability studies that fiber mats prepared under similar conditions will possess similar structural properties. These are related by a common geometrical factor, after separating the measurable controlling factors of porosity and surface area. The geometrical factor is represented by the Kozeny factor, when the Kozeny-Carman expression is used in the permeability analysis.

Ingmanson and coworkers (20) have characterized the Kozeny factors of high porosity mats prepared from the constant-rate filtration technique using well-defined cylindrical glass and nylon fibers. The Kozeny factors so characterized were expected to have a general applicability to mats of other types of fibers prepared under similar conditions. Ingmanson's correlation has been duplicated without difficulty (79), but was limited to the high porosity range.

For reasons not clearly understood at present, there has been no agreement among experimental permeability results for mats having been compressed to porosities lower than about 0.8. This has made permeability analyses rather difficult. Suggestions that surface area reduction and fiber shape variation may play important roles in mat permeability have been complicated by the disagreement of permeability data, per se, at porosities lower than 0.8.

One possible reason which might have been overlooked in the past is the load-induced error in the measurements of fiber mat thickness at porosities lower than 0.8. To elucidate this point, typical data of the relationships of the fiber mat thickness and the required compressive load as a function of mat porosity are depicted in Fig. 21, using Labrecque's (42) mat of cylindrical fibers as an example (his mat parameter is indicated in the figure). As can be

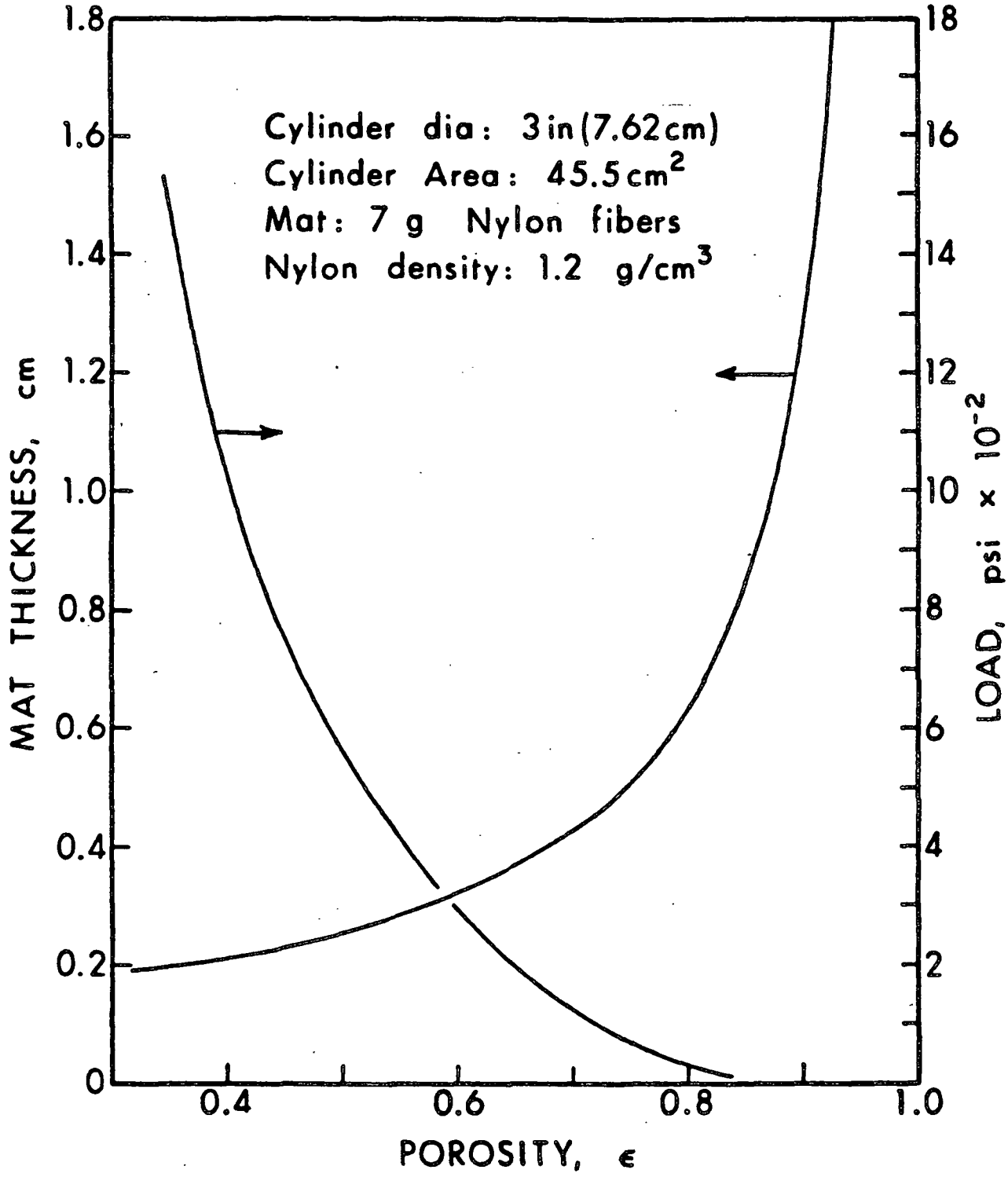

Figure 21. Fiber mat thickness and compressive load as a function of porosity.

seen for porosity higher than 0.8, the change of mat thickness with respect to porosity is substantial and can be measured with relative ease. For porosity lower than 0.8, from which disagreement of permeability results occurred, the change of mat thickness becomes ever-decreasing and more susceptable to error especially when a low basis weight mat is used. The difficulty can be further aggravated by the drastic, ever-increasing load required to compress the mat to the lower porosities. Recent experience had shown (82) that under such loading the framework supporting the commonly used permeability apparatus becomes distorted such that the bottom septum which was usually used as an immobile reference plane for mat thickness measurement is displaced along with the framework, the septum and piston wires (100 mesh wire over 1/4-inch piston holes as used by Labrecque) would easily be deflected into holes, rendering the measurement of mat thickness inaccurate. These sources of errors would vary with the mat basis weight and the mat compressibility. Comparison of permeability results either among or within the independent works using mats of different basis weight and of different compressibility would be impossible, should these errors occur.

With these possible complications in mind, a very rigid permeating cell without the need of supporting framework was constructed for the studies of low porosity mats. Piston wire and piston holes were designed in such a way as described in the experimental section that no wire deflection into piston holes would occur. A much higher basis weight (close to 7 times higher) was also preferred in order to eliminate the inaccuracy of the mat thickness measurements.

The permeability results obtained in this study were for fibers of three different aspect ratios in the porosity range from 0.85 to 0.4. The Darcy equation and the Kozeny-Carman equation were used as the basic relationships.

To determine the Darcy permeability at a given porosity, pressure drop measurements were made at as many as 13 different flow rates. Darcy's permeabilities were determined at 8 or 9 discrete descending porosities for each prepared mat. Triplicates were done on mats of each type fibers.

A typical example of permeation data is shown in Fig. 22, in which the volumetric flow rate, Q, is plotted against the pressure drop, ΔP, for nine discrete porosities of the same mat. Within the experimental range the data show direct proportionality in good agreement with Darcy's Law of Eq. (1). To calculate the Darcy permeability, the ratio of Q/A to $\Delta P/L$ was based on the slope of the straight line, where the mat area, A, was an accurately known constant and the mat thickness, L, was the measured value. The viscosity of the water at the temperature of each run was obtained from the CRC handbook. The porosity, ε, at each thickness, L, was evaluated from the ovendry weight of the mat, W, and the pycnometric density of the fibers, ρ, according to

$$\varepsilon = 1 - \frac{W}{\rho A L} \tag{26}$$

The Kozeny factor, k, was calculated from the Darcy's permeability, K, the measured porosity, ε, and the microscopically measured surface area, S_v, according to

$$k = \frac{\varepsilon^3}{K S_v^2 \, (1 - \varepsilon)^2} \tag{27}$$

The surface area was assumed unchanged over the investigated porosity range in this calculation. The Kozeny factor so obtained was termed "experimental" Kozeny factor.

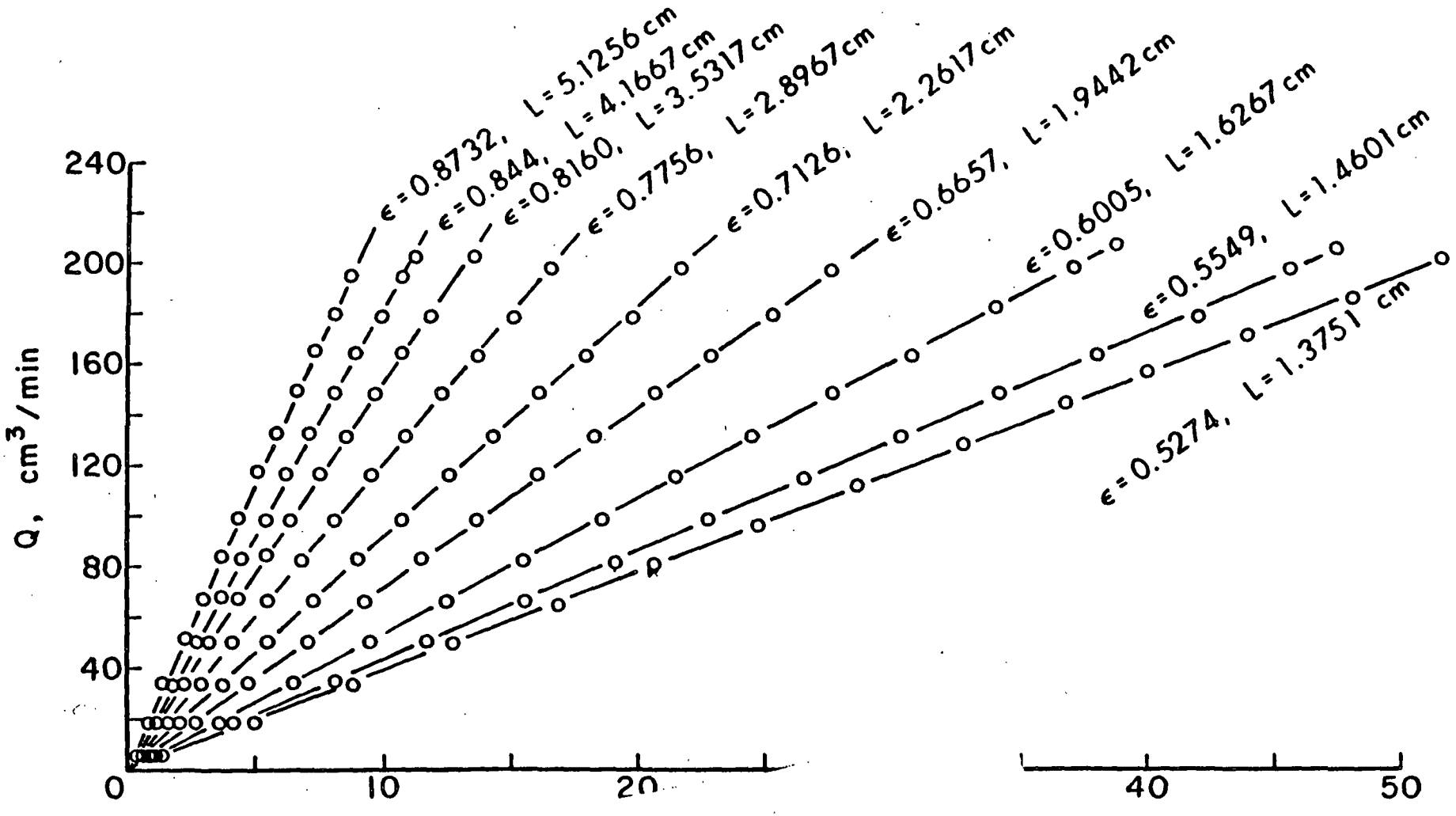

Figure 22. Typical volumetric flow rate vs. pressure drop plot for circular fibers.

The results of the experimental Kozeny factor as a function of porosity for mats of fibers of different aspect ratios are summarized in Fig. 23. The data of these measurements are given in Appendix III. These results show that fiber cross-sectional shape does not affect the experimental Kozeny factor at porosities higher than 0.8, as indicated by the convergence of the three curves. However, when compressed into lower porosities, the effect of fiber cross-sectional shape appears and becomes increasingly evident, as shown by the progressive divergence of the three curves. In addition, all the fiber mats have Kozeny factors deviating from the commonly found value of about 5.0 from particle beds at porosities lower than 0.8.

Polymer Adsorption of Compressed Mats

As a fiber mat composed of deformable fibers is compressed by a mechanical load, the compressive stresses are transmitted through the fiber intersections and distributed throughout the fibers. The surface area at the fiber intersections contributing to supporting the load will not contribute to the resistance to flow. Consequently, the assumption that the external surface area remain unchanged in the permeability consideration given in the preceding section is not a valid one.

The polymer adsorption technique was performed on the three types of fiber mats at various levels of compaction as a means of probing the change of the exposed surface area to the permeating liquid. Duplication runs were made for each type of mat. A known quantity of PEI-1000 was added to the adsorption system at pH 10.2. Thirty minutes contact time was allowed. The specific PEI adsorption of fibers of the compressed mat was compared to the specific adsorption of fibers in the free suspension at the same equilibrium concentration, and

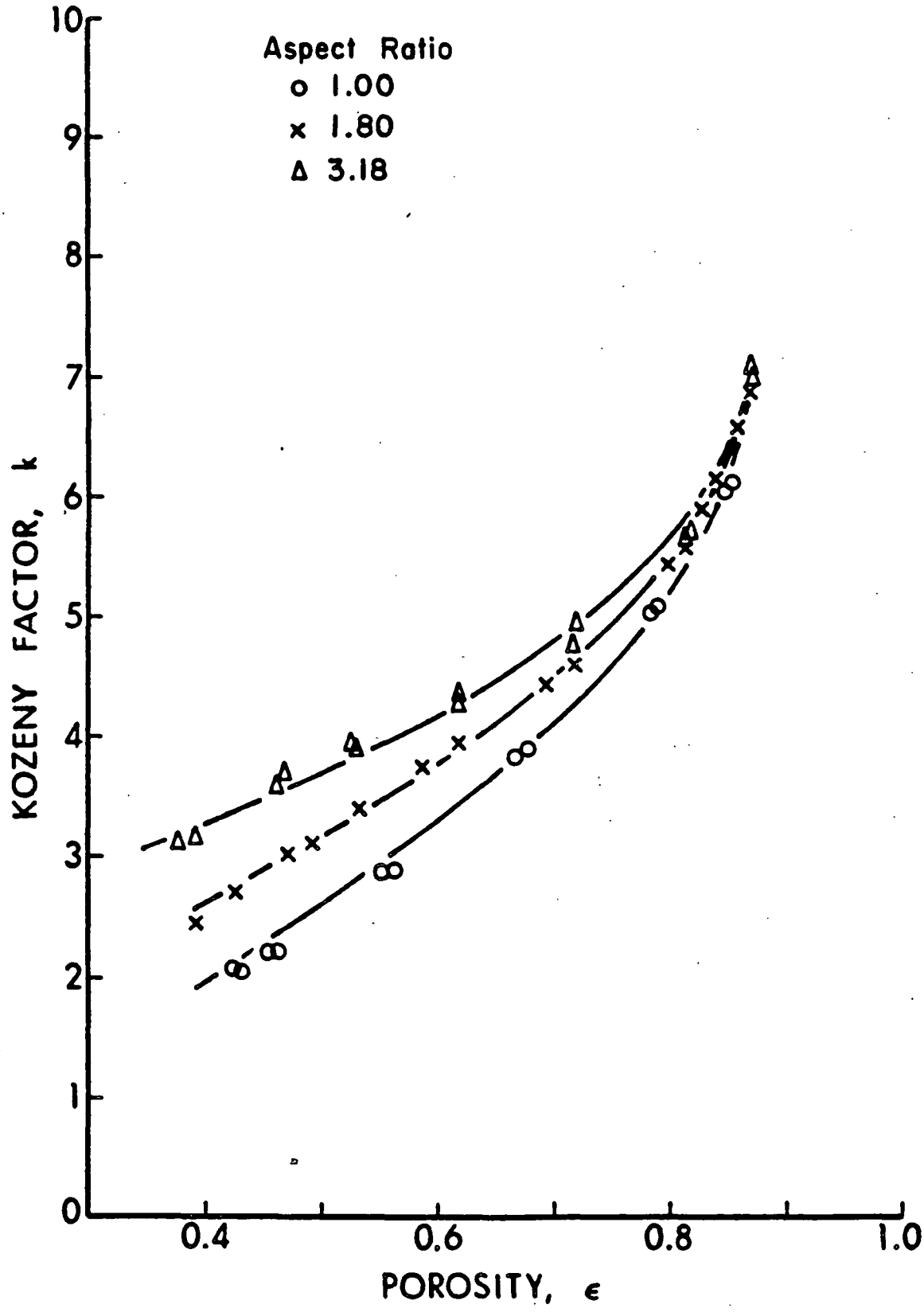

Figure 23. Experimental Kozeny factors as a function of porosity.

their ratio in percentage was interpreted as the % surface area exposed to the fluid.

The % surface area as a function of porosity for each type of fiber are depicted in Fig. 24 and the data summarized in Appendix III. It is interesting to find that, contrary to what was believed by the previous workers, the mats composed of flatter fibers can be brought to lower porosities before showing significant interfiber compaction and reduction of their surfaces. Approximately, the cylindrical-fiber mat starts to lose surface at $\varepsilon = 0.85$, the elliptical one with aspect ratio 1.80 starts at $\varepsilon = 0.80$, and the one with aspect ratio 3.18 starts at $\varepsilon = 0.75$. At any lower porosities, the higher the aspect ratio, the less the % surface area reduction.

Scanning electron micrographs of the three types of fibers removed from their respective mats after being compressed to porosity 0.4 are shown in Fig. 25. Fiber deformation by bending (kinking) and interfiber compression (denting) are readily observable from these micrographs. Among these three types of fibers, the cylindrical fibers show considerable extent of fiber deformation. The flatter fibers show less deformation, in qualitative agreement with the surface area reduction relationship.

Kozeny Factor-Porosity Correlations

Instead of assuming that the surface area does not change under compression, the surface area obtained from polymer adsorption technique was used to calculate the Kozeny factor as a function of porosity for the three different types of mats. The numerical results are given in Appendix III and are depicted in Fig. 26 by triangle symbols. It was found that all the data points of mats of fibers of various aspect ratios resolve into a single correlation, and the

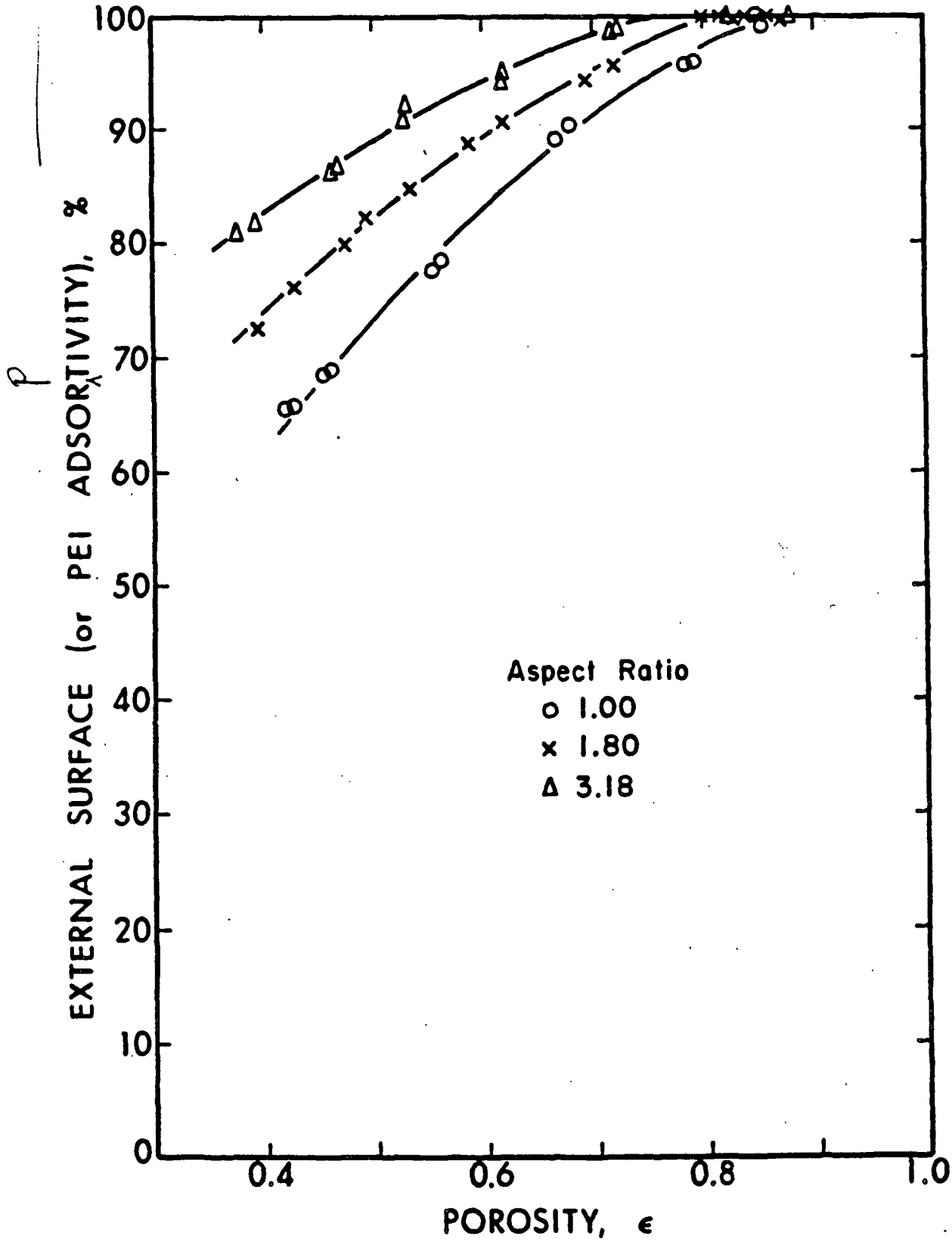

Figure 24. Percent surface area remained as a function of porosity.

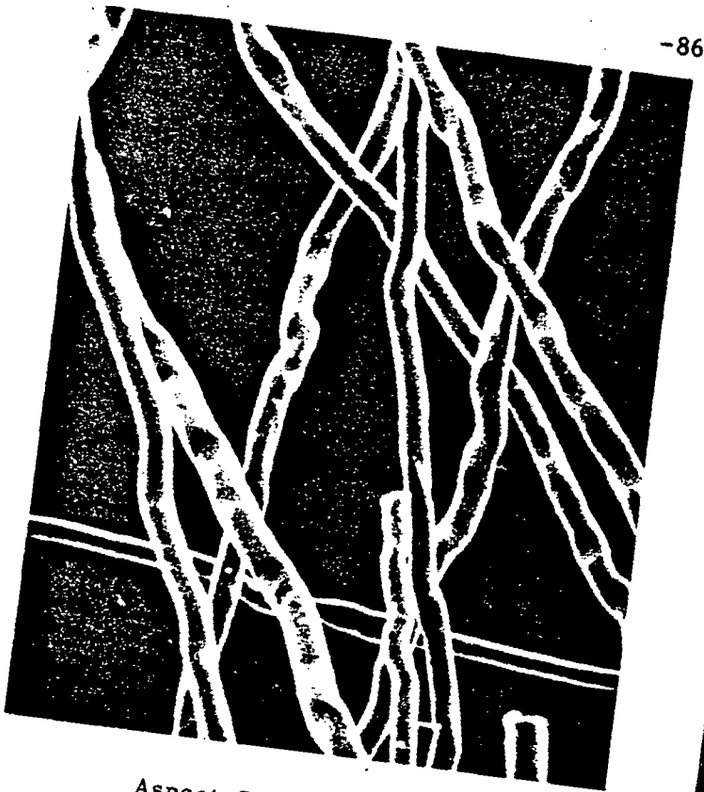

Aspect Ratio = 1.00

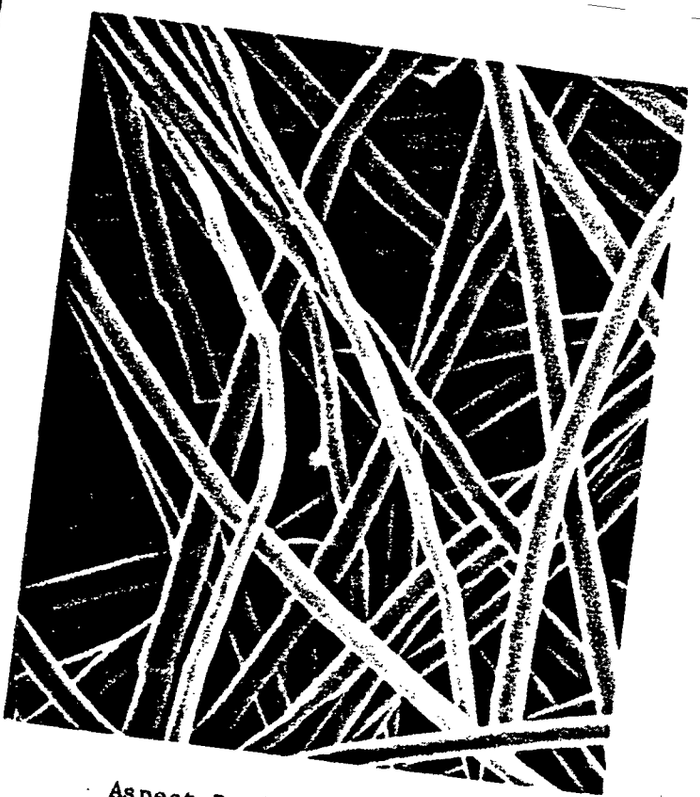

Aspect Ratio = 1.80

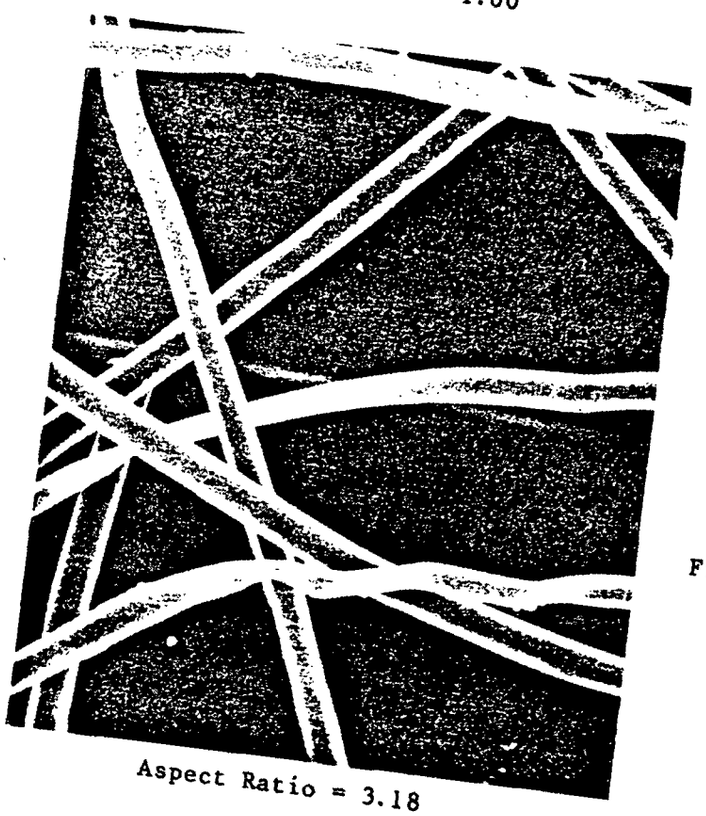

Aspect Ratio = 3.18

Figure 25. Fiber-to-fiber interactions at porosity 0.40 (magnification 300X).

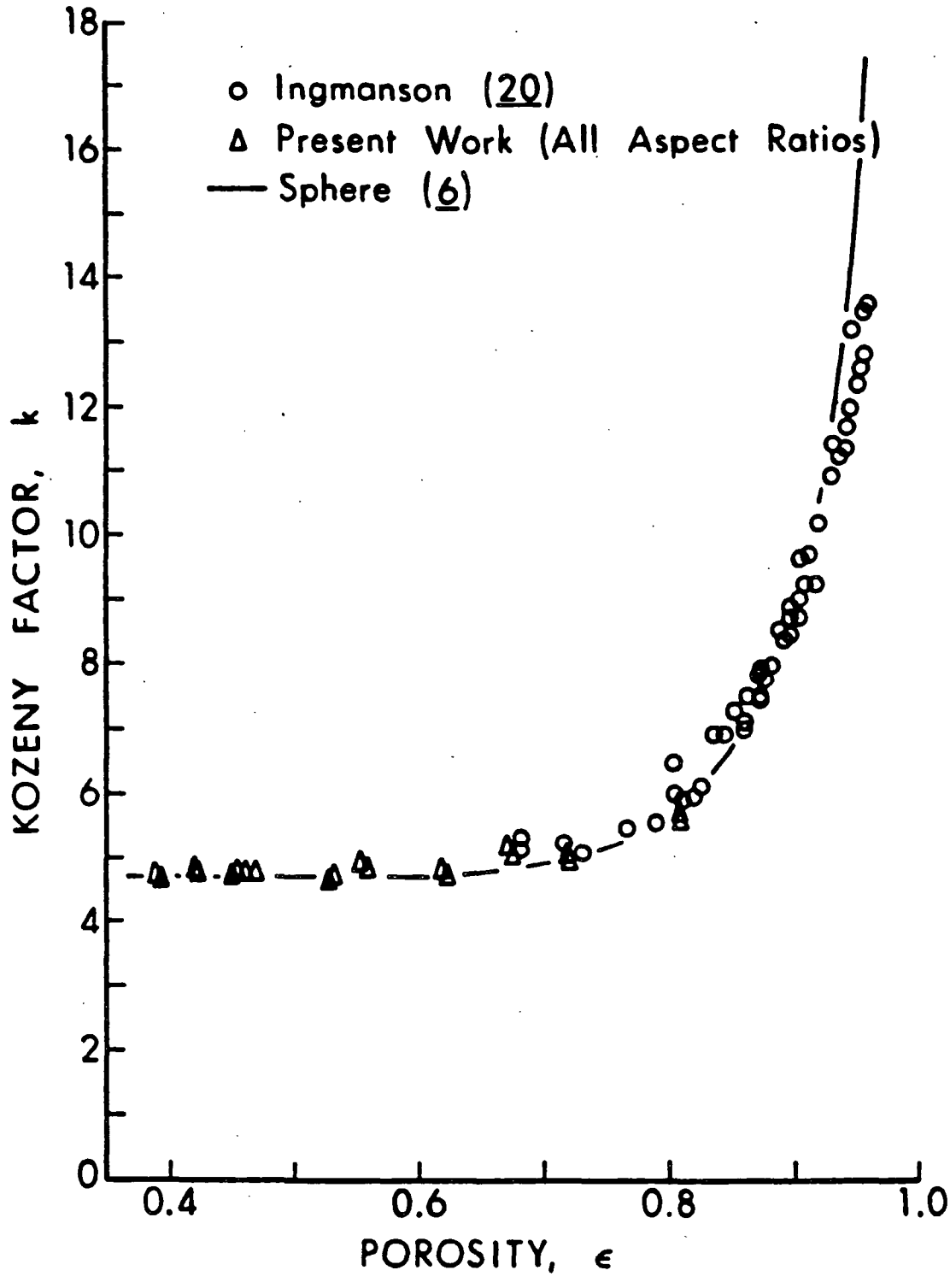

Figure 26. Kozeny factor - porosity correlations.

Kozeny factor appears to level off to a fairly constant value of 4.7 toward lower porosities, which is in close agreement with most of the reported values for particle beds.

In addition to the present data in the lower porosity range, Fig. 26 also includes Ingmanson's data (20), represented by circular symbols, in the higher porosity range where the surface area reduction does not occur. It shows that the two sets of data overlap and form a continuum covering a wide range of porosity from 0.96 to 0.40. The continuum can be correlated by

$$k = 4.7 + \exp\,[14\,(\varepsilon - 0.8)] \qquad (28)$$

This correlation can be considered as a calibration curve based on the known values of surface area and porosity. Therefore, for a fiber mat with well-defined porosities, the permeability technique can now be used to determine both the initial surface area at higher porosities and the progressive surface area reduction toward lower porosities, without further resorting to the tedious microscopic and polymer adsorption techniques used in this work.

A striking feature was also found when the correlation for fiber mats was compared to the correlation for sphere beds. The experimental correlation for sphere beds has been referred to in the literature review section and is plotted as a solid line here in Fig. 26. It shows that, although fiber represent an extreme departure in shape from sphere, the two agree well all the way up to a porosity around 0.92, beyond which they appear to diverge. The divergence at very high porosities has been predicted analytically, due to the increasing independence of the particles from one another. However, it is interesting to note that when fibers are randomly packed and densified to a porosity below 0.92, their original identifies become obscured, in fact, lost, and the fibers

exhibit essentially the same permeability characteristics as particle beds represented by spheres, regardless of its original shape, either elongated or flattened.

Compressibility of Fiber Mats

Since the surface area reduction is induced by the mechanical load transmitted through fiber intersections, it was felt that additional information could be gained from the compression behavior of the mats. Compressibility data were therefore obtained for all three types of mats and were carried out in duplicate.

The data of each mat could be represented by the conventional empirical relationship,

$$C = MP^N \tag{29}$$

where C is the mat density in g/cm^3, P is the applied load in $dyne/cm^2$. M and N are two compressibility constants, N being a pure number and M having a dimension of $(g/cm^3)/dyne/cm^2)^N$. This equation may be rearranged as follows:

$$\log C = \log M + N \log P \tag{30}$$

and a plot of the compressibility data on double logarithmic paper will yield a straight line. Such a plot for the three types of mats investigated are given in Fig. 27. The data are included in Appendix IV and are only shown on Fig. 27 in the load range of 10^6 - 10^8 $dyne/cm^2$. Data at loads lower than 10^6 $dyne/cm^2$ also extent the straight line relationships. In Table 3 are given values for the empirical constants, M and N. The unit of load was $dyne/cm^2$ to be consistent with most of the reported unit.

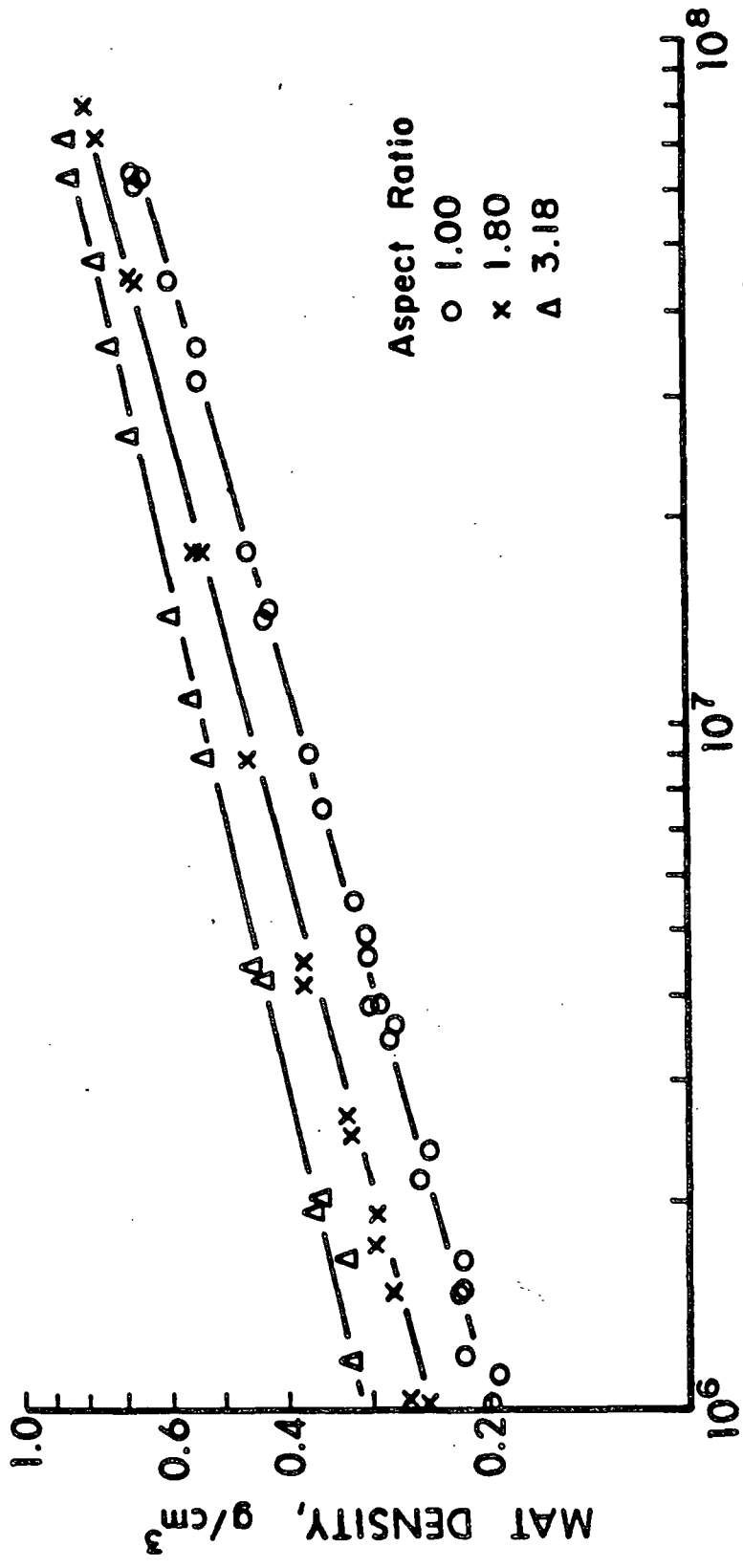

Figure 27. Compressibility of fiber mats of various aspect ratios.

Table 3. Compressibility constants for the equation, $C = MP^N$. (C, g/cm^3; P, dyne/cm^2).

Mat, Aspect Ratio	M	N
1.00	0.003579	0.289744
1.80	0.005830	0.270112
3.18	0.010865	0.241815

The compressibility constants, M and N, contains some physical character of the mat and the fibers, and have attracted a number of investigations (83-85,54, 18) devoted to identify them. Up to the present time, it is generally recognized that the compressibility cosntants, M and N, depend on such factors as fiber dimensions, fiber properties, modes of packing, and modes of deformation (e.g., fiber slipping, bending, and conformation). However, attempts to quantitatively break down the values of M and N into these factors has met with no particular success, primarily due to the apparent difficulties in quantifying all the conceivable modes of packing and modes of deformation. As a result, it has been virtually impossible to interpret the physical meaning directly from the empirical values of M and N. To appreciate the complexity of the subject, the readers are referred to the review by Han (18).

In view of the above-mentioned difficulties, a qualitative approach was attempted by plotting the compacting pressure vs. porosity for the three types of fiber mats, as shown in Fig. 28. It was found that as the fiber aspect ratio increases, the compacting pressure curve shifts to the lower porosity side, in exactly the same sequence as the shift of the "surface area reduction curve" previously given in Fig. 24. This means that the flatter the fiber, the lower the porosity the mat can be packed into before substantial compacting pressure arises and interfiber compaction occurs. It was also found that the "critical" porosity from which the mat begins to show a significant surface area reduction

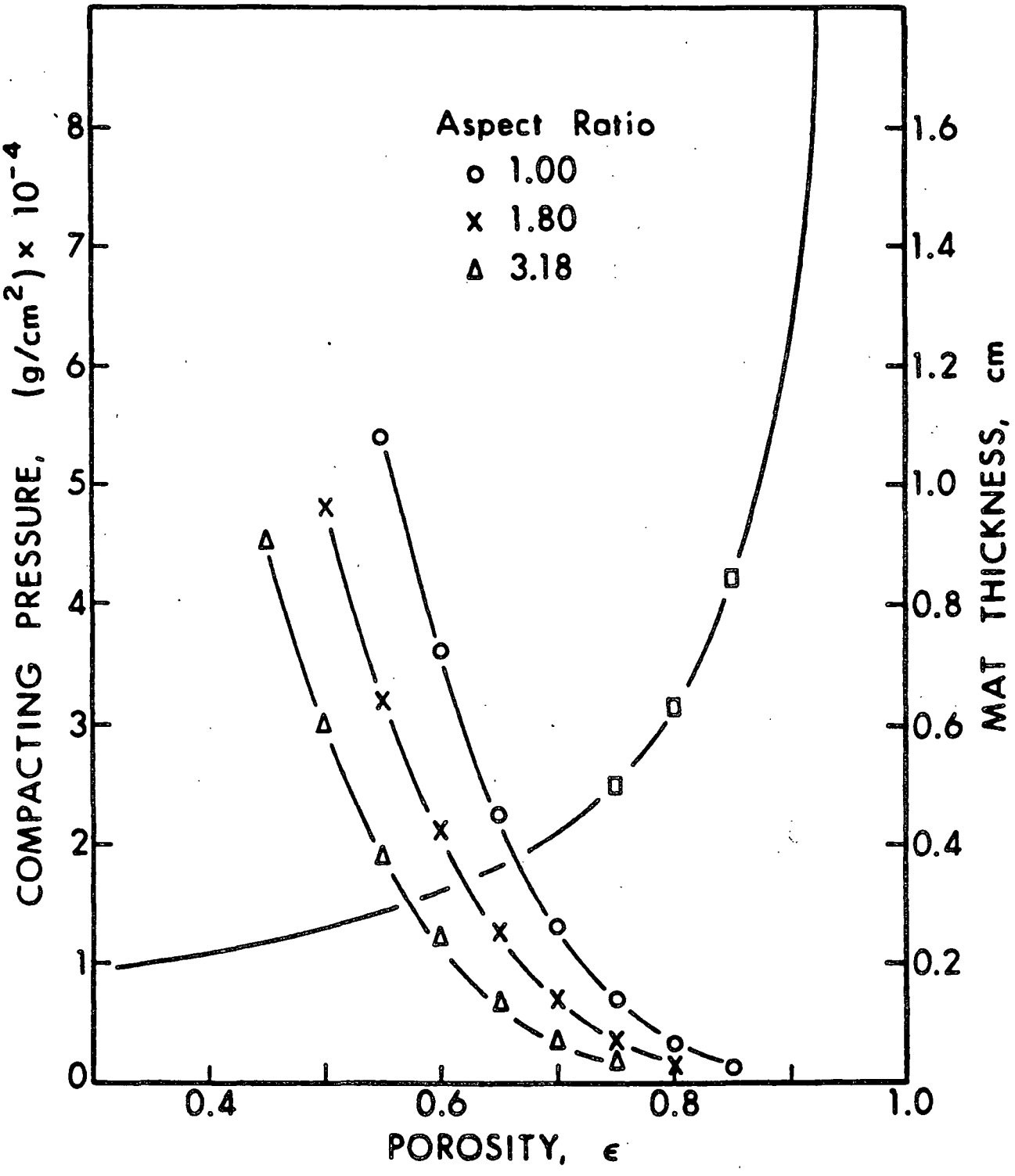

Figure 28. Compacting pressure and mat thickness as a function of porosity for mats of fibers of various aspect ratios.

and significant compacting pressure increase is about the same for each type of fiber. The mats of fibers of aspect ratio 1.00, 1.80, and 3.18 have their respective "critical" porosities occurring at 0.85, 0.80, and 0.75 for both surface area reduction (see Fig. 24) and compacting pressure increase (see Fig. 28).

The "critical" mat porosity appears to be influenced by the fiber thickness. On the right hand axis of Fig. 28, the mat thickness is plotted against porosity, and three squares are indicated on the mat thickness-porosity curve corresponding to the three "critical" porosities from which the significant surface area reduction and compacting pressure increase for three respective types of mats occur. It was noted that the mat thickness ratio of these three mats at their respective critical porosities of 0.85, 0.80, 0.75 is 1.0/0.75/0.60, and is about the same as the fiber thickness ratio of 1.0/0.75/0.56 of same size fibers of respective aspect ratios. This clearly indicates that for fibers piled up the same way, the thinner the fiber the lower the critical porosity it reaches before suffering from interfiber compaction and losing their surfaces.

Since the surface area reduction appears to be dependent on compacting pressure, the surface area loss of these three types of mats was plotted against the compacting pressure on a double-logarithmic paper, as shown in Fig. 29. The initial surface areas of the three types of fibers have been normalized to have the same cross-sectional size as the cylindrical fibers. As is evident, all the data of the three types of fibers fall onto the same surface area loss - compacting pressure relationships. It is thus concluded that the surface area reduction is caused by the compacting pressure.

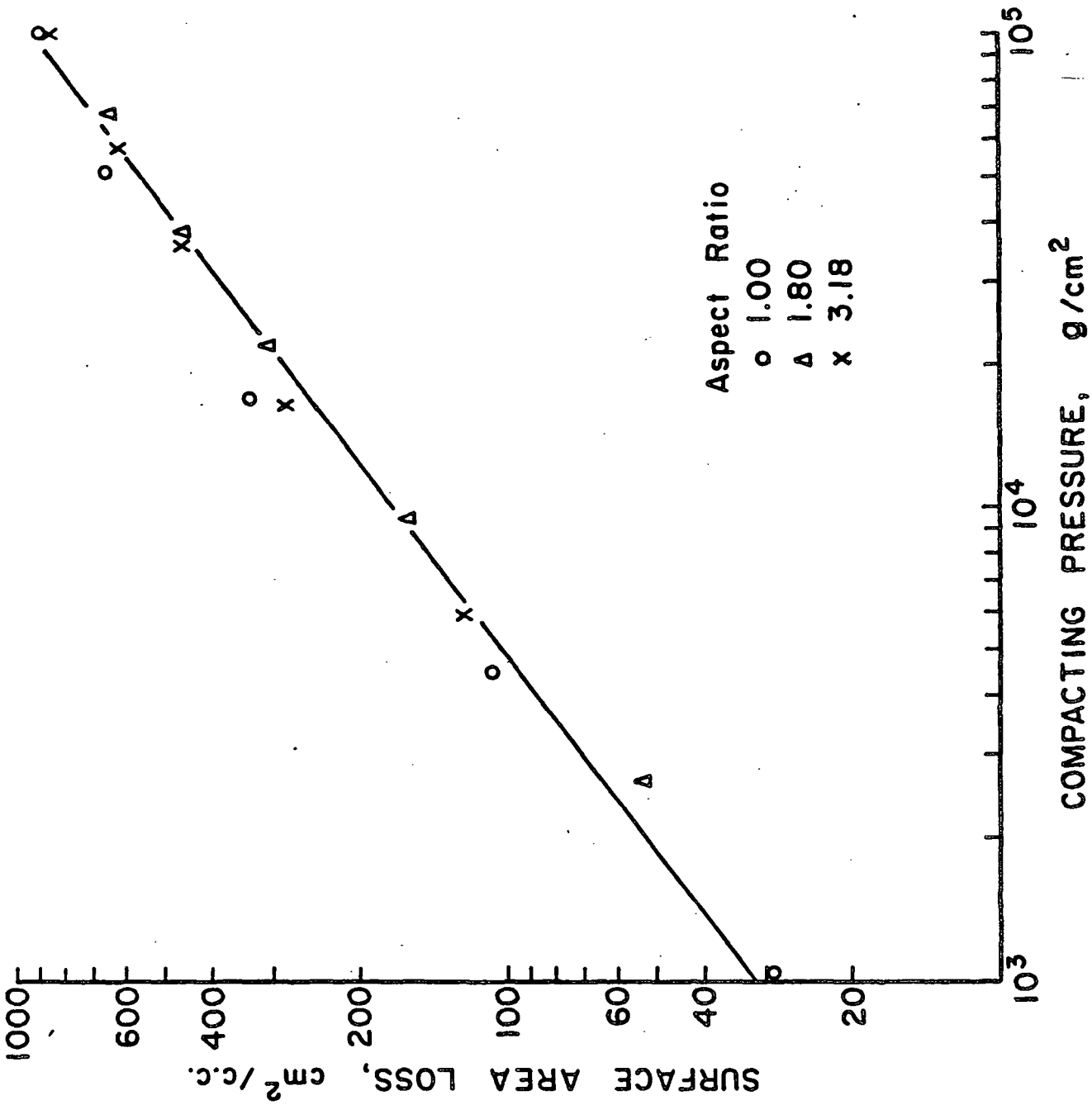

Figure 29. Surface area loss in relation to compacting pressure from mats of various aspect ratios.

Discussions on Structural Effect on Experimental Kozeny Factor

The resistance to compaction and the resistance to permeation are two of the most important physical properties of fiber mats. The resistance to compaction of a fibrous structure results from the solid-to-solid interaction, whereas the resistance to permeation stems from the solid-to-liquid interaction. Clearly, the more the surfaces participate in the solid-to-solid interaction, the less the surfaces are available for dragging the permeating fluid.

There are many factors other than the fiber cross-sectional shape that are known to influence the solid-to-solid interactions, as has been given in Jones' (54) and Elias' (85) mat compressibility studies and in a critical review by Han (18). These factors are expected to affect the extent of surface area reduction and concomittantly affect the experimental Kozeny factor.

The fiber "length-to-diameter ratio" will definitely play an important role in the experimental Kozeny factor detemination. Jones (54) has provided a comprehensive set of compressibility data for mats of cylindrical fibers with varying length-to-diameter ratio. He showed that when the length-to-diameter ratio becomes lower than certain critical values (about 500 for glass fibers, 100 for nylon fibers) the curve in the compacting pressure-porosity plot will shift to lower porosities. This is reasonable since the shorter fibers can be packed into mats of lower initial porosities. The experimental Kozeny factor below porosity 0.8 will undoubtedly swing upward and eventually coincide with the particle curve as the length-to-diameter ratio approaches 1.0. In other words reducing the length-to-diameter ratio will have the same effect as increasing the cross-sectional aspect ratio as shown in this study.

Mechanical conditioning can conceivably change the experimental Kozeny factor. It has been shown by Jones (54) that repeated cycles of loading-deloading will reorganize the mat structure into more compact initial structures and shift the compression curve to lower porosity side. As a result, the experimental Kozeny factor may be speculated to shift to higher values than that for unconditioned mats. Along the same line, vibration or pulsating flow rate during mat formation and any other mechanisms which cause a more compact initial structure of the mat will possibly result in the same effect.

Fiber slippage has often been mentioned (85) as one of the important factors influencing compression behavior. If so, the interfiber friction coefficient, adhesion characteristics, and surface roughness may be important.

CONCLUSIONS

The experimental observations made in this study have led to the following conclusions.

1. For filtration-formed fiber mats composed of conformable fibers, the "experimental" Kozeny factor (calculated by assuming point contacts) is not constant at porosities less than 0.8, but is a function of porosity and fiber cross-sectional shape.

2. The polymer adsorption technique can be used to estimate the external surface area of fibers exposed to flow. This technique gives results indicating the surface area reduction of the "compressed mats" is also a function of porosity and fiber cross-sectional shape.

3. The Kozeny factor when calculated with the surface area measured by polymer adsorption technique shows a fairly constant value of 4.7 toward lower porosities and is independent of fiber cross-sectional shape.

4. The surface area reduction is due to mechanical compaction.

SUGGESTIONS FOR FUTURE WORK

More work certainly deserves to be done in the area of fluid flow through a fiber mat, especially in the low porosity range, due to its importance to the wet pressing operation in paper manufacturing. But before studies in this area can be fruitful, studies on fiber mat compression at this low porosity range where the mechanism of fiber compaction dominates has to be systematically carried out. Important factors such as fiber mechanical properties, fiber surface properties, mechanical conditioning, fiber length to diameter ratio, fiber cross-sectional aspect ratio, and even fiber diameter distribution has to be taken into consideration. Compressibility along with permeability studies should yield valuable information for the understanding of fiber network structure and should provide a better background for theoretical development in the future.

Probably it will be advantageous to carry out permeation of Kirsch and Fuchs' model filter (31) to the low porosity range. The model filter can have fibers arranged in whatever pattern may be of interest and does not introduce interfiber compaction. The combination of a model filter study and Brown's (25) theoretical analysis may yield a more realistic theoretical background for fluid flow through low porosity mats.

Use of polymer adsorption techniques for measuring external surface area always needs thorough characterization depending upon the type of surface used. It, however, has the advantage over dye adsorption techniques because the polymer size can be varied to define the type (external or internal) of surface to be measured.

ACKNOWLEDGMENTS

The Board ot Trustees and member companies are thanked for their support to The Institute of Paper Chemistry.

My sincere appreciation is extended to the members of my Thesis Advisory Committee: Dr. Gary A. Baum, Chairman, Mr. Nai L. Chang, and Dr. Robert A. Stratton, for their continued advice and support. Special thanks and admiration fo to my former Thesis Chairman, Mr. S. T. Han who provided the initial enthusiasm, knowledge, and encouragement, and continued guidance after his retirement.

I am indebted to Messrs. Marvin C. Filz, Jr., and Paul F. Van Rossum for their aid in the construction of my equipment, to the American Enka Corporation, of Enka, North Carolina, for supplying the desired fiber samples, gratis, to the Down Chemical Company, of Midland, Michigan, for generously providing the polyamines, and to Mrs. H. Kaustinen for preparing the photomicrographs of the synthetic fiber cross sections. I am grateful to Mr. Bruce D. Andrews for many suggestions and sharing his vast experience relating to permeation experiments.

Special acknowledgment should be given to my wife, Hsiao-Shan, for her patience and encouragement throughout the course of this study.

NOMENCLATURE

A	= cross-section area of porous medium presented to flow, cm^2
A_f	= fiber cross-sectional area, cm^2
A_m	= projected area of a PEI molecule, $Å^2$
c	= mass of fibers per unit volume of the mat, g/cm^3
C_e	= equilibrium concentration of polymer, mg/L
d	= diameter of polymer molecule, Å
E	= modulus of elasticity, g/cm^2
F	= load for fiber elongation, g
K	= Darcy permeability or specific permeability, cm^2
K_L	= Langmuir constant, 1/mg
K_o	= proportionality factor of Darcy's Law, cm^2 sec/g
k	= Kozeny factor, dimensionless
k_{corr}	= Kozeny factor corrected with surface area, dimensionless
k_1, k_2	= constants in Davies and Ingmanson empirical correlations for Kozeny factor, dimensionless
$k_{(p)}$, $k_{(t)}$	= Kozeny factors for parallel and perpendicular flow past cylinders, dimensionless
L	= thickness of the medium, cm
L_o	= bed thickness at zero porosity, cm
l	= initial fiber length, cm
Δl	= elongation of fiber, cm
M	= compressibility constant, $g/cm^3/(dyne/cm^2)^N$
M_n	= number average molecular weight, g/mole
m	= hydraulic radius, cm
N	= compressibility constant, dimensionless
N_A	= Avogadro number, molecules/mole

P = mechanical load applied on fiber mat, g/cm^2

ΔP = pressure drop across the medium, $dyne/cm^2$

Q = volumetric flow rate, cm^3/sec

S_c = contact surface area, cm^2/cm^3

S_o = surface area per unit volume of the medium, cm^2/cm^3

S_v = surface area per unit volume of the particle, cm^2/cm^3

S_w = surface area per unit mass, cm^2/g

U = superficial flow velocity, cm/sec

v = effective specific volume of the fibers, cm^3/g

V_s = PEI sample volume, mL

V_t = total volume of sample for colorimetric measurement, mL

W = mass of particles or fibers in bed, g

$w(\varepsilon)$ = weighting function, dimensionless

y = difference in weight between the slurry-filled and water-filled pycnometer, g

ρ = density of fibers, g/cm^3

ρ_w = density of water at the test temperature, g/cm^3

μ = the viscosity of fluid, poises

ε = porosity, dimensionless

Γ_A = specific adsorption of polymer at equilibrium, mg/m^2

Γ_m = specific adsorption of polymer at surface saturation, mg/m^2

$\Gamma_{m,g}$ = specific adsorption of polymer at geometrically-allowed surface saturation, mg/m^2

LITERATURE CITED

1. Darcy, H. P. G. Les fontaines publiques de la ville de Dijon. Paris, Victor Dalamont, 1856.

2. Scheidegger, A. E. The physics of flow through porous media. Rev. ed. Toronto, University of Toronto Press, 1960.

3. Irmay, S., Trans. Am. Geophys. Union 39(4):702(1958).

4. Whittaker, S., Chem. Eng. Sci. 21(3):291-300(1966).

5. Carman, P. C., Trans. Inst. Chem. Engrs. (London) 15:150(1937).

6. Carman, P. C. Flow of gases through porous media. New York, Academic Press, 1956.

7. Snyder, L. J. and Steward, W. E., AIChE J. 12(1):167(1966).

8. Scarlett, B., Paper read to Inst. Chem. Eng. Symposium, Filtration, 1968.

9. Happel, J., AIChE J. 4(2):197-201(1958).

10. Kuwabara, S., J. Phys. Soc. Japan 14(4):527-32(1959).

11. Happel, J. and Brenner, H. Low Reynolds number hydrodynamics. New York, Prentice-Hall, Inc., 1965.

12. Brinkman, H. C., Appl. Sci. Res. A1:27(1947).

13. Steinour, H. H., Ind. Eng. Chem. 36:618, 840, 901(1944).

14. Mertes, T. S. and Rhodes, H. B., Chem. Eng. Progr. 51:429(1955); 51:517 (1955).

15. Verschoor, H., Appl. Sci. Research A2:155(1951).

16. Happel, J. and Epstein, N., Ind. Eng. Chem. 46:1187(1954).

17. Wilson, B. W., Australian J. Appl. Sci. 4:274(1953).

18. Han, S. T., Pulp Paper Mag. Can. 70(9):T134-46(1969).

19. Davies, C. N., Proc. Inst. Mech. Engrs. (London) B1:185(1952).

20. Ingmanson, W. L., Andrews, B. D., and Johnson, R. C., Tappi 42(10):840-9 (1959).

21. Carroll, C. W., unpublished work. Appleton, Wisconsin, The Institute of Paper Chemistry, 1965.

22. Emersleben, O., Phys. Z. 26:601(1925).

23. Langmuir, I. Filtration of aerosols and the development of filter materials. O.S.R.D. Report No. 865, Sept. 4, 1942.

24. Happel, J., AIChE J. 5(2):174-7(1959).

25. Brown, G. R. Creeping flow of fluids through assemblages of elliptic cylinders and its application to the permeability of fiber mats. Doctor's Dissertation, Appleton, Wisconsin, The Institute of Paper Chemistry, 1975.

26. Sparrow, E. M. and Loeffler, A. L., Jr., AIChE J. 5(3):325-30(1959).

27. Leibenson, L. S., Complete Works, Vol. 3, Moscow, 1955.

28. Hasimoto, H., J. Fluid Mech. 5:317-28(1959).

29. Sullivan, R. R., J. Appl. Phys. 13:725(1942).

30. Kirsch, A. A. and Fuchs, N. A., J. Phys. Soc. Japan 22(5):1251-5(1967).

31. Kirsch, A. A. and Fuchs, N. A., Ann. Occup. Hyg. 10:23-30(1967).

32. Meyer, H., Unpublished work, Appleton, Wisconsin, The Institute of Paper Chemistry, 1969.

33. Meyer, H., Tappi 54(9):1426-50(1971).

34. Han, S. T. The status of the sheet-forming process: a critical review. Appleton, Wisconsin, The Institute of Paper Chemistry, 1965.

35. Robertson, A. A. and Mason, S. G., Pulp Paper Mag. Can. 50(13):103(Dec., 1949).

36. Carroll, M. and Mason, S. G., Can. J. Technol. 30(12):321(1952).

37. Mason, S. G., Tappi 33(8):403(1950).

38. Fowler, J. L. and Hertel, K. L., J. Appl. Phys. 11:496(1940).

39. Brown, J. C., Jr. Determination of the exposed surface area of pulp fibers from air permeability measurements, using a modified Kozeny equation. Doctor's Dissertation, Appleton, Wisconsin, The Institute of Paper Chemistry, 1949.

40. Bliesner, W. C. A study of the porous structure of fibrous sheets using permeability techniques. Doctor's Dissertation, Appleton, Wisconsin, The Institute of Paper Chemistry, 1963.

41. Onogi, S. and Sasaguri, K., Tappi 44(12):874-80(1961).

42. Labrecque, R. P. An investigation of the effects of fiber cross-sectional shape on the resistance to the flow of fluids through fiber mats. Doctor's Dissertation, Appleton, Wisconsin, The Institute of Paper Chemistry, 1967.

43. Nguyen, C. T., A-291 Special Studies, The Institute of Paper Chemistry, 1977.

44. Moncrief, R. W., Man-made Fibers, Interscience Publisher, New York, N.Y., 1970.

45. Arnold, E. W., Tappi 46(4):250-6(1963).

46. Van Veld, R. D., Morris, G., and Billica, H. R., J. Appl. Polymer Sci. 12:2709(1968).

47. Kindler, W. A., Jr. Adsorption kinetics in the polyethylenimine-cellulose fiber system. Doctor's Dissertation, Appleton, Wisconsin, The Institute of Paper Chemistry, 1971.

48. Hostetler, R. E. A study of the diffusion into and adsorption of polyethylenimine onto silica gel. Doctor's Dissertation, Appleton, Wisconsin, The Institute of Paper Chemistry, 1973.

49. Lindquist, G. M. The role of polyelectrolyte charge density and molecular weight on the adsorption and flocculation of colloidal silica with polyethylenimine. Doctor's Dissertation, Appleton, Wisconsin, The Institute of Paper Chemistry, 1975.

50. Dick, C. R. and Ham, G. E., J. Macromol. Sci.-Chem. A4(6):1301-14(1930).

51. Van Den Berg, J. W. A., Bloys Van Treslong, C. J., and Polderman, A., Recueil 92:3-10(1973).

52. Allan, G. G., Akagane, K., Keogi, N., and Reif, W. M. In The physics and chemistry of wood pulp fibers - TAPPI Monograph STAP No. 8. New York, TAPPI, 1970.

53. Perrine, T. D. and Landis, W. R., J. Polymer Sci. Part A-15(8):1993-2005 (1967).

54. Jones, R. L. An investigation of the effect of fiber structural properties on the compression response of fibrous beds. Doctor's Dissertation, Appleton, Wisconsin, The Institute of Paper Chemistry, 1962.

55. Adamson, A. W., Physical Chemistry of Surfaces, 2nd ed., New York, Interscience, 1967. 747 p.

56. Henwood, A. and Garey, R. M., J. Franklin Inst. 221(4):531(1936); Analytical Group Method 52, Appleton, Wisconsin, The Institute of Paper Chemistry, June 1, 1964.

57. Hughes, R. E. and von Frankenburg, C. A. High polymers. In Annual Reviews of Physical Chemistry, Vol. 14, Palo Alto, CA, Annual Reviews, Inc. 1963. p. 291.

58. Silberberg, A., J. Phys. Chem. 66:1884-907(1962).

59. Patat, F., Killman, E., and Schliebener, C., Rubber Chem. Technol. 39: 36-87(1966).

60. Claesson, I. and Claesson, S., Phys. Rev. 73:1221(1948).

61. Hobden, J. F. and Jellinek, H. H. G., J. Polymer Sci. 11:365-78(1953).

62. Binford, J. S. and Gessler, A. M., J. Phys. Chem. 63:1376-8(1959).

63. Jankovics, L., J. Appl. Polymer Sci. 9:545-52(1965).

64. Rowland, F. W. and Eirich, F. R., J. Polymer Sci., Pt. A-1:2401-21(1966).

65. Rowland, F. W., Bulas, R., Rothstein, E., and Eirich, F. R., Ind. Eng. Chem. 57(9):46-52(1965).

66. Frisch, H. L., Simha, R., and Eirich, F. R., J. Phys. Chem. 21:365(1953).

67. Simha, R., Frisch, H. L., and Eirich, F. R., J. Phys. Chem. 57:584(1953).

68. Frisch, H. L. and Simha, R., J. Phys. Chem. 58:507(1959).

69. Emery, P. H. Polymer adsorption and fractionation in the polystyrene-dichloroethane-carbon black system. Doctor's Dissertation, Appleton, Wisconsin, The Institute of Paper Chemistry, 1965.

70. Farrar, N. O. Partitioning and reversibility of polymer adsorption in the polystyrene, 1,2-dichloroethane, carbon black system. Doctor's Dissertation, Appleton, Wisconsin, The Institute of Paper Chemistry, 1967.

71. Howard, G. J. and McConnell, P., J. Phys. Chem. 71:2974-95(1967).

72. Wilfinger, H., Papier 2:265(1948).

73. Trout, P. E., Tappi 34:539(1951).

74. Clapp, R. T. An investigation of the relation between carboxyl content and zeta potential. Doctor's Dissertation, Appleton, Wisconsin, The Institute of Paper Chemistry, 1972.

75. Allan, G. G. and Reif, W. M., Svensk Papperstid. 74:2, 25(1971).

76. McDonald, M. Paper recycling and the use of chemicals. Noyes Data Corp., Park Ridge, NJ. 1971.

77. Robson, H. L. Chloramines and chloroamines." Kirk-Othmer Encyclopedia of chemical technology. 2nd ed., Vol. 4, Interscience Publishers, A Division of John Wiley & Sons, Inc., New York, 1964. pp. 908-28.

78. Ingmanson, W. L. and Andrews, B. D., Tappi 42(1):29(1959).

79. Peterson, R. M. Two-dimensional flow of fluids in deformable porous media. Doctor's Dissertation, Appleton, Wisconsin, The Institute of Paper Chemistry, 1969.

80. Birkner, F. B. and Morgan, J. J., J. Am. Water Works Assoc. 60:175-91 (1968).

81. Kasper, D. R. Theoretical and experimental investigation of the flocculation of charged particles in aqueous solutions by polyelectrolytes of opposite charge. Doctor's Dissertation, Pasadena, CA, California Institute of Technology, 1971.

82. Chang, N. L., private communication, 1977.

83. Van Wyk, C. M., J. Textile Inst. 37:T-285(1946).

84. Wilder, H. D. The compression creep properties of wet pulp mats. Doctor's Dissertation, Appleton, Wisconsin, The Institute of Paper Chemistry, 1959.

85. Elias, T. C. An investigation of the compression response of ideal unbonded fibrous structures by direct observation. Doctor's Dissertation, Appleton, Wisconsin, The Institute of Paper Chemistry, 1965.

APPENDIX I

CALIBRATION OF THE PRESSURE DROP ACROSS THE PERMEATION SYSTEM

After installation, the rotameter was calibrated at several tube readings by measuring the time required for the collection of a measured volume of water. The rotameter was a F & P Co. Precision Bore Flowrator No. 2F 1/4 20-5/36. Its calibration curve is shown in Fig. 30. The pressure drop across the permeation system from Vessel (A) to Vessel (B) shown in Fig. 11 was then determined in the absence of fiber mat at various flow rates in the same manner as described in the Experimental Section. The calibration is shown in Fig. 31. In the fiber mat permeability determination, the pressure drop across the system containing a fiber mat is always subtracted by that across the system at the respective flow rate.

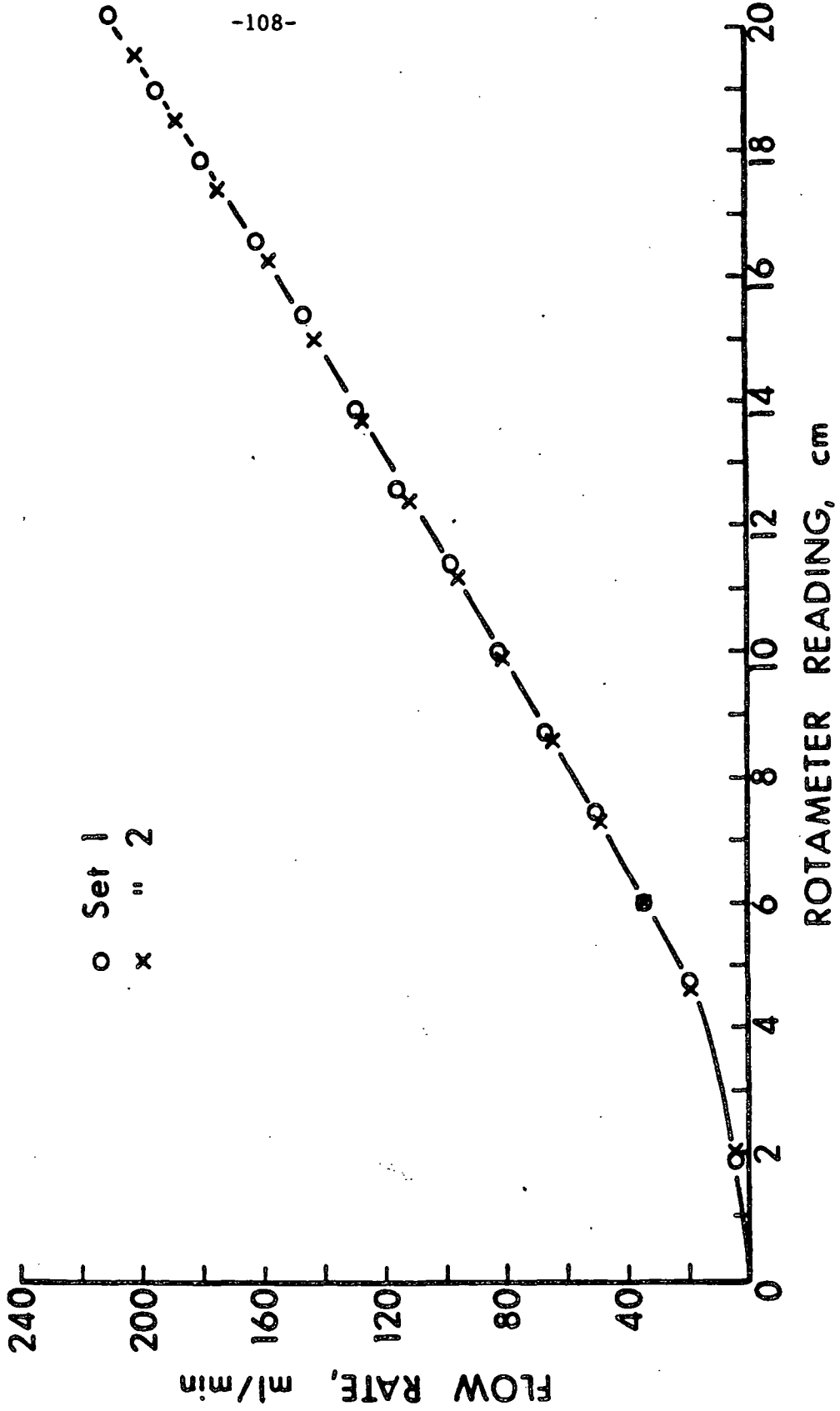

Figure 30. Rotameter calibration curve.

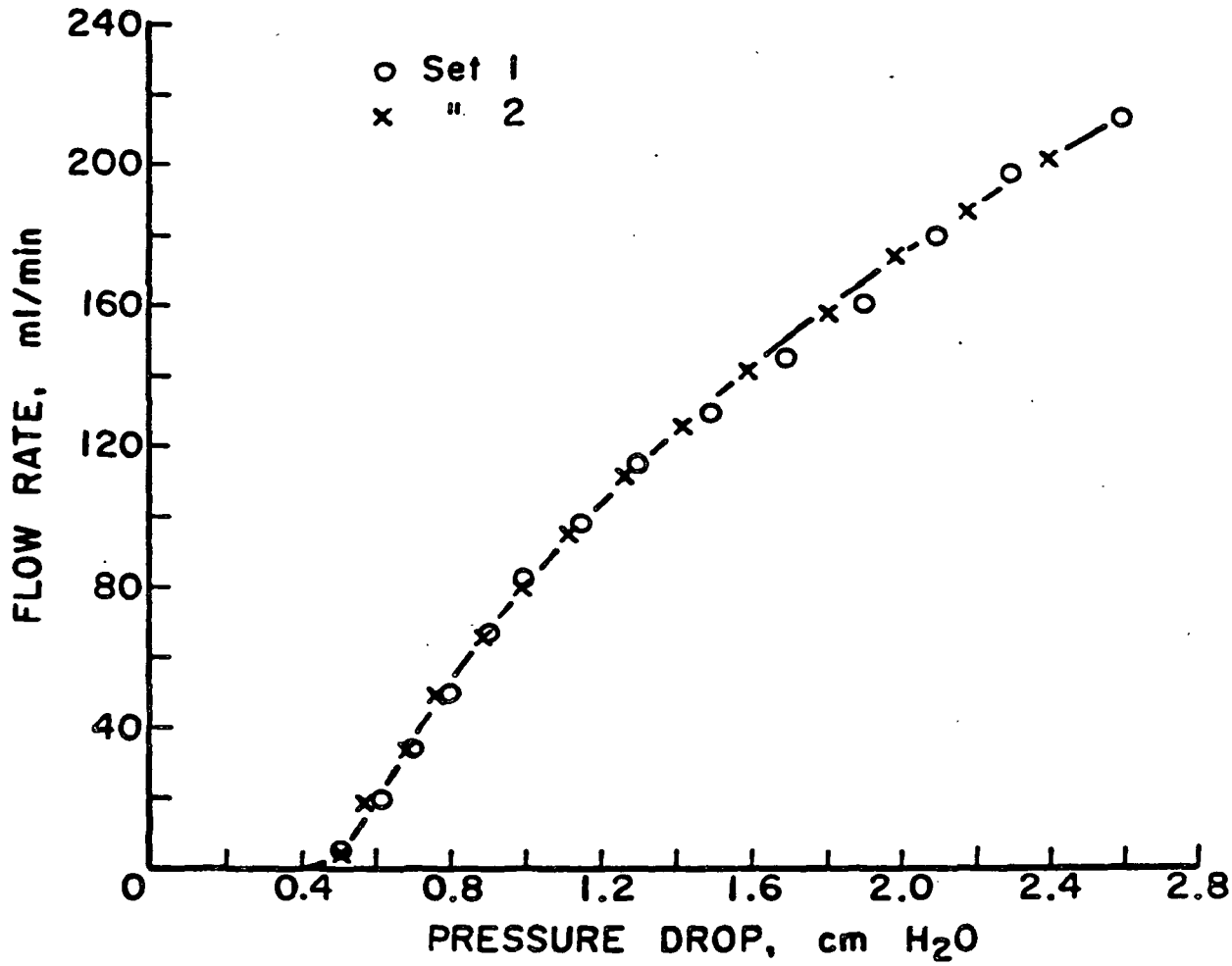

Figure 31. Flow resistance of permeation system.

APPENDIX II

EQUILIBRIUM ADSORPTION DATA

Table 4. Adsorption of PEI-1000 on cylindrical polyester fibers[a] as a function of pH.

pH	C_e, mg/L	Γ_A, mg/m^2[b]
3.51	14.85	0.0142
4.15	14.53	0.0460
5.10	13.98	0.0991
6.04	13.49	0.1469
7.00	12.83	0.2106
8.30	11.91	0.3009
8.80	11.41	0.3487
9.20	10.98	0.3912
9.80	9.94	0.4920
10.00	9.28	0.5558
10.20	8.96	0.5876
10.40	9.01	0.5823
10.60	12.94	0.2000
10.80	14.91	0.0088
11.00	14.96	0.0035
11.30	15.00	0.00

[a] 3 mg of PEI-1000 was added to each slurry containing 200 mL of H_2O and 10 g of fibers having a total surface area of 2.057 m^2.
[b] Specific adsorption, Γ_A, was calculated by: $\Gamma_A = (3 - 0.2\ C_e)/2.057$.

Table 5. Readsorption of PEI-1000 on water-alkali-acid washed fibers[a] as a function of pH.

pH	C_e, mg/L	Γ_A, mg/m^2[b]
7.8	14.96	0.0035
8.3	14.91	0.0088
8.9	14.53	0.0460
9.4	14.14	0.0832
9.8	13.54	0.1416
10.2	13.05	0.1894
10.4	13.49	0.1469
10.6	14.20	0.0779
10.8	14.96	0.0035
11.0	15.00	0.00
11.3	14.96	0.0035

[a] 3 mg of PEI-1000 was added to each slurry containing 200 mL of H_2O and 10 g of fibers having a total surface area of 2.057 m^2.
[b] Specific adsorption, Γ_A, was calculated by: $\Gamma_A = (3 - 0.2\ C_e)/2.057$.

Table 6. Ten cycles of adsorptions on NaOCl-alkali washed fibers.

Cycle No.	C_e, mg/L	Γ_A, mg/m^2
1	8.96	0.5876
2	9.01	0.5823
3	8.96	0.5876
4	9.07	0.5770
5	9.01	0.5823
6	8.96	0.5876
7	9.07	0.5770
8	9.07	0.5770
9	8.96	0.5876
10	8.96	0.5876

Same footnotes as Table 4, except the adsorption pH being controlled at 10.20 here.

Table 7. Adsorption of PEI-1000 on cylindrical polyester fibers as a function of contact time.

Contact time, min	C_e, mg/L	Γ_A, mg/m^2
0	--	--
5	9.393	0.5451
10	9.175	0.5664
15	8.956	0.5876
20	9.066	0.5770
30	8.956	0.5876
40	8.956	0.5876
60	9.011	0.5823
120	8.956	0.5876
240	9.011	0.5823

Same footnotes as Table 6.

Table 8. Adsorption of PEI-1000 on fibers of all aspect ratios[a] as a function of concentration.

PEI Added, mg	C_e, mg/L	Γ_A, mg/m^2[b]	C_e/Γ_A, m^2/L
Aspect Ratio = 1.00			
1.24	1.147	0.4912	2.335
2.48	6.444	0.5790	11.13
3.72	12.29	0.6136	20.03
4.96	18.35	0.6281	29.21
6.20	24.52	0.6298	38.93
7.44	30.64	0.6380	48.02
8.68	36.81	0.6408	57.44
9.92	42.98	0.6436	66.78
Aspect Ratio = 1.80			
1.24	0.665	0.4154	1.578
2.48	4.970	0.5566	8.929
3.72	10.54	0.6038	17.46
4.96	16.44	0.6264	26.24
6.20	22.55	0.6327	35.65
7.44	28.67	0.6389	44.88
8.68	34.84	0.6411	54.35
9.92	40.96	0.6473	63.28
Aspect Ratio = 3.18			
1.24	0.492	0.3923	1.253
2.48	4.478	0.5444	8.226
3.72	9.776	0.6064	16.12
4.96	15.84	0.6159	25.71
6.20	21.90	0.6254	35.02
7.44	27.96	0.6349	44.04
8.68	34.19	0.6331	54.00
9.92	40.30	0.6388	63.09

[a]The adsorption system contains 10 g of fibers in 0.2 liter of water, resulting in a total surface area of 2.057 m^2 for Aspect Ratio (A.R.) 1.00, of 2.670m^2 for A.R. 1.80, and of 2.911 m^2 for A.R. 3.18.

[b]Specific adsorption, Γ_A, was obtained by:

Γ_A = (PEI added - 0.2 C_e)/2.057 for A.R. 1.00
Γ_A = (PEI added - 0.2 C_e)/2.670 for A.R. 1.80
Γ_A = (PEI added - 0.2 C_e)/2.911 for A.R. 3.18

Table 9. Adsorption of PEI on cylindrical polyester fibers[a] as a function of molecular weight.

PEI-1000
$\underline{M}_n$: 75,000
pH: 10.20

PEI Added, mg	$\underline{C}_e$, mg/L	Γ_A, mg/m^2[b]	$\underline{C}_e/\Gamma_A$, m^2/L
1.24	0.328	0.1817	1.804
2.48	0.928	0.3504	2.650
3.72	2.348	0.4800	4.892
4.96	4.915	0.5548	8.859
6.20	8.356	0.5880	14.210
7.44	12.015	0.6105	19.680
8.68	16.056	0.6149	26.110
9.92	19.988	0.6246	32.000
11.16	24.139	0.6237	38.700
12.40	28.125	0.6307	44.590
13.64	32.112	0.6377	50.360

PEI-600
$\underline{M}_n$: 50,000
pH: 10.2

PEI Added, mg	$\underline{C}_e$, mg/L	Γ_A, mg/m^2[b]	$\underline{C}_e/\Gamma_A$, m^2/L
1.24	0.328	0.1817	1.804
2.48	1.038	0.3452	3.006
3.72	2.567	0.4696	5.466
4.96	5.297	0.5365	9.874
6.20	8.793	0.5670	15.510
7.44	12.670	0.5792	21.880
8.68	16.493	0.5940	27.770
9.92	20.643	0.5933	34.790
11.16	24.575	0.6029	40.760
12.40	28.617	0.6072	47.130
13.64	32.767	0.6065	54.030

[a]The adsorption system contains 30.5416 g of cylindrical fibers and 0.3 liter of water, providing a total surface area of 6.2824 m^2.
[b]Specific adsorption, Γ_A, was obtained by: $\Gamma_A = (\text{PEI added} - 0.3\ \underline{C}_e)/6.2824$.

Table 9 (Contd.). Adsorption of PEI on cylindrical polyester fibers[a] as a function of molecular weight.

PEI-400
$\underline{M}_n$: 35,000
pH: 10.2

PEI Added, mg	$\underline{C}_e$, mg/L	Γ_A, mg/m^2[b]	$\underline{C}_e/\Gamma_A$, m^2/L
1.24	0.382	0.1791	2.135
2.48	1.092	0.3426	3.188
3.72	2.731	0.4617	5.914
4.96	5.516	0.5261	10.480
6.20	9.066	0.5545	16.350
7.44	12.834	0.5714	22.460
8.68	16.875	0.5758	29.310
9.92	20.807	0.5854	35.540
11.16	24.598	0.5846	42.080
12.40	28.890	0.5942	48.620
13.64	33.095	0.5908	56.020

PEI-200
$\underline{M}_n$: 25,000
pH: 10.2

PEI Added, mg	$\underline{C}_e$, mg/L	Γ_A, mg/m^2[b]	$\underline{C}_e/\Gamma_A$, m^2/L
1.24	0.437	0.1765	2.475
2.48	1.049	0.3447	3.044
3.72	3.004	0.4487	6.694
4.96	5.844	0.5104	11.450
6.20	9.393	0.5384	17.450
7.44	13.271	0.5506	24.100
8.68	17.039	0.5680	30.000
9.92	21.189	0.5672	37.360
11.16	25.122	0.5768	43.550
12.40	29.272	0.5759	50.830
13.64	33.313	0.5804	57.400

[a]The adsorption system contains 30.5416 g of cylindrical fibers and 0.3 liter of water, providing a total surface area of 6.2824 m^2.
[b]Specific adsorption, Γ_A, was obtained by: Γ_A = (PEI added - 0.3 $\underline{C}_e$)/6.2824.

Table 9 (Contd.). Adsorption of PEI on cylindrical polyester fibers[a] as a function of molecular weight.

PEI-18
$\underline{M}_n$: 1,800
pH: 10.2

PEI Added, mg	$\underline{C}_e$, mg/L	Γ_A, mg/m^2[b]	$\underline{C}_e/\Gamma_A$, m^2/L
1.24	0.765	0.1608	4.755
2.48	2.458	0.2774	8.859
3.72	5.297	0.3392	15.620
4.96	8.902	0.3644	24.430
6.20	12.779	0.3771	33.890
7.44	16.602	0.3915	42.410
8.68	20.753	0.3906	53.130
9.92	24.739	0.3977	62.210
11.16	28.835	0.3994	72.200

PEI-12
$\underline{M}_n$: 1,200
pH: 10.2

PEI Added, mg	$\underline{C}_e$, mg/L	Γ_A, mg/m^2[b]	$\underline{C}_e/\Gamma_A$, m^2/L
1.24	0.874	0.1556	5.616
2.48	2.676	0.2670	10.020
3.72	5.625	0.3235	17.390
4.96	9.229	0.3488	26.460
6.20	13.162	0.3584	36.720
7.44	16.930	0.3758	45.050
8.68	21.189	0.3698	57.300
9.92	25.231	0.3742	67.430
11.16	29.217	0.3812	76.650

[a]The adsorption system contains 30.5416 g of cylindrical fibers and 0.3 liter of water, providing a total surface area of 6.2824 m^2.
[b]Specific adsorption, Γ_A, was obtained by: Γ_A = (PEI added - 0.3 $\underline{C}_e$)/6.2824.

Table 9 (Contd.). Adsorption of PEI on cylindrical polyester fibers[a] as a function of molecular weight.

PEI-6
$\underline{M}_n$: 600
pH: 10.2

PEI Added, mg	$\underline{C}_e$, mg/L	Γ_A, mg/m^2[b]	$\underline{C}_e/\Gamma_A$, m^2/L
1.24	0.928	0.1530	6.068
2.48	2.949	0.2539	11.610
3.72	6.062	0.3027	20.030
4.96	9.776	0.3227	30.290
6.20	13.653	0.3354	40.710
7.44	17.749	0.3367	52.710
8.68	21.626	0.3489	61.980
9.92	25.831	0.3455	74.770
11.16	29.818	0.3525	84.590

PEI-3
$\underline{M}_n$: 300
pH: 10.2

PEI Added, mg	$\underline{C}_e$, mg/L	Γ_A, mg/m^2[b]	$\underline{C}_e/\Gamma_A$, m^2/L
1.24	1.147	0.1426	8.042
2.48	3.441	0.2305	14.930
3.72	6.717	0.2714	24.750
4.96	10.431	0.2914	35.800
6.20	14.363	0.3010	47.720
7.44	18.459	0.3028	60.960
8.68	22.282	0.3176	70.160
9.92	26.596	0.3090	86.070
11.16	30.419	0.3238	93.940

[a]The adsorption system contains 30.5416 g of cylindrical fibers and 0.3 liter of water, providing a total surface area of 6.2824 m^2.
[b]Specific adsorption, Γ_A, was obtained by: $\Gamma_A = (\text{PEI added} - 0.3\ \underline{C}_e)/6.2824$.

APPENDIX III

TITLE

Table 10. Permeability and polymer adsorption data of compressed mats.

Aspect Ratio: 1.00
Mat Weight: 29.5802 g

ε	$\underline{K} \times 10^8$, cm^2	$\underline{k}$	$\underline{C_e}$, mg/L	Γ_A, mg/m^{2a}	Γ_{AO}, mg/m^{2b}	Γ_A/Γ_{AO}[c]	$\underline{k}$ corr.
0.8469	49.96	6.15	12.288	0.6169	0.6114	1.009	6.04
0.7814	23.57	5.02	12.888	0.5873	0.6133	0.958	5.47
0.6687	8.425	3.83	13.653	0.5496	0.6155	0.893	4.80
0.5538	3.508	2.88	15.073	0.4796	0.6191	0.775	4.80
0.4545	1.406	2.21	16.165	0.4257	0.6214	0.685	4.71
0.4217	1.282	2.07	16.493	0.4096	0.6220	0.658	4.77
Aspect Ratio: 1.00 Mat Weight: 27.8975 g							
0.8532	55.83	6.12	13.107	0.6085	0.6140	0.991	6.23
0.7890	15.71	5.10	13.435	0.5913	0.6149	0.962	5.52
0.6764	9.028	3.88	14.090	0.5569	0.6167	0.903	4.76
0.5587	3.710	2.86	15.455	0.4852	0.6199	0.783	4.67
0.4546	2.682	2.21	16.547	0.4279	0.6221	0.688	4.67
0.4211	1.288	2.05	16.930	0.4078	0.6228	0.655	4.78

[a]Each polymer adsorption was conducted by adding 7.44 mg of PEI-1000 to the system of constant volume (water + fibers) of 321 ml. Thus, the specific adsorption, Γ_A, was obtained by:

$$\Gamma_A = \{7.44 - [0.321 - (\text{mat weight}/\text{fiber density})]\ \underline{C_e}\}/\text{mat weight} \times \underline{S_w}.$$

[b]The specific adsorption of fibers in the free suspension, Γ_{AO}, at the same equilibrium concentration was calculated from the calibrated Langmuir's equation:

$$\Gamma_{AO} = = \underline{K_L}\ \Gamma_m \underline{C_e}/(1 + \underline{K_L C_e}) = 1.138 \times 0.655 \times \underline{C_e}/(1 + 1.138\ \underline{C_e}).$$

[c]Γ_A/Γ_{AO} is considered to be the fraction of original surface area available for adsorption.

Table 10 (Contd.). Permeability and polymer adsorption data of compressed mats.

Aspect Ratio: 1.80
Mat Weight: 24.3259 g

ε	$\underline{K} \times 10^8$, cm^2	$\underline{k}$	$\underline{C_e}$, mg/L	Γ_A, mg/m^2[a]	Γ_{AO}, mg/m^2[b]	Γ_A/Γ_{AO}[c]	$\underline{k}$ cor:
0.8709	41.92	6.90	11.523	0.6072	0.6087	0.997	6.94
0.8423	28.39	6.17	11.523	0.6072	0.6087	0.997	6.20
0.8152	20.66	5.60	11.469	0.6097	0.6085	1.002	5.58
0.7187	7.435	4.60	12.015	0.5842	0.6106	0.957	5.02
0.6192	3.022	3.95	12.615	0.5561	0.6125	0.908	4.79
0.5324	1.480	3.40	13.380	0.5204	0.6148	0.847	4.74
0.4722	0.9161	3.01	13.981	0.4923	0.6164	0.799	4.72
0.3944	0.4977	2.45	14.909	0.4489	0.6187	0.726	4.65
Aspect Ratio: 1.80							
Mat Weight: 26.4537 g							
0.8597	35.59	6.61	10.486	0.6052	0.6045	1.001	6.59
0.8285	23.91	5.90	10.540	0.6028	0.6047	0.997	5.94
0.7991	16.91	5.45	10.486	0.6052	0.6045	1.001	5.44
0.6941	5.876	4.43	11.250	0.5725	0.6077	0.942	5.00
0.5859	2.280	3.75	11.960	0.5421	0.6103	0.888	4.75
0.4915	1.080	3.10	12.834	0.5048	0.6132	0.823	4.57
0.4261	0.6343	2.70	13.653	0.4698	0.6155	0.763	4.64

[a]Each polymer adsorption was conducted by adding 7.44 mg of PEI-1000 to the system of constant volume (water + fibers) of 321 ml. Thus, the specific adsorption, Γ_A, was obtained by:

$$\Gamma_A = \{7.44 - [0.321 - (\text{mat weight/fiber density})]\ \underline{C_e}\}/\text{mat weight} \times \underline{S_w}.$$

[b]The specific adsorption of fibers in the free suspension, Γ_{AO}, at the same equilibrium concentration was calculated from the calibrated Langmuir's equation:

$$\Gamma_{AO} = = \underline{K_L}\ \Gamma_m \underline{C_e}/(1 + \underline{K_L C_e}) = 1.138 \times 0.655 \times \underline{C_e}/(1 + 1.138\ \underline{C_e}).$$

[c]Γ_A/Γ_{AO} is considered to be the fraction of original surface area available for adsorption.

Table 10 (Contd.). Permeability and polymer adsorption data of compressed mats.

Aspect Ratio: 3.18
Mat Weight: 24.4391 g

ε	$\underline{K} \times 10^8$, cm^2	$\underline{k}$	$\underline{C_e}$, mg/L	Γ_A, mg/m^{2a}	Γ_{AO}, mg/m^{2b}	$\Gamma_A/\Gamma_{AO}{}^c$	$\underline{k}$ corr.
0.8702	34.99	6.88	10.376	0.6035	0.6040	0.999	6.89
0.8141	16.97	5.66	10.431	0.6012	0.6042	0.995	5.72
0.7170	5.949	4.76	10.540	0.5965	0.6047	0.986	4.89
0.6168	2.311	4.26	11.141	0.5709	0.6073	0.940	4.82
0.5295	1.065	3.88	11.414	0.5593	0.6083	0.919	4.59
0.4690	0.6144	3.67	12.124	0.5590	0.6109	0.866	4.89
0.3907	0.3160	3.13	12.779	0.5010	0.6130	0.817	4.68
Aspect Ratio: 3.18 Mat Weight: 23.4697 g							
0.8736	36.92	6.96	10.868	0.6055	0.6061	0.999	6.98
0.8180	17.82	5.71	10.868	0.6055	0.6061	0.999	5.72
0.7201	5.918	4.96	10.977	0.6006	0.6066	0.990	5.06
0.6171	2.254	4.38	11.469	0.5788	0.6085	0.951	4.84
0.5255	1.006	3.94	12.015	0.5544	0.6105	0.908	4.78
0.4610	0.5826	3.56	12.615	0.5277	0.6125	0.862	4.80
0.3762	0.2715	3.10	13.325	0.4961	0.6146	0.807	4.76

[a]Each polymer adsorption was conducted by adding 7.44 mg of PEI-1000 to the system of constant volume (water + fibers) of 321 ml. Thus, the specific adsorption, Γ_A, was obtained by:

$$\Gamma_A = \{7.44 - [0.321 - (\text{mat weight/fiber density})]\ \underline{C_e}\}/\text{mat weight} \times \underline{S_w}.$$

[b]The specific adsorption of fibers in the free suspension, Γ_{AO}, at the same equilibrium concentration was calculated from the calibrated Langmuir's equation:

$$\Gamma_{AO} = = \underline{K_L}\ \Gamma_m \underline{C_e}/(1 + \underline{K_L C_e}) = 1.138 \times 0.655 \times \underline{C_e}/(1 + 1.138\ \underline{C_e}).$$

[c]Γ_A/Γ_{AO} is considered to be the fraction of original surface area available for adsorption.

APPENDIX IV

FIBER MAT COMPRESSIBILITY DATA

(Mat Area = 25.65 cm^2)

Aspect Ratio: 1.00
Mat Weight: 18.2313 g

Load, g/cm^2	Mat Thickness, cm	Mat Density, g/cm^3
26.94	9.123	0.0779
35.77	8.522	0.0834
53.50	7.708	0.0922
80.05	7.086	0.1003
124.7	6.334	0.1122
186.4	5.797	0.1226
275.4	5.253	0.1351
511.6	4.384	0.1621
595.4	4.171	0.1704
1037	3.587	0.1981
1480	3.234	0.2197
4574	2.371	0.3000
8995	1.959	0.3627
17840	1.571	0.4525
44360	1.202	0.5911
67350	1.063	0.6688

Aspect Ratio: 1.00
Mat Weight: 12.8001 g

26.94	11.71	0.07923
35.77	11.11	0.08351
53.50	10.02	0.09260
80.05	9.191	0.1010
124.7	8.432	0.1101
186.4	7.640	0.1214
175.4	7.121	0.1303
511.6	6.275	0.1550
621.9	5.214	0.1780
1205	4.198	0.2210
2160	3.690	0.2515
3425	3.309	0.2804
3867	3.235	0.2868
5458	2.981	0.3112
14570	2.219	0.4180
35520	1.711	0.5421
62040	1.457	0.6366
106300	1.254	0.7400

FIBER MAT COMPRESSIBILITY DATA

(Mat Area = 25.65 cm^2)

Aspect Ratio: 1.00
Mat Weight: 25.9439 g

Load, g/cm^2	Mat Thickness, cm	Mat Density, g/cm^3
26.94	12.21	0.08283
35.77	11.66	0.08674
53.50	10.73	0.09426
80.05	9.771	0.1035
124.7	8.879	0.1139
186.4	8.008	0.1263
175.4	7.335	0.1379
511.6	6.375	0.1586
684.0	5.722	0.1768
1126	5.214	0.1940
1621	4.706	0.2149
2364	4.198	0.2410
3602	3.690	0.2741
3867	3.404	0.2971
7492	2.896	0.3492
14390	2.388	0.4235
31450	1.880	0.5380
62040	1.538	0.6578
105300	1.322	0.7653

Aspect Ratio: 1.80
Mat Weight: 28.0036 g

26.94	11.97	0.09124
35.77	11.24	0.09717
53.50	10.04	0.1088
80.05	8.935	0.1222
124.7	7.925	0.1378
186.4	7.295	0.1496
275.4	6.448	0.1693
511.6	5.431	0.2010
551.1	5.214	0.2094
683.8	4.960	0.2201
825.2	4.706	0.2320
1037	4.401	0.2481
1480	3.964	0.2754
1922	3.664	0.2979
2664	3.360	0.3249
4486	2.896	0.3770
8895	2.414	0.4523
17840	2.020	0.5404
44360	1.601	0.6820
79730	1.372	0.7954
106300	1.296	0.8422

FIBER MAT COMPRESSIBILITY DATA

(Mat Area = 25.65 cm^2)

Aspect Ratio: 1.80
Mat Weight: 28.0241 g

Load, g/cm^2	Mat Thickness, cm	Mat Density, g/cm^3
26.94	11.74	0.09310
35.77	11.11	0.09840
53.50	9.930	0.1100
80.05	8.655	0.1262
124.7	7.755	0.1409
186.4	7.090	0.1541
275.4	6.400	0.1707
511.6	5.805	0.1882
648.4	4.917	0.2222
1037	4.198	0.2602
1736	3.690	0.2961
2514	3.372	0.3240
4132	2.896	0.3772
8895	2.427	0.4502
17840	2.048	0.5334
44360	1.652	0.6614
70880	1.435	0.7612
106300	1.310	0.8341

Aspect Ratio: 3.18
Mat Weight: 23.7043 g

26.94	7.568	0.1221
35.77	6.835	0.1352
53.50	6.206	0.1489
80.05	5.697	0.1622
124.7	5.025	0.1839
186.4	4.616	0.2002
275.4	4.116	0.2245
511.6	3.520	0.2625
861.0	3.230	0.2861
949.0	3.080	0.3000
1922	2.572	0.3592
4397	2.064	0.4476
8995	1.747	0.5290
14300	1.556	0.5938
35520	1.277	0.7237
62040	1.125	0.8218
106300	1.023	0.9034

FIBER MAT COMPRESSIBILITY DATA

(Mat Area = 25.65 cm^2)

Aspect Ratio: 3.18
Mat Weight: 25.5560 g

Load, g/cm^2	Mat Thickness, cm	Mat Density, g/cm^3
26.94	7.180	0.1388
35.77	7.115	0.1400
53.50	6.850	0.1454
80.05	6.123	0.1627
124.7	5.406	0.1843
186.4	4.860	0.2050
275.4	4.426	0.2251
511.6	3.827	0.2603
789.9	3.429	0.2905
1170	3.186	0.3127
1656	3.065	0.3250
2010	2.811	0.3544
4220	2.303	0.4325
10760	1.795	0.5549
26680	1.458	0.6835
47900	1.287	0.7738
70880	1.191	0.8366
106300	1.110	0.8980